MODELING OF PARTICLE FILLED RESIN IMPREGNATION IN COMPRESSION RESIN TRANSFER MOLDING

HATİCE SİNEM ŞAŞ

JULY 2010

MODELING OF PARTICLE FILLED RESIN IMPREGNATION IN COMPRESSION RESIN TRANSFER MOLDING

A THESIS SUBMITTED TO
THE GRADUATE SCHOOL OF NATURAL AND APPLIED SCIENCES
OF
MIDDLE EAST TECHNICAL UNIVERSITY

BY

HATİCE SİNEM ŞAŞ

IN PARTIAL FULFILMENT OF THE REQUIREMENTS
FOR
THE DEGREE OF MASTER OF SCIENCE
IN
MECHANICAL ENGINEERING

JULY 2010

Approval of the thesis:

MODELING OF PARTICLE FILLED RESIN IMPREGNATION IN COMPRESSION RESIN TRANSFER MOLDING

submitted by **HATİCE SİNEM ŞAŞ** in partial fulfillment of the requirements for the degree of **Master of Science in Mechanical Engineering Department, Middle East Technical University** by,

Prof. Dr. Canan Özgen _____
Dean, Graduate School of **Natural and Applied Sciences**

Prof. Dr. Suha Oral _____
Head of Department, **Mechanical Engineering**

Assist. Prof. Dr. Merve Erdal _____
Supervisor, **Mechanical Engineering Dept., METU**

Examining Committee Members:

Prof. Dr. Levent Parnas _____
Mechanical Engineering Dept., METU

Assist. Prof. Dr. Merve Erdal _____
Mechanical Engineering Dept., METU

Assist. Prof. Dr. Almıla Güvenç Yazıcıoğlu _____
Mechanical Engineering Dept., METU

Assist. Prof. Dr.Cüneyt Sert _____
Mechanical Engineering Dept., METU

Fikret Şenel, M.Sc. _____
Barış Elektrik End. A.Ş.

Date: 08.07.2010

I hereby declare that all information in this document has been obtained and presented in accordance with academic rules and ethical conduct. I also declare that, as require by these rules and conduct, I have fully cited and referenced all material and results that are not original to this work.

Name, Last Name : Hatice Sinem, Şaş

Signature :

ABSTRACT

MODELING OF PARTICLE FILLED RESIN IMPREGNATION IN COMPRESSION RESIN TRANSFER MOLDING

Şaş, Hatice Sinem

M.Sc., Department of Mechanical Engineering

Supervisor: Assist. Prof. Dr. Merve Erdal

July 2010, 137 pages

Compression Resin Transfer Molding (CRTM) is an advanced liquid molding process for producing continuous fiber-reinforced composite parts in relatively large dimensions and with high fiber volume fractions. This thesis investigates this process for the purpose of producing continuous fiber reinforced composites with particle fillers. In many composites, fillers are used within the resin for various reasons such as cost reduction and improvement of properties. However, the presence of fillers in a process involving resin impregnation through a fibrous medium can result in a composite with non-homogeneous microstructure and properties. This work aims to model the resin impregnation and particle filtration during injection and compression stages of the process. For this purpose, a previously developed particle filtration model is adapted to CRTM. An appropriate commercial software tool is used for numerical solution after a survey of available packages. The process is analyzed based on the developed model for various process scenarios. The results of this study aim to enhance the understanding of particle-filled resin impregnation and particle filtration phenomena in the CRTM process and are likely to be used towards designing optimum process configurations for a desired outcome in the future.

Keywords: Compression Resin Transfer Molding (CRTM), Resin Transfer Molding (RTM), Particle-fillers, Resin Flow, Filtration, Numerical Analysis

ÖZ

PRESLEMELİ REÇİNE TRANSFER KALIPLAMA YÖNTEMİNDE PARÇACIK DOLGULU REÇİNE EMİLİMİNİN MODELLENMESİ

Şaş, Hatice Sinem
Yüksek Lisans. Makina Mühendisliği Bölümü
Tez Yöneticisi: Yrd. Doç. Dr. Merve Erdal

Temmuz 2010, 137 sayfa

Preslemeli Reçine Transfer Kalıplama Yöntemi, büyük ebatlarda ve yoğun elyaf oranına sahip kompozitlerin üretimine yönelik geliştirilmiş bir ileri kompozit kalıplama tekniğidir. Bu yüksek lisans tez çalışması, bu yöntemi parçacık dolgulu sürekli elyaflarla takviyeli kompozit parça üretimi için incelemektedir. Birçok kompozit malzemede parçacık dolgu malzemeleri maliyet düşürmek veya malzemenin çeşitli özelliklerini geliştirmek gibi çeşitli amaçlarla kullanılmaktadır. Ancak, reçinenin emdirilmesi sırasında parçacık dolgu malzemelerinin kompozit içinde düzgün dağılmaması, üretilen kompozitin homojen olmayan bir mikro yapıya ve istenilen özelliklere sahip olmamasına sebep olabilir. Bu çalışma, üretimin enjeksiyon ve baskı aşamalarında, reçinenin elyaf içindeki akışını ve parçacık dolgu malzemelerinin filtrasyonunu modellemeyi hedeflemektedir. Bu amaçla daha önceden geliştirilmiş bir parçacık filtrasyon modeli baskılı reçine transfer kalıplama yöntemine uyarlanmıştır. Mevcut ticari yazılım paketlerinin incelenmesinin ardından uygun bir paket yazılım seçilmiş ve sayısal analiz için kullanılmıştır. Geliştirilen modelle çeşitli üretim senaryoları için proses analiz edilmiştir. Bu araştırma sonucunda preslemeli reçine transfer kalıplama üretiminde parçacık dolgulu reçine emdiriliminin ve parçacık filtrasyonunun anlaşılması amaçlanmıştır. Bu

çalışmanın sonuçlarının, ileride istenilen malzeme özellikleri için gerekli optimum üretim konfigürasyonlarının tasarımına yönelik kullanılabileceği düşünülmektedir.

Anahtar kelimeler: Preslemeli Reçine Transfer Kalıplama, Reçine Transfer Kalıplama, Dolgu Parçacıkları, Reçine Akışı, Filtrasyon, Sayısal Analiz

To my lovely sister Senem

ACKNOWLEDGEMENTS

I am heartily thankful to my supervisor Assist. Prof. Dr. Merve Erdal for her encouragement, guidance and support from the initial to the final level of my graduate education. Her endless motivations to help not only about the thesis study but also about my future career are deeply appreciated.

I owe my deepest gratitude to my mother, my father and also my sister Senem for their precious support and endless love. I also want to express my special thanks to Alp Emre not only for his encourage but also for his advices that solve any kind of problems.

Additionally, I would like to thank my dear friends Adem, Almıla, Aşkın, Gökhan, Mehmet, Onur, Özlem, Salih, Tuğçe and Ulaş for their friendship and support. It is a pleasure to thank to the members of the great working environment, Ali Murat, Ural and Mustafa, and Ender in CFD laboratory. Also, I am grateful to all my colleagues in the Department of Mechanical Engineering. And precious help of Gönenç during my thesis study is appreciated.

Finally, the financial support of The Scientific Technological Research Council of Turkey (TÜBİTAK) and Middle East Technical University Office of Scientific and Research Projects Coordination are gratefully acknowledged.

TABLE OF CONTENTS

LIST OF TABLES

TABLES

LIST OF FIGURES

FIGURES

LIST OF SYMBOLS

SYMBOLS

C: concentration of particles in the polymer (volume of particles/volume of suspension

K: domain permeability [m^2]

$\dot{m}$: mass flow rate [kg/s]

p: pressure [Pa]

Q: volumetric flux per width [m^2/s]

S: specific surface area [1/m]

t: time [s]

u, v, w: superficial velocity components in x-, y- and z- directions [m/s]

u', v', w': actual velocity components in x-, y- and z- directions [m/s]

U_z: mold closing speed [m/s]

V: superficial velocity [m/s]

V': actual (interstitial) velocity [m/s]

$\forall$: volume [m^3]

ν_f: fiber volume fraction (volume of fibers/volume of mold cavity), $\nu_f = \nu_{f0} + \sigma$

x,y,z: cartesian coordinates

ε: porosity (volume of pores/volume of mold cavity), $\varepsilon = \varepsilon_0 - \sigma$

μ: viscosity [Pa·s]

ρ: density [kg/m^3]

σ: specific particle deposit (volume of filtered particles/volume of mold cavity)

ϕ: level set function (a scalar function)

SUBSCRIPTS

c: particles in the resin

injection: corresponding to end of the injection

o: corresponding to unfiltered domain

u: corresponding to clogging state (ultimate value)

σ: filtered particles

p: resin

a: air

s: suspension

initial: before compression

final: at the end of compression

ABBREVIATIONS

ALE: Arbitrary Lagrangian-Eulerian

CRTM: Compression Resin Transfer Molding

LSM: Level Set Method

PDE: Partial Differential Equations

RTM: Resin Transfer Molding

UMFPACK: Unsymmetric MultiFrontal PACKage

VARTM: Vacuum-Assisted Resin Transfer Molding

CHAPTER 1

INTRODUCTION

1.1 The Resin Transfer Molding Process

Resin Transfer Molding (RTM) is a liquid composite molding process that is used for the manufacturing of continuous fiber reinforced advanced composites. RTM has several advantages over other advanced composite manufacturing processes. Manufacturing of neat-shaped advanced composites with smooth surface finish and uniform wall thickness is enabled. This process offers relatively good control over the dimensions, shape and quality of the final composite product. The clamping force to keep the mold closed is relatively low compared to compression molding during manufacturing. Perhaps the most advantageous feature of RTM is the ability to produce complex shaped products in a repeatable manner, with relatively fast cycle times. High fiber loadings can be imparted, yielding strong mechanical behavior of the product [2-3]. However, the equipment and tooling cost of RTM is relatively high rather than other composite manufacturing techniques due to mold design and manufacturing process.

The advanced composite produced by the RTM process possess certain advantages in critical engineering applications like aerospace or automobile

applications. For example the light weight products produced by using RTM process contribute to decrease in fuel consumption. These composites yield high mechanical performance and structural strength. Furthermore, with the RTM process, more integrated parts can be produced, decreasing the amount of parts required for assembly [4].

In RTM advanced composites are manufactured with continuous fiber reinforcement. In such a composite, the continuous fiber reinforcement is the load carrying part of the composite and the fibers are embedded in a resin matrix that transfers the load between the fibers. In RTM of continuous fiber reinforcements the fabric layers or continuous strand mats are previously shaped in the final shape of the product and this final shape is called preform. Usually glass and carbon fibers are preferred as fiber reinforcements. The resins are thermosetting polymers such as epoxy used in advanced applications. RTM is mostly used for polymeric composite manufacturing but ceramic composite production is also possible. Figure 1.1 presents a variety of textile preforms and mats manufactured from various fiber materials that are available as the reinforcing components.

Figure 1.2 presents the processing steps of the RTM process. Layers of fibrous fabric are placed in a mold cavity, cut in the shape of the final product to be produced (fibrous preform). After the placement of the fibrous preform, the mold is closed. The injection of the resin into the mold cavity begins. The injection from the inlet gate is performed by constant flow rate or constant inlet gate pressure. Upon completion of the injection where the fibrous medium has been impregnated with the resin, the resin cures (hardens by the cross-linking of polymer molecules) and the final composite product is formed (Figure 1.2.f). In order to decrease the cure time, the impregnated fibrous preform is put into oven after the impregnated preform is waited for same time in the mold and it is called post-curing.

Since RTM is an expensive process due to molding equipment costs and it is time consuming, this process should be designed in terms of process parameters, such

as; mold configuration parameters: vent and inlet gate location, reinforcement parameters: volume of the fibers per mold cavity (fiber volume fraction), alignment and type of the reinforcement, permeability of the domain, flow parameters: material properties of the resin, inlet injection velocity or pressure. The determination of these process parameters with trial and error is not cost effective and it is time consuming. The numerical study of this process satisfies several advantages. In literature, the RTM process is studied from several points of view. There are several reliable computer simulations for resin impregnation. Simulations are performed mainly to provide effective filling of the preform with resin, to get knowledge on process parameters, and with the knowledge obtained, optimize the production [5]. Tan and Springer introduce a dynamic mold filling simulation program that some parameters can be changed during the simulation for 3-D mold configurations [6].

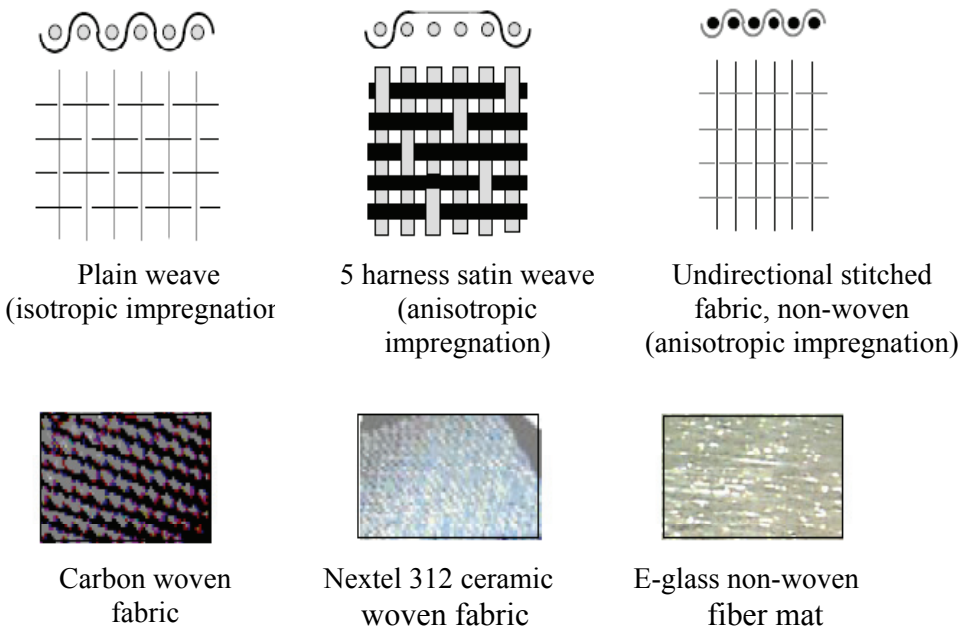

Figure 1.1. Examples of various preform weave configurations and reinforcing fabrics [7]

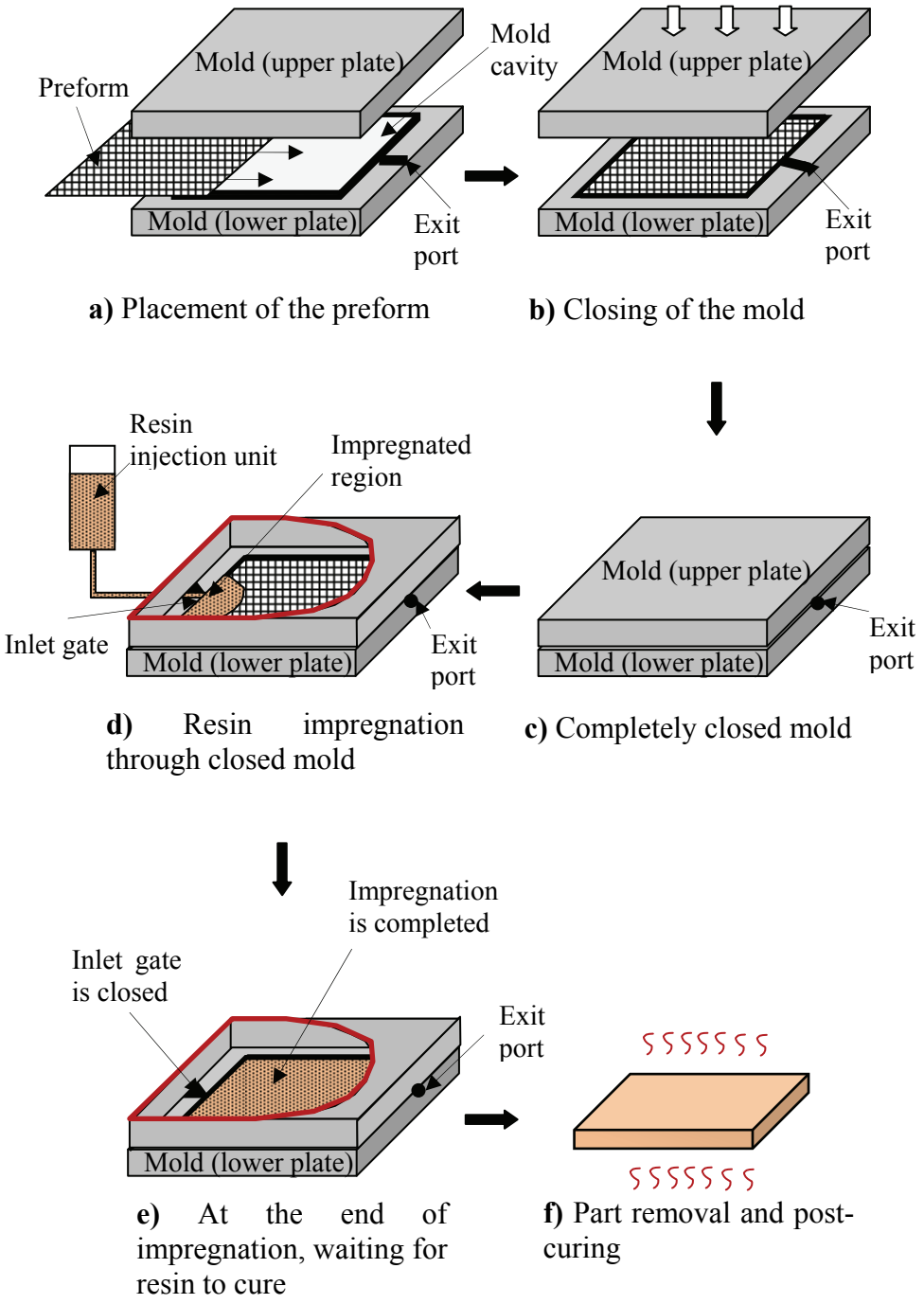

a) Placement of the preform

b) Closing of the mold

c) Completely closed mold

d) Resin impregnation through closed mold

e) At the end of impregnation, waiting for resin to cure

f) Part removal and post-curing

Figure 1.2. Description of Resin Transfer Molding process

Some of the RTM simulations include the experimental validation of the developed impregnation models. A mathematical model for the resin flow using Hele-Shaw flow assumption with planar dimensions is presented by Hieber and Shen [8]. The numerical results obtained for unbalanced mold configurations are validated with experimental results and observations are performed about short-shot, and pressure traces, which directly affects the quality of the final composite product. Anisotropy is an important issue in RTM which basically affects the flow characteristics of the resin. In anisotropic preform the permeability value is different in different flow directions and this difference should be controlled according to the design requirements. Bruschke and Advani's studies about mold filling through anisotropic fibrous medium includes the effects of anisotropy to the resin flow [9].

The control over process parameters is investigated to determine the optimum process. [10-14]. The selection of optimum parameters ease the application of the RTM process with minimum cost and maximum performance of the final product. The optimization study of Lin *et. al.* is performed for gate location for minimum fill time and domain permeability is changed to obtain minimum resin waste and minimum fill time [15]. Moreover, the deformation of the preform during the impregnation is investigated [16]. The observation of the deformation of the preform during impregnation is important in terms of quality of the final part. Deformation of the preform leads non-homogeneous part properties and mechanically weaker composites.

Bruschke and Advani developed a numerical model using finite element/control volume method to track the free surface (flow front) for irregular mold cavities, which is another important parameter of RTM [9]. Thus, the fibrous medium is enlarging with impregnation; so the portion of the impregnated region should be followed. The domain permeability values are determined experimentally and the numerical solutions are validated with experimental studies on regular geometries. Frederick and Phelan proposed a FAN (Flow Analysis Network) technique to

track the flow front and the process parameters are studied for complex mold configurations [17]. Bickerton *et. al.* performed series of experiments to show the effect of mold geometry on mold filling [18].

1.2 Description of Compression Resin Transfer Molding

Compression Resin Transfer Molding (CRTM) is a modification of the RTM process, which is used for manufacturing continuous fiber reinforced composites for structural applications. The potential advantage of CRTM over RTM is the improvement in the wettability of the fibers with the resin and better consolidation of the composite. Because the impregnation is performed through uncompressed preform, then the mold is closed, especially for larger product and high fiber loadings. The uncompressed preform has lower fiber volume fraction and higher permeability values which eases the injection phase. After the injection phase, the impregnation is completed with compression and final product with high fiber volume fraction and lower permeability can be obtained. In addition, CRTM is a candidate process for manufacturing large structural composites.

In advanced composite manufacturing the benefits introduced by RTM give rise to some restrictions for products with high fiber loadings and/or large dimensions. For instance, as the fiber content is increased the domain permeability decreases so the pressure increases for constant inlet flow rate, the fill time increases; for constant inlet pressure, which both leads an increase in cost of the process and in the risk of the gelatin of the resin [19]. For the production of parts with large dimensions the inlet pressure is to be higher which results in preform deformation. So, injection pressure should be increased for effective filling. However, increase in injection pressure leads to the deformation of the preform and a decrease in the product quality. At this point CRTM process which is the combination of RTM and Compression Molding is introduced to overcome the drawbacks of RTM and to have the advantages of RTM at the same time.

In literature, the description of the CRTM process shows some differences. In one description, after placement of the preform in the final shape the mold upper plate is not closed. Resin impregnation from the upper mold plate is throughout the gap between upper mold plate and preform. During the impregnation phase, the resin spreads out mostly through the gap rather than fibrous medium (preform). The resin impregnation through porous medium (fibrous preform) is achieved mainly during the compression phase [2, 4, 20-22]. In another CRTM variation, the resin is injected through uncompressed fibrous preform where it penetrates directly into the preform (not in the final shape) without a gap. The injection is then followed by compression [1, 23]. Figure 1.3 depicts the processing stages of the CRTM process. Injection phase of CRTM is quite similar to the conventional RTM process as described in the description of RTM. Fibrous preform which will be in the shape of the final product after the compression phase is placed to the mold cavity (Figure 1.3.a) and mold is closed partially contrary to conventional RTM process (Figure 1.3.b). In, RTM process mold is closed, and injection of the resin is performed while the fiber preform is compressed to the design (product) volume fraction. In CRTM, the resin is injected to the uncompressed fibrous preform as presented in Figure 1.3.c, in which the fiber volume fraction is less than the designed value. Thus injection phase can be achieved at low injection pressures and low fiber volume fractions. After sufficient amount of the neat resin is injected (Figure 1.3.d), the mold top plate begins to closed down compressing the partially filled preform, so that the resin inside can spread out the rest of the preform and wet the fibers uniformly and effectively, as shown in Figure 1.3.e. During the compression, the injection gate is closed so that there is no injection. The excessive resin may be bled out from the mold vents. Following the injection and the compression stages, the final part is obtained by curing of the resin and the part is removed from the mold cavity.

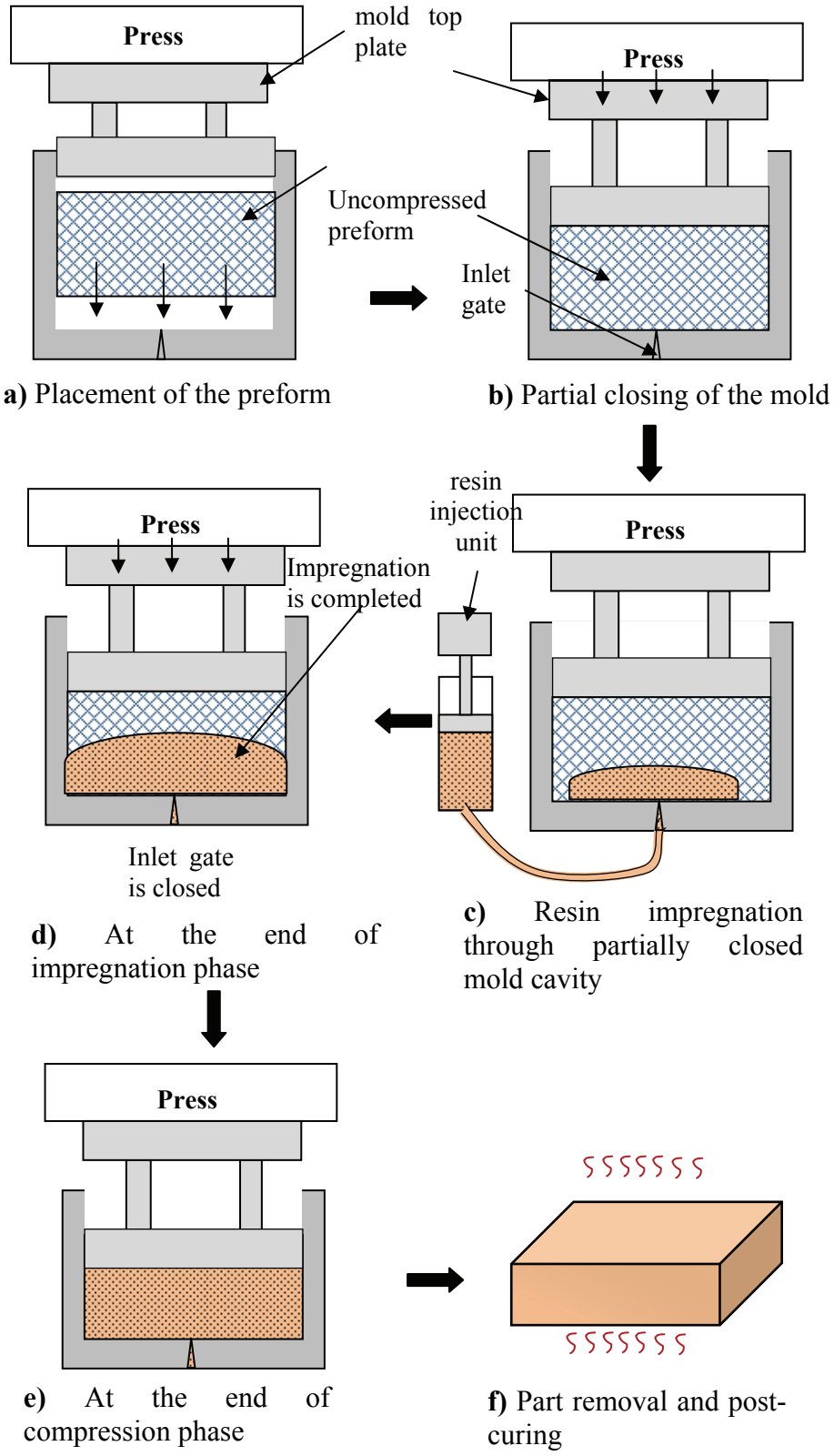

Figure 1.3. Injection and Compression Phases of CRTM

In literature, several studies on CRTM have been performed. Young and Chiu [24] stated that the flexural strength and modulus of composite materials produced by RTM and CRTM does not lead significant differences. However, as Brockmann and Michaeli pointed out, that with CRTM the pressure values during the injection phase of the process is reduced significantly rather than the values during the RTM process. [25]

Some experimental studies are performed regarding to injection and compression phases of CRTM. In the experimental study performed by Wirth and Gauvin, two different sets of experiments have been conducted [26]. These experiments corresponding to the two approaches to the CRTM process have been explained before. In these experiments, the pressure distributions during the process are measured and the effectiveness of the filling is investigated. In one set of experiments, the resin is injected into the gap between the preform and the mold plate, followed by the compression phase to impregnate the resin through the glass fiber preform. In this set, the final fiber volume fraction is considerably increased after the compression phase. In the second set of experiments, impregnation is performed through continuous strand glass fiber mat and both injection and compression phases occur simultaneously (with no gap space during injection). In this case, the fiber volume fraction is not changed significantly through the compression phase. The results of these experiments demonstrate the effectiveness of manufacturing high fiber loadings composites with relatively low pressure values with CRTM process. However, CRTM does not present a significant benefit at low fiber volume fractions.

Han *et. al.* offer a numerical solution for the neat resin flow and heat transfer in CRTM and perform experiments using a tub-shaped mold to show the agreement of the numerical solution with experimental results [27].

Buntain and Bickerton conducted experiments of RTM and CRTM. The main aim of their study is to observe the effect of elastic behavior of fiber reinforcements on clamping forces [23]. This study focuses of the forces due to tooling during RTM

and CRTM to monitor the effective process parameters that decreases the tooling cost and forces and increase the performance of the final product at the same time. The contributions of fluid and fiber forces are compared for two reinforcements with different compaction behavior and close permeability values. It is proposed by Somashekar *et. al.* that non-elastic behavior of fiber should be considered and the effects of stress relaxation, fluid lubrication and permanent deformation of the reinforcements is investigated and Buntain and Bickerton demonstrate the importance of these parameters with the numerical simulations [28].

Several numerical solutions are performed to express the effects of the process parameters of CRTM and evaluate the CRTM process [2, 4, 20-22]. Bhat *et. al* present the effect of non-dimensional parameters on the filling time and it increases as the compression and/or stiffness of the preform are increased [20]. Chang proposed that high compression speed and small initial gap increases the performance of the CRTM process [21]. Shojaei demonstrated that injection time and flow front progression is closely related with fiber type, fiber stacking sequence and the gap between the preform and mold plate, which ease the injection process [2]. Using the numerical solution developed by Shojaei the filling parameters such as; flow front progression, pressure distribution and clamping force can be evaluated [22]. In addition, the numerical results are compared with analytical solutions for regular shaped mold cavities. Simacek *et. al.*, investigated the mold filling simulations in CRTM for detailed automobile parts and the results are compared with comprehensive experiments [4]. Although it is stated that the numerical solution could not be validated by the researchers, the solutions were reasonable for the position of vent locations to prevent the short-shots.

The numerical study of Pham and Trochu is validated by both experimental study using the results of Wirth and Gauvin and by analytical solutions for one and two dimensional simple mold configurations [1]. That study explains the effect of

compression speed, injection pressure and closing/opening of injection gate during the compression phase of CRTM process.

1.3 Use of Particle-Fillers in Advanced Composites

In the continuous strive to improve material properties to match the ever increasing demands of technology; newer and innovative composite materials with higher performance are sought. The aim is to have final products with increased functionality and to obtain the designed final product.

A method for the improvement of the composites or change desired properties to a composite material can be accomplished by the addition of particle-fillers to the resin. The filler particles possess certain qualities that can change the overall properties of the composite part. The use of particle-fillers for composite materials are performed by the addition of the particle-fillers to the neat resin prior to injection for various purposes like adding different functionalities to the composite material. Nano- or micro particles within the composite are added to resin to give improved part toughness, improved thermal properties (e.g. fire resistance), electromagnetic shielding properties, self-healing properties, and reduce processing cost/time (in ceramic composites) [29-30].

Use of particle-fillers for RTM is performed by mixing particle-fillers and neat resin before the process and this suspension (particle-fillers and resin mixture) is injected from injection unit through the tight fibrous preform. As the suspension flows, the fibrous preform acts as a filter to the impregnating particle-filled resin suspension. Due to filler inclusion, the viscosity of the suspension (neat resin and particle-fillers) increases. Then, higher injection pressure is required for particle filled resin impregnation rather than neat resin. Moreover, during the injection of the suspension, particles distribute non-homogeneously in the part. Thus, non-homogeneous filler distribution results in non-homogeneous final product properties.

Using particle-filled resin for CRTM overcomes the drawbacks of particle-filled RTM process. Previously mixed particle-fillers and the neat resin mixture is injected through the uncompressed fibrous preform rather than tight preform in RTM process. Thus, the injection is performed at a lower fiber volume fraction than the designed value that leads several advantages over the particle-filled RTM process. Firstly, the injection pressure is lower and filtration effect of the fibrous preform is decreased. As the filtration decrease the particles retained in the resin can be distributed along the product, which is the filler distribution becomes homogenous. More homogenous filler distribution leads more homogenous properties of the final part. After the completion of the particle-filled resin injection at lower fiber volume fraction, the final value of the designed fiber volume fraction is reached at the end of compression phase. Consequently, use of particle-fillers for CRTM enables manufacturing of advanced composite products with complex geometries and high fiber loadings. Besides, the improvements and modifications offered by particle-filler addition is implemented to CRTM can be accomplished effectively, especially rather than implementation to RTM process.

The filtration of the particle-fillers has been investigated in several areas: water flow [31-32], oil well studies [33-34] or paper industry [35].

There are several studies on particle deposition. Jung and Tien investigated the dynamic behavior of filtration using a particle trajectory approach [36]. Following the streamline of the suspension flow the effect of deposition on particle filtration is shown. However, this study does not consider the changes of other process parameters with filtration. Another method is using statistical models, in which the fibrous preform is considered to have infinite sets of pores and a network of passage ways for the particle-fillers [37-38]. Additionally, using network model from the analogy between Darcy flow and an electric circuit Chohra *et. al.* model filtration as a dual-scale porous media [39-40]. These models estimate the concentration distribution along the fibrous medium and experimental data are generated for the validation of the model. Li and Park use Effective Medium

Approximation (EMA) to predict the permeability and filtration rate in the porous medium and analytical solutions are developed for various particle sizes and fibrous medium characteristics [41]. The effects of process parameters are investigated.

Considering the particle-to-fibrous medium, particle-to-fluid and particle-to-particle interaction forces in a filtering medium, Nazarboland *et. al.* developed a numerical solution to observe the effect of particle size and shape on the filtration[42]. Composite parts with particle-fillers are generally manufactured by RTM and VARTM (Vacuum-Assisted Resin Transfer Molding-a variation of RTM). In these processes particle-filled resin suspension is injected through fibrous preform. Besides issues for the neat resin impregnation, the clogging of the particles in the fibrous medium is an issue for particle-filled resin impregnation. The particle deposition as the suspension flows through porous medium has several process parameters that need to be considered: amount of deposited particle-fillers, concentration of the particle-fillers in the suspension, flow rate of the suspension, distribution of the particles in the final part, the characteristics of the fibrous medium and size and shape of the particle-fillers [29]. Moreover for the manufacturing of composite parts with particle-filler, two particle deposition mechanisms is presented by Nordlund *et. al.* [29]: "filtration during the fiber bundle impregnation and filtration induced by stationary flow through fiber bundles" and suggestions for the manufacturing of homogenous composite products are presented. Erdal *et. al* presents a mathematical model based on conservation equation and empirical relations to model particle-filled impregnation of RTM and observe the effect of process parameters [7]. Then, Lefevre *et. al.* proposed a numerical solution based on Erdal *et. al* study and focus more on particle retention [43-44],[7]. These results are compared with experimental data.

All above presented studies involve either particle filtration in RTM or its variants, or neat resin impregnation in CRTM. To date, there is no study in the literature regarding to the use of particle-fillers for CRTM process.

1.4 Need for Modeling in Developing Advanced Composites

RTM and CRTM offer several advantages over many other composite manufacturing techniques, i.e. good surface finish, better dimensional accuracy, relatively fast cycle times, products with high fiber volume fractions and geometrically complex parts. Both processes involve a large number of processing variables. A successful operation must yield near-net shape fabrication of the composite with the desired microstructure, while satisfying the performance, reliability and cost objectives. To achieve this, several processing issues need to be addressed. A crucial factor for achievement of defect-free, homogeneous microstructure is the assurance of void-free impregnation for RTM and impregnation and compression for CRTM. Formation of voids inhibits the structural integrity of the composite as well as the surface finish quality. Factors affecting the progression of the flow front such as fiber wetting, complex flow patterns at micro-level due to three-dimensionality of the fiber geometry and permeability of the fibrous medium need to be taken into account during process the design. The geometric complexity of the part must be considered during preform selection for the processability as well as the structural design performance objectives.

High fiber volume fraction in the end-product is a desirable feature that has implications in both preform design and impregnation. As the fiber content rises, the injection pressure increases requiring costly injection apparatus and tooling. The fiber-resin adhesion should be strong enough to prevent de-lamination but must also accommodate fiber de-bonding and pull-out under high loadings for toughening mechanism. From a processing cost perspective, the cycle times must

be relatively short with acceptable surface finish and repeatability. The tool design and impregnation conditions must accommodate the complex geometries ranging from 3-D structures to inserts. To provide science base for intelligent processing of advanced composite systems, a shift from costly “trial - and - error” type processing to development of “predict - and - verify” type design tools must take place, enabling reliable modeling and optimization prior to processing.

Computer simulations can be used for optimizing mold features such as location of injection gates and venting ports, as well as for eliminating dry spots, calculating and reducing fill times, determining pressure distribution and the clamping force, particle concentration distribution, filtration rate. Mold filling simulations can also yield information about optimum processing parameters such as resin optimum injection pressure and flow rate.

1.5 Scope and the Organization of the Thesis Study

In this study, particle-filled impregnation and compression phases of the Compression Resin Transfer Molding process are investigated in order to understand how various process parameters (injection velocity, inlet particle concentration, fiber preform permeability, mold closing speed, etc.) interact during impregnation and compression to evaluate the performance of the process. In this study, the mathematical model developed by Erdal [7] is used for impregnation and a mathematical model for compression phases of CRTM is developed. Mathematical models for impregnation and compression phases are solved numerically by using commercial software. The model is based on porous flow through the fibrous media with negligence of inertial effects, i.e. a Darcy flow. The particle distribution is modeled by a filtration kinetics equation. Darcy law and the kinetics equation are coupled with mass conservation equations to complete the model.

In the first chapter of this thesis study (the current chapter), the descriptions of the RTM and the CRTM processes have been presented. The background leading to the need for the current study has been explained.

In Chapter 2, mathematical models that are developed for modeling the impregnation and the compression phases of the particle-filled CRTM stage are presented.

In Chapter 3, the numerical implementation of the mathematical models that are developed in the second chapter is presented. The commercial software COMSOL Multiphysics® that is used in the numerical solution is explained. The application modes of the commercial software to impose the governing equations and constitutive relations regarding this study are explained. Details of the implementation are given.

In Chapter 4, simulation results of the presented CRTM model are given. In addition, some model validations are done by comparing the results with analytical solutions and experimental data from the literature. The process is investigated in terms of pressure distribution and total particle distribution for RTM and CRTM processes and the results are compared. Moreover, an analysis to observe the effects of process parameters is conducted to express the process condition that makes the CRTM process favorable.

Finally, Chapter 5 presents the conclusions and future work of this study.

CHAPTER 2

THE MATHEMATICAL MODEL FOR COMPRESSION RESIN TRANSFER MOLDING OF PARTICLE-FILLED COMPOSITES

As described in the first chapter the CRTM has two phases: Injection and compression. The processing steps for the injection phase are same with RTM. In this chapter mathematical modeling for injection and compression phases are given in detail. Then, governing equations and constitutive relations are expressed for both phases with the boundary and initial conditions for the solution.

2.1 Mathematical Modeling of Resin Transfer Molding (Injection Phase) with Particle-Fillers

2.1.1 Flow of Particle-Filled Resin through Porous Medium

Modeling of resin through porous medium is based on Darcy's Law which simply relates the velocity of the fluid to the pressure drop through a proportionality factor of medium permeability over the viscosity of the fluid [22, 30]. For incompressible flows during the filling stage, the problem can be treated as a quasi-steady Darcy flow through fibrous (porous) medium and the Darcy flow can be generalized to multi-dimensional flow as:

$$\vec{V} = -\frac{1}{\mu}(K \cdot \nabla p) \tag{2.1}$$

where $\vec{V}$ is the velocity vector, μ is the particle-filled resin viscosity, p is the pressure and K is the fibrous (porous) medium permeability tensor, which is given by,

$$\underline{\underline{K}} = \begin{bmatrix} K_{xx} & K_{xy} & K_{xz} \\ K_{xy} & K_{yy} & K_{zy} \\ K_{xz} & K_{yz} & K_{zz} \end{bmatrix} \tag{2.2}$$

The diagonal elements are permeability values along the coordinate axes and the rest relate the effect of pressure gradients in transverse directions to flow. If the coordinate axes are rotated appropriately, they coincide with the principle directions of the porous medium (the fibrous preform). In the current modeling, the coordinate axes are chosen to coincide with the principle directions of the permeability tensor, rendering the permeability tensor a diagonal matrix.

The particle-filled resin mixture is treated as a homogeneous fluid with continuous and averaged properties. The velocity term, $\vec{V}$ in equation (2.1) is the bulk velocity that would be attained in the absence of the preform and called superficial velocity. The actual suspension velocity (interstitial velocity) is the increased velocity through the fibrous preform due to existence of solid phase (the porous medium) and it is expressed as

$$\vec{V}' = \frac{\vec{V}}{1 - \upsilon_f} = \frac{\vec{V}}{\varepsilon} \tag{2.3}$$

where υ_f is the total solid (fiber and filtered particles) volume fraction, and ε is the porosity of fibrous medium, $(1 - \upsilon_f)$.

2.1.2 Conservation Equations

An infinitesimal control volume in the flow domain (through the fibrous preform in the mold cavity) is presented in Figure 2.1 where the incoming suspension flow passes through a unit volume element. Particle-fillers in the process are classified into two groups: Those that are carried along with the moving resin and those that have been stuck within the fibrous preform (filtered). This is an artificial distinction (not a different species), only for the purpose of mathematical modeling. The conservation laws for the particle filled resin flow through a fibrous medium are investigated for three different species: Particles in the resin, the neat resin and filtered particles.

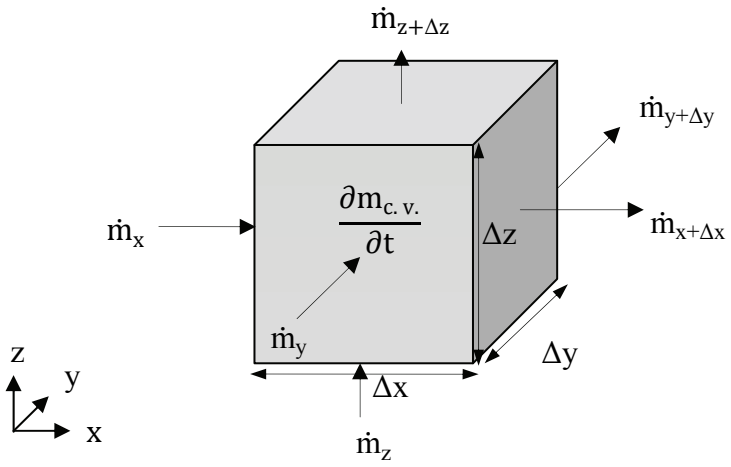

Figure 2.1. Flow domain control volume for the conservation equations during impregnation

Particles retained in the resin: Conservation equation (equation (2.4)) over the control volume in Figure 2.1 consists of inflow and outflow mass rate, rate of change of mass in the control volume (stored mass) and mass generation rate for particles in the resin. Mass generation rate for particles in the resin represents the

change (reduction or increase) in the content of filler particles in the resin due to filtration. Here, the "mass generation" relates to the increase/decrease in the particles retained in the polymer which is the same amount of decrease/increase in filtered particles.

$$\dot{m}_{in} - \dot{m}_{out} + \dot{m}_{generated,c} = \dot{m}_{stored} \tag{2.4}$$

The mass flux across the boundaries can be expressed as

$$\dot{m} = \rho_c V' A_c \tag{2.5}$$

where ρ_c is the density of the particle-fillers, V' is the actual flow velocity, and A_c is the cross-sectional area that particle-fillers pass through.

The rate of change of mass in the control volume (stored mass) is expressed as

$$\dot{m}_{stored} = \rho_c[\forall_c|_{t+\Delta t} - \forall_c|_t] \tag{2.6}$$

where $[\forall_c|_{t+\Delta t} - \forall_c|_t]$ is the rate of change of the volume of the particles retained in the unit control element.

Integrating equation (2.4) over unit time, Δt results in

$$\begin{aligned}&\left[\rho_c u_c' A_c \Delta t|_x + \rho_c v_c' A_c \Delta t|_y + \rho_c w_c' A_c \Delta t|_z\right] \\ &\quad - \left[\rho_c u_c' A_c \Delta t|_{x+\Delta x} + \rho_c v_c' A_c \Delta t|_{y+\Delta y} + \rho_c w_c' A_c \Delta t|_{z+\Delta z}\right] \\ &\quad + \dot{m}_{generated,c} \Delta t = \rho_c[\forall_c|_{t+\Delta t} - \forall_c|_t]\end{aligned} \tag{2.7}$$

The volume occupied by the particles those in the resin is

$$\forall_c = \forall_0 . \varepsilon C \tag{2.8}$$

where $\forall_0$ is the volume of the control volume element and C is the concentration of the particles in the impregnated suspension (volume of particles in the suspension per volume of the suspension). The net area which particles in the resin pass through is

$$A_c = A_0 . \varepsilon C \tag{2.9}$$

where A_0 represents the area of the volume element normal to the incoming flow.

Putting equation (2.8) and (2.9) into equation (2.7) yields

$$\begin{aligned}&\left[\rho_c u_c' A_0 \varepsilon C \Delta t|_x + \rho_c v_c' A_0 \varepsilon C \Delta t|_y + \rho_c w_c' A_0 \varepsilon C \Delta t|_z\right] \\ &\quad - \left[\rho_c u_c' A_0 \varepsilon C \Delta t|_{x+\Delta x} + \rho_c v_c' A_0 \varepsilon C \Delta t|_{y+\Delta y}\right. \\ &\quad \left. + \rho_c w_c' A_0 \varepsilon C \Delta t|_{z+\Delta z}\right] + \dot{m}_{generated,c} \Delta t \\ &\quad = \rho_c [\forall_0 \varepsilon C\,|_{t+\Delta t} - \forall_0 \varepsilon C|_t]\end{aligned} \tag{2.10}$$

Rearranging the equation (2.10) and dividing the equation by "$\rho_c \Delta t \forall_0$" yields

$$\begin{aligned}&\frac{A_0}{\forall_0}\left\{[u_c' \varepsilon C|_x - u_c' \varepsilon C|_{x+\Delta x}] + \left[v_c' \varepsilon C|_y - v_c' \varepsilon C|_{y+\Delta y}\right]\right. \\ &\quad \left. + [w_c' \varepsilon C|_z - w_c' \varepsilon C|_{z+\Delta z}]\right\} + \frac{\dot{m}_{generated,c}}{\rho_c \forall_0} \\ &\quad = \frac{[\varepsilon C\,|_{t+\Delta t} - \varepsilon C|_t]}{\Delta t}\end{aligned} \tag{2.11}$$

The frontal areas along the x, y and z directions can be expressed as

$$A_0|_x = \Delta y \Delta z$$

$$A_0|_y = \Delta x \Delta z \tag{2.12}$$

$$A_0|_z = \Delta x \Delta y$$

The volume of the control volume, presented in Figure 2.1, is

$$\forall_0 = \Delta x \Delta y \Delta z \tag{2.13}$$

The unit volume element does not deform during impregnation, Δx, Δy and Δz are constant. Using equations (2.12) and (2.13), equation (2.11) is simplified as

$$\frac{[u_c'\varepsilon C|_x - u_c'\varepsilon C|_{x+\Delta x}]}{\Delta x} + \frac{[v_c'\varepsilon C|_x - v_c'\varepsilon C|_{x+\Delta x}]}{\Delta y} + \frac{[w_c'\varepsilon C|_x - w_c'\varepsilon C|_{x+\Delta x}]}{\Delta z} + \frac{\dot{m}_{generated,c}}{\rho_c \forall_0} = \frac{[\varepsilon C\,|_{t+\Delta t} - \varepsilon C|_t]}{\Delta t} \tag{2.14}$$

As $\Delta t \to 0, \Delta x \to 0, \Delta y \to 0$ and $\Delta z \to 0$ above equation becomes

$$-\left[\frac{\partial(\varepsilon C u_c')}{\partial x} + \frac{\partial(\varepsilon C v_c')}{\partial y} + \frac{\partial(\varepsilon C w_c')}{\partial z}\right] + \frac{\dot{m}_{generated,c}}{\rho_c \forall_0} = \lim_{\Delta t \to 0}\left[\frac{[\varepsilon C\,|_{t+\Delta t} - \varepsilon C)|_t]}{\Delta t}\right] \tag{2.15}$$

As $\Delta t \to 0$, the right hand side of equation (2.15) for non-deformable control volume yields to

$$\lim_{\Delta t \to 0}\left[\frac{[\varepsilon C\,|_{t+\Delta t} - \varepsilon C|_t]}{\Delta t}\right] = \frac{\partial(\varepsilon C)}{\partial t} \tag{2.16}$$

Thus, equation (2.15) with equation (2.16) gives

$$-\left[\frac{\partial(\varepsilon C u_c')}{\partial x}+\frac{\partial(\varepsilon C v_c')}{\partial y}+\frac{\partial(\varepsilon C w_c')}{\partial z}\right]+\frac{\dot{m}_{generated,c}}{\rho_c \forall_0}=\frac{\partial(\varepsilon C)}{\partial t} \tag{2.17}$$

Thus the continuity equation for the particles moving with the resin, during injection of suspension is derived as

$$\frac{\partial[\varepsilon C]}{\partial t}+\nabla\cdot\left\{\varepsilon C\vec{V}_c'\right\}=\frac{\dot{m}_{generated,c}}{\forall_0 \rho_c} \tag{2.18}$$

Neat Resin: For the mass balance of the neat resin, there is no artificially introduced generation term. Then, continuity equation can be expressed as

$$\dot{m}_{in}-\dot{m}_{out}=\dot{m}_{stored} \tag{2.19}$$

Expressing the mass flux across the boundaries as

$$\dot{m}=\rho_p V' A_p \tag{2.20}$$

where ρ_p is the density of the neat resin, V' is the actual flow velocity, and A_p is the cross-sectional area that neat resin pass through.

The rate of change of mass of neat resin in the control volume (stored mass) is expressed as

$$\dot{m}_{stored}=\rho_p\left[\forall_p\big|_{t+\Delta t}-\forall_p\big|_t\right] \tag{2.21}$$

where $\left[\forall_p\big|_{t+\Delta t}-\forall_p\big|_t\right]$ is the rate of change of the volume of the neat resin in the unit control element.

Integration of equation (2.19) over unit time, Δt gives

$$\left[\rho_p u'_p A_p \Delta t\big|_x + \rho_p v'_p A_p \Delta t\big|_y + \rho_p w'_p A_p \Delta t\big|_z\right] - \left[\rho_p u'_p A_p \Delta t\big|_{x+\Delta x} + \rho_p v'_p A_p \Delta t\big|_{y+\Delta y} + \rho_p w'_p A_p \Delta t\big|_{z+\Delta z}\right] = \rho_p \left[\forall_p\big|_{t+\Delta t} - \forall_p\big|_t\right] \quad (2.22)$$

The volume of the neat resin in the control volume is

$$\forall_p = \forall_0 . \varepsilon(1 - C) \quad (2.23)$$

The net area through which neat resin flows is

$$A_p = A_0 . \varepsilon(1 - C) \quad (2.24)$$

Putting (2.23) and (2.24) into equation (2.22)

$$\left[\rho_p u'_p A_0 \varepsilon(1 - C)\Delta t\big|_x + \rho_p v'_p A_0 \varepsilon(1 - C)\Delta t\big|_y + \rho_p w'_p A_0 \varepsilon(1 - C)\Delta t\big|_z\right] - \left[\rho_p u'_p A_0 \varepsilon(1 - C)\Delta t\big|_{x+\Delta x} + \rho_p v'_p A_0 \varepsilon(1 - C)\Delta t\big|_{y+\Delta y} + \rho_p w'_p A_0 \varepsilon(1 - C)\Delta t\big|_{z+\Delta z}\right] = \rho_p[\forall_0 \varepsilon(1 - C)|_{t+\Delta t} - \forall_0 \varepsilon(1 - C)|_t] \quad (2.25)$$

Rearranging the equation (2.25) and dividing the equation by "$\rho_p \Delta t \forall_0$" yields

$$\frac{A_0}{\forall_0}\Big\{\Big[u_p'\varepsilon(1-C)\Big|_x - u_p'\varepsilon(1-C)\Big|_{x+\Delta x}\Big] + \Big[v_p'\varepsilon(1-C)\Big|_y - v_p'\varepsilon(1-C)\Big|_{y+\Delta y}\Big] + \Big[w_p'\varepsilon(1-C)\Big|_z - w_p'\varepsilon(1-C)\Big|_{z+\Delta z}\Big]\Big\} = \frac{[\varepsilon(1-C)|_{t+\Delta t} - \varepsilon(1-C)|_t]}{\Delta t\forall_0} \tag{2.26}$$

The simplified equation of equation (2.26) is obtained via equations (2.12) and (2.13) as

$$\frac{\Big[u_p'\varepsilon(1-C)\Big|_x - u_p'\varepsilon(1-C)\Big|_{x+\Delta x}\Big]}{\Delta x} + \frac{\Big[v_p'\varepsilon(1-C)\Big|_x - v_p'\varepsilon(1-C)\Big|_{x+\Delta x}\Big]}{\Delta y} + \frac{\Big[w_p'\varepsilon(1-C)\Big|_x - w_p'\varepsilon(1-C)\Big|_{x+\Delta x}\Big]}{\Delta z} = \frac{[\varepsilon(1-C)|_{t+\Delta t} - \varepsilon(1-C)|_t]}{\Delta t} \tag{2.27}$$

As $\Delta t \to 0, \Delta x \to 0, \Delta y \to 0$ and $\Delta z \to 0$ equation (2.27) is

$$-\left[\frac{\partial(\varepsilon(1-C)u_p')}{\partial x} + \frac{\partial(\varepsilon(1-C)v_p'))}{\partial y} + \frac{\partial(\varepsilon(1-C)w_p'))}{\partial z}\right] = \lim_{\Delta t\to 0,}\left[\frac{[\varepsilon(1-C)\,|_{t+\Delta t} - \varepsilon(1-C)|_t]}{\Delta t}\right] \tag{2.28}$$

The right hand side of the equation (2.28) can be expressed for non-deformable control volume as

$$\lim_{\Delta t\to 0,}\left[\frac{[\varepsilon(1-C)\,|_{t+\Delta t} - \varepsilon(1-C)|_t]}{\Delta t}\right] = \frac{\partial\big(\varepsilon(1-C)\big)}{\partial t} \tag{2.29}$$

Then, equation (2.28) using equation (2.29) gives

$$-\left[\frac{\partial(\varepsilon(1-C)u_p')}{\partial x}+\frac{\partial(\varepsilon(1-C)v_p'))}{\partial y}+\frac{\partial(\varepsilon(1-C)w_p'))}{\partial z}\right]=\frac{\partial\left(\varepsilon(1-C)\right)}{\partial t} \quad (2.30)$$

Thus, the continuity equation for the polymer resin, during injection of suspension through the inlet mold gate

$$\frac{\partial[\varepsilon(1\text{-}C)]}{\partial t}+\nabla\cdot\left\{\vec{V}_p'\varepsilon(1-C)\right\}=0 \quad (2.31)$$

Filtered Particles: In the control volume, the filtered particles are stuck to the preform hence there is no influx or out-flux of the filtered particles. The rate of change of filtered particles in a given volume is only dependent on the amount of filtration, which is represented by the artificial change of mass. Then, the mass conservation for filtered particles is

$$\dot{m}_{generated,\sigma}=\dot{m}_{stored,\sigma} \quad (2.32)$$

The rate of change of mass of filtered particles in the control volume (stored mass) is expressed as

$$\dot{m}_{stored}=\rho_\sigma[\forall_\sigma|_{t+\Delta t}-\forall_\sigma|_t] \quad (2.33)$$

where ρ_σ is the density of the filtered particles and $[\forall_\sigma|_{t+\Delta t}-\forall_\sigma|_t]$ is the rate of change of the volume of the filtered particles in the unit control element.

Integration of equation (2.32) over unit time, Δt gives

$$\dot{m}_{generated,\sigma}\Delta t=\rho_\sigma[\forall_\sigma|_{t+\Delta t}-\forall_\sigma|_t] \quad (2.34)$$

Volume of the filtered particles

$$\forall_\sigma = \forall_0 \sigma \tag{2.35}$$

where σ is the specific particle deposit, that is the volume of filtered particles per volume of the mold cavity.

Using equation (2.35) and dividing the equation (2.34) by '$\rho_\sigma \Delta t \forall_0$' gives

$$\frac{\dot{m}_{generated,\sigma}}{\rho_\sigma \forall_0} = \frac{[\sigma|_{t+\Delta t} - \sigma|_t]}{\Delta t} \tag{2.36}$$

As $\Delta t \to 0$, equation (2.36) is reduced to

$$\frac{\dot{m}_{generated,\sigma}}{\rho_\sigma \forall_0} = \lim_{\Delta t \to 0,} \left[\frac{[(\sigma)|_{t+\Delta t} - (\sigma)|_t]}{\Delta t}\right] \tag{2.37}$$

Thus, the continuity equation for the filtered particles during injection of suspension through the mold gate can be expressed as

$$\frac{\dot{m}_{generated,\sigma}}{\rho_\sigma \forall_0} = \frac{\partial(\sigma)}{\partial t} \tag{2.38}$$

From continuity, the generation term for filtered particles and the generation term for the particles retained in the resin must be equal to each other with a sign change. This relation can be expressed as

$$\dot{m}_{generated,\sigma} = -\dot{m}_{generated,c} \tag{2.39}$$

Another point to be considered is that filtered particles are the same particles that are in the polymer, therefore

$$\rho_\sigma = \rho_c \tag{2.40}$$

The fiber volume fraction is the ratio of the volume of the fibers to the volume of the mold cavity. Porosity indicates the available space in the mold cavity through which the suspension flow takes place; it is defined as the ratio of the volume of the available space to the volume of mold cavity.

As the particle filled resin impregnates the fibrous preform, filtered particles alter the unfiltered (initial) domain porosity, ε_0 and unfiltered (initial) fiber volume fraction, v_{f0}. Relations between fiber volume fraction and specific particle deposit; and porosity and specific particle deposit are

$$v_f = v_{f0} + \sigma \tag{2.41}$$

$$\varepsilon = \varepsilon_0 - \sigma \tag{2.42}$$

In equation (2.42), porosity of the flow domain at any time instant is related to initial porosity of the flow domain and specific particle deposit which changes with time. Taking the derivative with respective to time of equation (2.42) and noting that initial values are constant

$$\frac{\partial \varepsilon}{\partial t} = -\frac{\partial \sigma}{\partial t} \tag{2.43}$$

Equation (2.38) with equations (2.39) and (2.40) can be written as:

$$-\frac{\dot{m}_{generated,c}}{\rho_c \forall_0} = \frac{\partial(\sigma)}{\partial t} \tag{2.44}$$

Combining equation (2.18) with equation (2.44) will lead to the concentration conservation equation

$$\frac{\partial[\varepsilon C]}{\partial t} + \nabla \cdot \{\vec{V}_c' \varepsilon C\} = -\frac{\partial(\sigma)}{\partial t} \tag{2.45}$$

From equation (2.43) into the equation (2.45) yields

$$\frac{\partial[\varepsilon C]}{\partial t}+\nabla\cdot\left\{\vec{V}_c'\varepsilon C\right\}=\frac{\partial(\varepsilon)}{\partial t} \tag{2.46}$$

Arranging the equation (2.46) gives:

$$-\frac{\partial[\varepsilon(1\text{-}C)]}{\partial t}+\nabla\cdot\left\{\vec{V}_c'\varepsilon C\right\}=0 \tag{2.47}$$

Using equation (2.31) in equation (2.47) yields:

$$\nabla\cdot\left\{\vec{V}_p'\varepsilon(1-C)\right\}+\nabla\cdot\left\{\vec{V}_c'\varepsilon C\right\}=0 \tag{2.48}$$

The relative velocity between the particles retained in the resin and the resin is negligible [7], i.e. $\vec{V}_p'=\vec{V}_c'$. The concentration conservation equation takes the final form:

$$\nabla\cdot\left\{\vec{V}_p'\varepsilon\right\}=0 \tag{2.49}$$

Since all velocities are the same (resin and the particles), the subscript of the velocity terms can be dropped:

$$\nabla\cdot\left\{\vec{V}'\varepsilon\right\}=0 \tag{2.50}$$

$\vec{V}'$ is the actual (interstitial) velocity. Using the relation between superficial velocity, $\vec{V}$ and actual velocity, $\vec{V}'$ from equation (2.3) , the final form of continuity equation for neat resin is obtained as:

$$\nabla\cdot\vec{V}=0 \tag{2.51}$$

2.1.3 Filtration Kinetics

During the particle-filled resin flow, particle filtration rate per length of the flow is stated to be proportional to the volumetric flux of the suspension by an amount of filtration coefficient, α [45-46]:

$$\frac{\partial \sigma}{\partial t} = \alpha VC \tag{2.52}$$

For the purpose of modeling, as the particles are filtered, filtrates are assumed to deposit evenly on the inner walls of the capillary that the suspension flows, as shown in Figure 2.2. As the flow area through which the suspension flows is clogged by the particles, the porosity of the fibrous medium decreases. So, the actual velocity of the suspension increases with increasing particle deposit according to equation (2.3). Filtration does not continue indefinitely. After a while some of the filtered particles may be introduced back to the flow due to shearing.

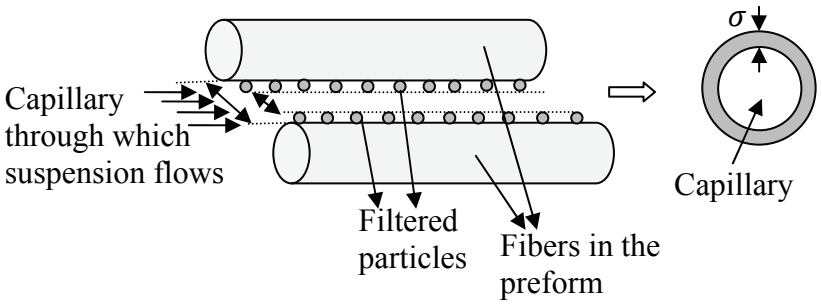

Figure 2.2. Filtration through fibrous preform

Then, equation (2.52) is modified as

$$\frac{\partial \sigma}{\partial t} = \alpha V C - \beta \sigma \tag{2.53}$$

where β indicates the amount of regained particles and it is called the detachment coefficient. As the particles deposit to the preform and filtration continues, the medium will eventually reach a saturation point so that the filtration rate will become zero. Defining the specific deposit value at the instant when filtration rate becomes zero as σ_u, equation (2.53) equals to zero:

$$\frac{\partial \sigma}{\partial t} = \alpha V C - \beta \sigma_u = 0 \tag{2.54}$$

Then, the detachment coefficient β can be expressed as:

$$\beta = \frac{\alpha V C}{\sigma_u} \tag{2.55}$$

Thereafter, filtration kinetics equation is obtained as [7]:

$$\frac{\partial \sigma}{\partial t} = \alpha V C \left(1 - \frac{\sigma}{\sigma_u}\right) \tag{2.56}$$

The ultimate specific deposit σ_u is an empirical constant and its value must be less than the initial porosity, ε_0 of the fibrous medium.

2.1.4 Filtration Coefficient

The filtration coefficient α is an empirical parameter related to the particle deposit. In literature there are mainly two mechanisms regarding to particle filtration: transportation of the particle-fillers and surface chemistry.

Several studies [47-48] indicate that suspension flows where the surface interactions are kept in minimum degree, in terms of transportation the filtration coefficient is found to be constant at the initial stage of the filtration. The changes at the initial stages arise from surface chemistry. However, this study focuses on the effect of changes of the geometry of the fibers in the preform (and pores in the fibrous medium) with filtration and the surface chemistry is completely neglected.

In this manner, the approach for the formulation of the filtration coefficient set out by Erdal [7] is used.

Erdal [7] assumed that α varies with respect to the changing specific deposit.

$$\alpha = \alpha_0 f(\sigma) \tag{2.57}$$

where α_0 is the initial coefficient for the undeposited preform. The filter coefficient α is assumed to increase proportionally to the specific surface of the preform pores on which particles are deposited; this relation is expressed by,

$$\alpha = \alpha_0 \left(\frac{S}{S_0}\right) \tag{2.58}$$

where S is the specific surface area and S_0 is the initial specific surface area without particle deposition. The increasing local velocities due to clogging of the pores are likely to promote detachment of the filtered particles back into the flow, which retards filtration. Therefore, α becomes inversely proportional to the local velocity. However, the effect of increasing local velocities is implicitly implemented in equation (2.56).

In the absence of particles, the permeability of the flow domain is dependent largely on the preform architecture (fiber diameter, weave, fiber volume fraction, etc.) and, consequently, the specific surface area of the medium. This relation is often expressed by the Kozeny–Karman relation as,

$$K \propto \frac{\varepsilon^3}{S^2(1-\varepsilon)^2} \tag{2.59}$$

which assumes that the permeability K is inversely proportional to the specific surface area and is directly proportional to the porosity, ε of the medium. Thus, α is expressed in terms of K and ε as by Erdal [7] as:

$$\alpha = \alpha_0 \left[\left(\frac{K}{K_0} \right)^{-1/2} \left(\frac{\varepsilon}{\varepsilon_0} \right)^{3/2} \right]^{a_1} \tag{2.60}$$

where a_1 is a positive model constant, K_0 is unfiltered domain permeability and ε_0 is unfiltered domain porosity.

2.1.5 Domain Permeability

Since filtration of the particles leads to a decrease in the area of the suspension flow, permeability of the porous medium is affected by the clogging. As a result, the specific surface area of the pores, denoted by S, changes locally and the porosity of the medium, ε decreases, as shown in Figure 2.2. In order to determine the specific surface area, the geometry of the fibrous medium should be considered. For the purpose of modeling, the pores of the fibrous preform are assumed to be composed of cylindrical grains and capillary, and the fiber diameter in the preform is assumed to be much larger than particle-filler diameter, as shown in Figure 2.2. The particle-fillers deposited onto these fibers are assumed to be distributed evenly and create a uniform layer around the fiber. In addition, the pores of the fibrous preform are assumed to be composed of cylindrical fiber and capillaries that the suspension flows formed between the fibers.

In order to obtain a relation for the domain permeability, the Kozeny-Karman equation is taken as the basis of the formulation. First, the specific surface areas of the pores are the combination the surface of the fibers in the preform and the

surface of the particles attached to the fibers. The grain model assumes that the particles are deposited uniformly around fibers, thus increasing the grain size. In the capillary model, the capillary pores are formed by the surrounding fibers, and the particle deposit on the fiber surface in the capillary narrows the flow passage. The specific surface area of the pores through which the suspension flows is related to the porosity. The permeability is expressed as a function of the original (unfiltered domain) permeability, changing as the specific surface area changes due to the filtration.

With the above definitions Erdal [7] proposed a permeability model as:

$$K = K_0 \left[\left(\frac{\varepsilon}{\varepsilon_0} \right) \left(\frac{1-\varepsilon}{1-\varepsilon_0} \right)^{-2} \right]^{a_2} \tag{2.61}$$

where a_2 is a model parameter which changes with the process conditions and properties of the fibrous preform. K_0 is the initial domain (unfiltered preform) permeability.

2.1.6 Resin Viscosity

Suspension viscosity is dependent to the particle loading in the medium. The following relation presented by Erdal [7] expresses the relation between suspension viscosity and concentration as,

$$\mu = \mu_o \left(1 - \frac{C}{A} \right)^{-2} \tag{2.62}$$

where μ_o is the neat resin viscosity and A, is an empirical constant. The above relation is defined at constant shear rates. In this study, resin is assumed to be a Newtonian fluid because the effect of shear dependence is small due to very low

viscosity of the neat resin. This relation is used as the viscosity term in Darcy's Law. The change of the viscosity with temperature and time is neglected.

The governing equations for the fiber impregnation in the RTM are continuity equation for the neat resin (equations (2.51), Darcy's Law (equation (2.1)), the concentration conservation equation (equation (2.45)) and filtration equation (equation (2.56)) with the unknowns: Pressure field p, velocity field $\vec{V}$, concentration C and filtration σ. The remaining equations necessary for solution are the porosity (equation (2.42), filtration coefficient (equation (2.60)), the domain permeability (equation 2.58)) and the suspension viscosity (equation 2.59)). These equations are the same equations that are used in modeling the impregnation stage of the CRTM process.

2.2 Compression with Particle-Fillers

2.2.1 Mathematical Modeling

For the impregnation phase, the suspension flow through fibrous medium during the compression phase is modeled with Darcy Law through equation (2.1) . The relation between the actual velocity and the superficial velocity during the compression phase is same as that for the impregnation phase which is presented in equation (2.3).

The derivation for the governing equations in the compression phase of CRTM is performed in a manner similar to the previous section. For conservation equations, an infinitesimal deformable control volume which is compressed (slowly closed) along z-direction with constant mold closing speed, U_z, is presented in Figure 2.3. As in the impregnation case, the suspension flow during the compression phase passes through a fibrous medium. However, in CRTM modeling, there is no injection and the injection gate is closed. The particles carried along moving resin

and particles stuck within the preform (filtered) are considered separately. As before, the conservation equations are derived for three "different" species during compression phase: particles in the resin, the neat resin and the filtered particles.

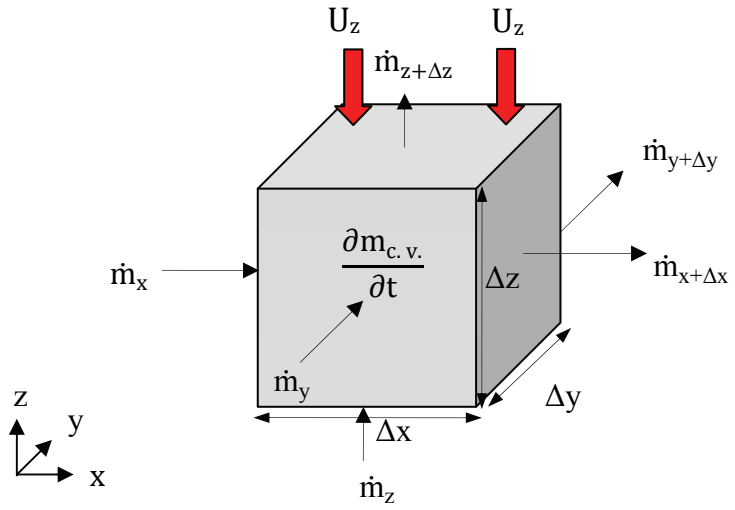

Figure 2.3. Flow domain control volume for the conservation equations during compression

Particles retained in the resin: For the deformable control volume given in Figure 2.3 the conservation equation is

$$\dot{m}_{in} - \dot{m}_{out} + \dot{m}_{generated,c} = \dot{m}_{stored} \tag{2.63}$$

which is the same relation as the conservation equation of particles retained in the polymer for impregnation phase. Thus, the integration of equation (2.63) over unit time, Δt results in the same equation with equation (2.7) for compression phase. Using the volume and area definitions of the particles retained in the resin in equations (2.8) and (2.9), and dividing the equation (2.7) by "$\rho_c \Delta t \forall_0$" yields:

$$\frac{A_0}{\forall_0}\{[u_c'\varepsilon C|_x - u_c'\varepsilon C|_{x+\Delta x}] + [v_c'\varepsilon C|_y - v_c'\varepsilon C|_{y+\Delta y}] + [w_c'\varepsilon C|_z - w_c'\varepsilon C|_{z+\Delta z}]\} + \frac{\dot{m}_{generated,c}}{\rho_c \forall_0} = \frac{\rho_c[\varepsilon C\,|_{t+\Delta t} - \varepsilon C|_t]}{\rho_c \Delta t} \tag{2.64}$$

Using equation (2.12) and (2.13) equation 2.56 is simplified to

$$\frac{[u_c'\varepsilon C|_x - u_c'\varepsilon C|_{x+\Delta x}]}{\Delta x} + \frac{[v_c'\varepsilon C|_x - v_c'\varepsilon C|_{x+\Delta x}]}{\Delta y} + \frac{[w_c'\varepsilon C|_x - w_c'\varepsilon C|_{x+\Delta x}]}{\Delta z} + \frac{\dot{m}_{generated,c}}{\rho_c \forall_0} = \frac{[\varepsilon C\,|_{t+\Delta t} - \varepsilon C|_t]}{\Delta t} \tag{2.65}$$

Δx and Δy are constants as mold is closed, but as the mold is closed Δz decreases. Thus Δx and Δy components at the right hand side of the equation can be eliminated. Then, as $\Delta t \to 0, \Delta x \to 0, \Delta y \to 0$ and $\Delta z \to 0$ equation (2.65) is

$$-\left[\frac{\partial(u_c'\varepsilon C)}{\partial x} + \frac{\partial(v_c'\varepsilon C)}{\partial y} + \frac{\partial(w_c'\varepsilon C)}{\partial z}\right] + \frac{\dot{m}_{generated,c}\Delta t}{\rho_c \Delta t \forall_0} = \lim_{\Delta t\to 0,\Delta z\to 0}\left[\frac{[\Delta z\varepsilon C\,|_{t+\Delta t} - \Delta z\varepsilon C|_t]}{\Delta t \Delta z}\right] \tag{2.66}$$

As $\Delta t \to 0$ and $\Delta z \to 0$, the right hand side of equation (2.66) becomes

$$\lim_{\Delta t\to 0,\Delta z\to 0}\left[\frac{[\Delta z\varepsilon C\,|_{t+\Delta t} - \Delta z\varepsilon C|_t]}{\Delta t \Delta z}\right] = \frac{\Delta z}{\Delta z}\frac{\partial(\varepsilon C)}{\partial t} + \varepsilon C\left[\frac{1}{\Delta z}\frac{\partial(\Delta z)}{\partial t}\right] \tag{2.67}$$

For the preform modeled as a one continuous layer, the preform thickness which is also the cavity gap thickness, can be thought as the sum of M equal infinitesimal gap thicknesses, i.e. $H = M\Delta z$. As the mold upper plate is closes,

each infinitesimal element is assumed to compress with the same amount (one continuous layer) while their number remains same (M=constant). Then,

$$U_z = \frac{dH}{dt} = \frac{d(M\Delta z)}{dt} = M\frac{d(\Delta z)}{dt} = M\frac{\Delta z}{\Delta z}\frac{d(\Delta z)}{dt} = \frac{H}{\Delta z}\frac{d(\Delta z)}{dt} \tag{2.68}$$

where H is the overall thickness of the mold cavity which changes with compression and U_z is the constant mold closing speed. Then, using equations (2.67) and (2.68), equation (2.66) yields to the conservation equation for the particles in the resin for the suspension flow during the compression phase:

$$\frac{\partial[\varepsilon C]}{\partial t} + \varepsilon C\frac{U_z}{H} + \nabla\cdot\{\varepsilon C\vec{V}_c'\} = \frac{\dot{m}_{generated,c}}{\forall_0\rho_c} \tag{2.69}$$

Neat Resin: For the mass balance of the neat resin, as impregnation phase, there is no artificially introduced generation term for the compression phase. The conservation equation for the neat resin is:

$$\dot{m}_{in} - \dot{m}_{out} = \dot{m}_{stored} \tag{2.70}$$

which is the same relation with the conservation equation for the impregnation phase, equation (2.19). Integration of equation (2.70) over unit time,Δt, yields to equation (2.22). Using the volume and area definitions of the particles retained in the resin in equations (2.23) and (2.24), and dividing the equation (2.22) by "$\rho_p\Delta t\forall_0$" yields:

$$\frac{A_0}{\forall_0}\Big\{\Big[u_p'\varepsilon(1-C)\Big|_x - u_p'\varepsilon(1-C)\Big|_{x+\Delta x}\Big] + \Big[v_p'\varepsilon(1-C)\Big|_y - v_p'\varepsilon(1-C)\Big|_{y+\Delta y}\Big] + \Big[w_p'\varepsilon(1-C)\Big|_z - w_p'\varepsilon(1-C)\Big|_{z+\Delta z}\Big]\Big\} = \frac{[\varepsilon(1-C)|_{t+\Delta t} - \varepsilon(1-C)|_t]}{\Delta t\forall_0} \tag{2.71}$$

Δx and Δy are constants as mold is closed, but as the mold is closed Δz decreases. Thus Δx and Δy components at the right hand side of the equation can be eliminated. Then, equation (2.71) using equations (2.12) and (2.13) is simplified to:

$$\frac{\Big[u_p'\varepsilon(1-C)\Big|_x - u_p'\varepsilon(1-C)\Big|_{x+\Delta x}\Big]}{\Delta x} + \frac{\Big[v_p'\varepsilon(1-C)\Big|_x - v_p'\varepsilon(1-C)\Big|_{x+\Delta x}\Big]}{\Delta y} + \frac{\Big[w_p'\varepsilon(1-C)\Big|_x - w_p'\varepsilon(1-C)\Big|_{x+\Delta x}\Big]}{\Delta z} = \frac{[\varepsilon(1-C)|_{t+\Delta t} - \varepsilon(1-C)|_t]}{\Delta t} \tag{2.72}$$

Then, as $\Delta t \to 0, \Delta x \to 0, \Delta y \to 0$ and $\Delta z \to 0$ equation (2.72) yields to:

$$-\left[\frac{\partial(u_p'\varepsilon(1-C))}{\partial x} + \frac{\partial(v_p'\varepsilon(1-C))}{\partial y} + \frac{\partial(w_p'\varepsilon(1-C))}{\partial z}\right] = \lim_{\Delta t\to 0,\Delta z\to 0}\left[\frac{[\Delta z\varepsilon(1-C)\,|_{t+\Delta t} - \Delta z\varepsilon(1-C)|_t]}{\Delta t\Delta z}\right] \tag{2.73}$$

As $\Delta t \to 0$ and $\Delta z \to 0$, the right hand side of equation (2.72) gives:

$$\lim_{\Delta t\to 0,\Delta z\to 0}\left[\frac{[\Delta z\varepsilon(1-C)\,|_{t+\Delta t}-\Delta z\varepsilon(1-C)|_t]}{\Delta t\Delta z}\right] = \frac{\Delta z}{\Delta z}\frac{\partial(\varepsilon(1-C))}{\partial t}+\varepsilon(1-C)\left[\frac{1}{\Delta z}\frac{\partial(\Delta z)}{\partial t}\right] \tag{2.74}$$

Then, using equations (2.74) and (2.68), equation (2.73) yields to the conservation equation for the neat resin for the suspension flow during the compression phase

$$\frac{\partial[\varepsilon(1\text{-}C)]}{\partial t}+\varepsilon(1\text{-}C)\frac{U_z}{H}+\nabla\cdot\{\varepsilon(1-C)\vec{V}_p'\}=0 \tag{2.75}$$

Filtered particles: The conservation equation for the filtered particles during the compression phase is obtained in the same manner as that in the impregnation phase, as given in equation (2.32). Similarly, using equation (2.35), equation (2.32) is,

$$\frac{\dot{m}_{generated,\sigma}}{\rho_\sigma \forall_0}=\frac{[(\Delta z\sigma)|_{t+\Delta t}-(\Delta z\sigma)|_t]}{\Delta t\Delta z} \tag{2.76}$$

Δx and Δy terms at the right hand side of the equation can be canceled. Also flow is assumed to be incompressible, so density is constant.

As $\Delta t \to 0$ and $\Delta z \to 0$ equation (2.76) gives:

$$\frac{\dot{m}_{generated,\sigma}}{\rho_\sigma \forall_0}=\lim_{\Delta t\to 0,\Delta z\to 0}\left[\frac{[(\Delta z\sigma)|_{t+\Delta t}-(\Delta z\sigma)|_t]}{\Delta t\Delta z}\right] \tag{2.77}$$

Using the relation in equation (2.68) for single layer preform assumption, equation (2.77) is expressed as

$$\frac{\dot{m}_{generated,\sigma}}{\rho_\sigma \forall_0} = \frac{\partial(\sigma)}{\partial t} + \sigma \frac{U_z}{H} \tag{2.78}$$

The derivative of the equation (2.42) includes the time rate of change of the initial porosity. As the mold is compressed same amount of fibers exists in a smaller mold cavity that increases the fiber volume fraction ν_f. Thus, the derivative of this equation is

$$\frac{\partial \varepsilon}{\partial t} = \frac{\partial \varepsilon_0}{\partial t} - \frac{\partial \sigma}{\partial t} \tag{2.79}$$

Equation (2.78) with equations (2.39) and (2.40) can be expressed as

$$-\frac{\dot{m}_{generated,c}}{\rho_\sigma \forall_0} = \frac{\partial(\sigma)}{\partial t} + \sigma \frac{U_z}{H} \tag{2.80}$$

Continuity equation for the particles retained in the resin, (2.69) using equation (2.80) simplified to

$$\frac{\partial[\varepsilon C]}{\partial t} + \varepsilon C \frac{U_z}{H} + \nabla \cdot \left\{ \varepsilon C \vec{V}_c' \right\} = -\frac{\partial(\sigma)}{\partial t} - \sigma \frac{U_z}{H} \tag{2.81}$$

Using the equation (2.79) and continuity equation for the neat resin in equation (2.75), equation (2.81) is rearranged and " $-\varepsilon \frac{U_z}{H}$ " is added to both sides of the equation which yields

$$\nabla \cdot \left\{ \varepsilon (1 - C) \vec{V}_p' \right\} + \nabla \cdot \left\{ \varepsilon C \vec{V}_c' \right\} = -(\varepsilon + \sigma) \frac{U_z}{H} - \frac{\partial \varepsilon_0}{\partial t} \tag{2.82}$$

The relative velocity between the resin is assumed to be zero [7, 30]. Then the subscripts in the velocity terms are dropped and equation (2.82) reduces to

$$\nabla \cdot \{\varepsilon \vec{V}'\} = -\varepsilon_0 \frac{U_z}{H} - \frac{\partial \varepsilon_0}{\partial t} \tag{2.83}$$

The total volume of the fibers, $\forall_{fiber}$ can be related to the mold cavity volume, $\forall_0$ as

$$\forall_{fiber} = \forall_0 (1 - \varepsilon_0) \tag{2.84}$$

Since the total volume of the fiber does not change as the mold is compressed, (assuming fibers are not compressible)

$$\frac{\partial \forall_{fiber}}{\partial t} = \frac{\partial \forall_{mold}}{\partial t} - \varepsilon_0 \frac{\partial \forall_0}{\partial t} - \forall_{mold} \frac{\partial \varepsilon_0}{\partial t} = 0 \tag{2.85}$$

The cavity gap, H, is related to the cavity volume as

$$\forall_0 = HA \tag{2.86}$$

where A is the cavity area perpendicular to the z-direction (mold closing direction). Assuming the cavity geometry is such that A remains constant and differentiating equation (2.86)

$$\frac{\partial \forall_0}{\partial t} = A \frac{\partial H}{\partial t} = AU_z \tag{2.87}$$

Using equations (2.86) and (2.87), time rate change of the unfiltered domain porosity is obtained as

$$\frac{\partial \varepsilon_0}{\partial t} = \frac{U_z}{H} (1 - \varepsilon_0) \tag{2.88}$$

Thus, with equation (2.88), continuity equation for the neat resin in equation (2.83) is simplified to

$$\nabla \cdot \{\varepsilon \vec{V}'\} = -\frac{U_z}{H} \tag{2.89}$$

$\vec{V}'$ is the actual velocity. Using the relation between superficial velocity, $\vec{V}$and actual velocity, $\vec{V}'$ from equation (2.3) , the final form of continuity equation for neat resin during the compression phase is obtained as:

$$\nabla \cdot \{\vec{V}\} = -\frac{U_z}{H} \tag{2.90}$$

Equation (2.90) is found to be same with the continuity equation derived in [2, 22] for the continuity equation for the neat resin impregnation for the compression phase for the CRTM process.

The four equations for the four unknowns of the process, pressure p, velocity $\vec{V}$, particle concentration in the suspension C and the filtrate, specific particle deposit σ are the continuity equation for the neat resin (equations (2.90)), Darcy's Law (equation (2.1)), concentration equation (equation (2.81)) and filtration equation (equation (2.56)). Additionally, the relation of the domain porosity (equation (2.42)), the equation for filtration coefficient (equation (2.60)), the equation for the domain permeability (equation 2.58)) and the equation for the suspension viscosity (equation 2.59)) are used during the solution of the model.

2.3 Boundary and Initial Conditions

In the injection phase of CRTM and RTM processes, there are four unknowns ($p, \vec{V}, C$ and σ) and the equations for the solution of these four unknowns are equation (2.1) , equation (2.51), equation (2.45) and equation (2.56). For the solution to be complete, boundary and initial conditions must be supplied. These conditions are shown in Figure 2.4.

For the solution of the p and $\vec{V}$, Darcy's Law (equation (2.1)) and the continuity equation (equation (2.51)) are used. In order to solve these differential equations, boundary conditions must be specified. At the inlet gate either the inlet gage pressure, p_{inlet} or the inlet velocity, u_{inlet} is defined. Since the mold cavity is open to the environment (air vents exists) the flow front of the suspension is a free surface, the pressure at the flow front is zero gage (atmospheric). On the side walls, the suspension is allowed to flow only along the side walls (no flow along normal direction of the side walls) which results in slip condition at the side walls of the mold cavity.

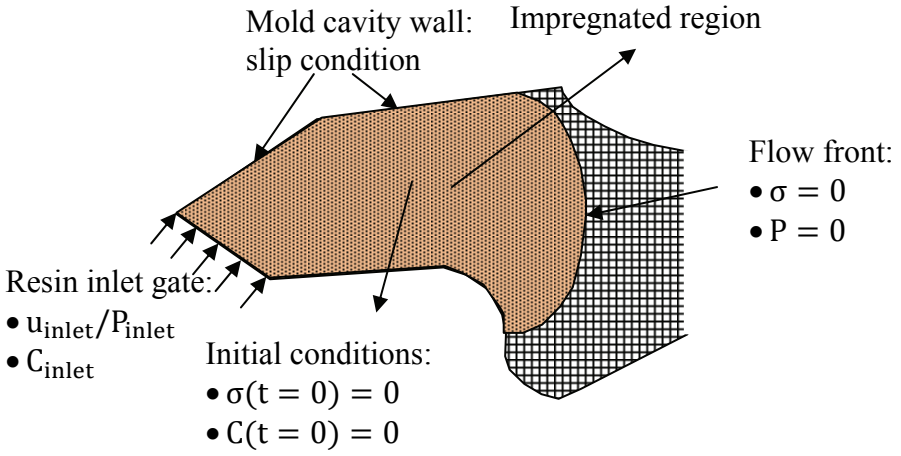

Figure 2.4. Boundary and initial conditions for injection phase

For the solution of the unknowns C and σ, the concentration equation (equation (2.45)) and the filtration equation (equation (2.56)) are used. The concentration equation (equation (2.45)) has first order time and space derivatives, so the solution necessitates one initial condition, C(t = 0) and one boundary condition, C_{inlet}, as shown in Figure 2.4. Initially the mold cavity is not filled with

suspension and there is no particle in the mold cavity, therefore $C(t = 0)$ is zero. As a boundary condition the concentration of the suspension at the inlet gate (the concentration value of the suspension at the injection unit), C_{inlet} is specified.

The filtration equation (equation (2.56)) has only first order time derivative, and one initial condition is needed. Initially, the mold is not impregnated with suspension and there is no particle resin mixture that can lead any particle deposit. The initial value of the specific deposit is zero.

During the compression phase of CRTM there are again four unknowns ($p, \vec{V}, C$ and σ) and the equations for the solution of these four unknowns are equation (2.1) , equation (2.90), equation (2.81) and equation (2.56). The boundary and initial conditions are figured out in Figure 2.5.

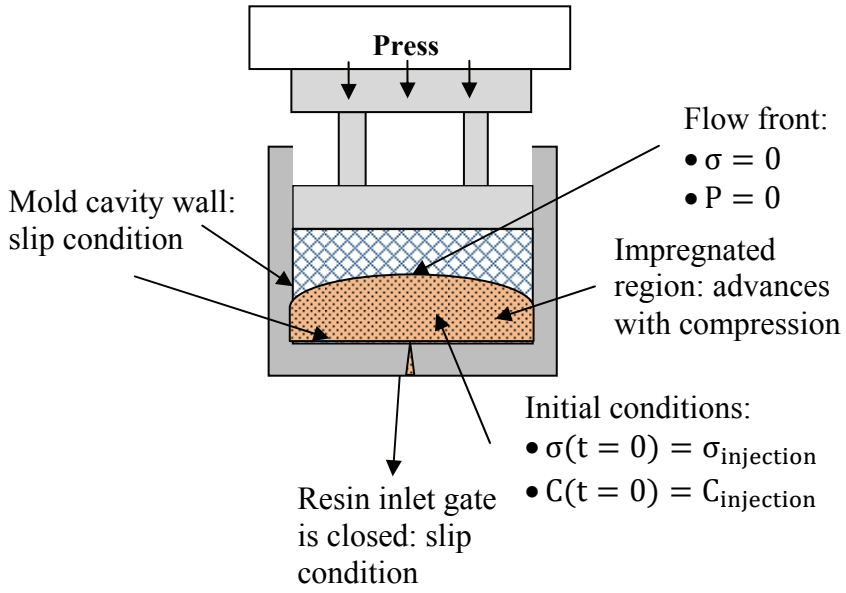

Figure 2.5. Boundary and initial conditions for compression phase

During the compression phase, there will not be any suspension addition. The amount of suspension that was impregnated during the injection will be dispersed throughout the rest of the preform by compression. For the solution of Darcy's Law (equation (2.1)) and continuity equation for the neat resin (equation equations (2.90)) there is no gate boundary condition.

The solution obtained at the end of injection phase is considered as an initial condition for all of the governing equations. The pressure field, velocity field, concentration and filtrate levels attained at the end of injection are prescribed as the initial conditions for the corresponding governing equations.

CHAPTER 3

NUMERICAL IMPLEMENTATION AND SOLUTION METHODOLGY

The numerical implementation and solution of the injection and the compression phases of CRTM are performed on COMSOL Multiphysics®, a commercial software package. The package is capable of solving a wide variety of well-known and/or user defined partial differential equations about a range of scientific and engineering problems which can be coupled or uncoupled. Several built-in physics modes are available for the solution of multiphysics problem. COMSOL Multiphysics® version 3.5a has been used by others in some plastics processing methods such as injection molding [49-51]. However, it has not been used before the purpose of modeling composites manufacturing and resin impregnation, let alone, particle-filled resin impregnation and compression phases.

The program allows in the definition/input of constant and variables as well as mathematical and logical functions to define material properties, loads, sources, boundary conditions, etc. Functions/logical expressions can be entered to the program using script language or MATLAB®.

The user can enter - by drawing – the problem geometry or import the geometry from another drawing tool. After the problem geometry is complete and parameters are defined, COMSOL Multiphysics® generates the solution mesh. User has control over the details of the mesh generation, such as mesh size, type, concentration, boundary layer meshing, size function definitions, etc.

The underlying mathematical structure of this package is a variety of partial differential equations (PDEs). The available application modules and their brief description are given in Table 3.1. Comsol Multiphysics and Chemical Enginnering modules of the software tool are used for numerical simulations. The solutions of these PDEs are performed via finite element method (FEM). A variety of numerical solvers are used when performing finite element analysis. The solvers and their usage are summarized in Table 3.2. The program offers both direct and iterative solvers with a wide range of pre-conditioners for iterative solvers and "time dependent" Direct (UMFPACK) is used. By default, COMSOL Multiphysics® chooses an appropriate solver for the selected application mode. In this study, all the simulations are performed by Time dependent solver. For multiphysics modeling the selection of the solver is done for the ruling application mode, so user should consider the performance of the selected solver for the rest of physics.

The postprocessing tools in the program for plotting and graphical representations can be used in all models and parameters. Alternatively, the results can be exported to programs such as MATLAB® or MS Excel® for post-processing.

Analysis of the injection and compression phases includes the simultaneous solution of the equations that are presented in the formulation of the problem chapter (Chapter 2). The chemical engineering module of COMSOL Multiphysics® is used in this study. The program has a built-in Darcy equation in the Chemical Engineering Module for analyzing porous flow. The equations for filtration kinetics and the conservation of particles in the suspension (concentration equations) for injection and compression phases are introduced via PDE application mode in the COMSOL Multiphysics application module. Enlarging flow domain (movement of the flow front) is tracked by the Level Set Method which is a built-in application mode in Chemical Engineering Module. Compression of the flow domain during the mold closing is modeled via ALE

(Arbitrary Lagrangian Eulerian) formulations which are built-in functions in COMSOL Multiphysics Module.

Table 3.1. Application modules of COMSOL Multiphysics® and their descriptions

Application Modules	**Description**
Comsol Multiphysics	Application modes for fundamental physics and for defining equations
AC/DC Module	Simulates electrical components and devices that depend on electrostatics, magnetostatics
Acoustics Module	Contains built-in application modes and boundary settings for the modeling of acoustic wave propagation in solids and stationary fluids
Chemical Engineering Module	Analyzes CFD and mass and energy balances coupled to chemical reaction kinetics and transport phenomena
Earth Science Module	Models single and coupled processes for geological and environmental phenomena particularly based around subsurface flow.
Heat Transfer Module	Consists of advanced application modes for the analysis of heat transfer by conduction, convection, and radiation.
MEMS Module	Represents coupled processes in MEMS and microfluidic devices
RF Module	Characterizes electromagnetic fields, currents, and waves for RF, microwave, optical, and other high-frequency devices.
Structural Mechanics Module	Performs classical stress-strain analyses with full multiphysics capabilities.

Table 3.2. COMSOL Multiphysics® solvers [52]

SOLVER TYPE	***USAGE***
Stationary	For steady PDE problems
Time dependent	For time-dependent PDE problems
Eigenvalue	For eigenvalue PDE problems
Parametric	For parameterized sets of steady PDE problems
Stationary segregated	For steady multiphysics PDE problems
Parametric segregated	For parameterized sets of steady multiphysics PDE problems
Time dependent segregated	For time-dependent multiphysics PDE problems
Adaptive	For steady PDE problems or linear eigenvalue PDE problems using adaptive mesh refinement
Sensitivity	For sensitivity analysis of steady PDE problems
Optimization	For optimization of steady PDE problems

3.1 Darcy Law and Continuity Equation

In a porous medium, the global transport of momentum by shear stresses in the fluid is often negligible because the pore walls hinder the momentum transport to the fluid outside the individual pores. Generally, a detailed description for each pore is not feasible. Alternatively, the porous medium and flow domain is reduced to a single homogenous. Darcy's law together with the continuity equation and equation of state for the fluid (or gas) provide a complete mathematical model suitable for a wide variety of applications involving porous media flows, for which the pressure gradient is the major driving force.

Darcy's law operates with the volume-averaged flow variables such as the flow velocity, pressure, and density, etc. These averaged properties are defined at any point inside the medium by means of averaging of the actual fluid properties over a certain volume surrounding the point. The volume is small compared to the typical macroscopic dimensions of the problem, but it is large enough to contain many pores and solid matrix elements. The Darcy's Law application mode in the Chemical Engineering Module combines Darcy's law with the continuity equation:

$$\delta_{ts}\frac{\partial(\rho\varepsilon)}{\partial t}+\nabla\cdot\left[\rho\left(-\frac{K}{\eta}\cdot\nabla p\right)\right]=F \tag{3.1}$$

where δ_{ts} is the time scaling coefficient, ρ is density, ε is porosity, κ is the permeability, η indicates dynamic viscosity and F is the source term. These parameters can be defined from the "subdomain settings" option of the program.

Boundary conditions one can impose in the Darcy's Law application mode comprise the pressure condition, a slip or symmetric boundary condition and a specific inflow/outflow perpendicular to the boundary.

In the Chemical Engineering Module of COMSOL Multiphysics® 3.5a, permeability, K is defined isotropic as default. In order to have anisotropic permeability tensor some modifications in the "equation system" is allowed.

3.2 Concentration and Filtration Equations

User-defined functions or PDE's are introduced to COMSOL Multiphysics® using the below built-in partial differential equation form:

$$e_a\frac{\partial^2 u}{\partial t^2}+d_a\frac{\partial u}{\partial t}+\nabla\cdot(c\nabla u-\alpha u+\gamma)+au+\beta\cdot\nabla u=f \tag{3.2}$$

where;

c : diffusion coefficient

a: absorption coefficient

f: source term

e_a: mass coefficient

d_a: damping/mass coefficient

α: mass conservative flux convection coefficient

β: convection coefficient

γ: conservative flux source term

u: dependent variable

The equations for the filtration kinetics (equation (2.56)) and the conservation equation during the injection phase (equation (2.45)) and the compression phase (equation (2.81)) are introduced to the program via this PDE application mode in the COMSOL Multiphysics® module. Definition of the constants of equation (3.2) corresponding to filtration kinetics and concentration equations for injection and compression phases are presented in Table 3.3.

The initial conditions of the problem can be imposed to COMSOL Multiphysics® from the subdomain settings of the program. Since there is no particle impregnated before the injection, the initial value of the specific particle deposit, σ and particle concentration, C are set to zero. The spatial derivative is not needed for the filtration kinetics equation, thus this equation has no boundary condition. For the concentration equation during the impregnation phase, the initial concentration is introduced at the inlet gate and there is no need to define boundary conditions on any of the remaining boundaries.

Table 3.3. Coefficients for introducing the filtration kinetics and concentration equations for injection and compression phases

Coefficients	**Filtration kinetics**	**Concentration equation during injection**	**Concentration equation during compression**
c	0	0	0
a	$\frac{\alpha VC}{\sigma_u}$	$\frac{\partial[\varepsilon]}{\partial t}$	$\frac{\partial[\varepsilon]}{\partial t}+(\varepsilon\text{-}1)\frac{U_z}{H}$
f	αVC	$-\frac{\partial(\sigma)}{\partial t}$	$-\frac{\partial(\sigma)}{\partial t}-\sigma\frac{U_z}{H}$
e_a	1	0	0
d_a	0	ε	0
α	0	0	0
β	0	$\vec{V}$	$\vec{V}$
γ	0	0	0
u	σ	C	C

3.3 Flow Front Tracking Using Level Set Method

The solution of injection and compression phases of the CRTM process includes an enlarging flow domain with free surface. Thus, this enlarging flow domain should be tracked. In the level set method (LSM) the interface is defined as the zero level set of a smooth function. Although, the conservation properties are not taken into account in this method, the computation algorithm is relatively easy and the solution is performed on a fixed mesh [53].

The level set method is an implicit method for describing the evolution of an interface between two fluids. It makes use of a distance function, referred to as the level-set function, ϕ which labels every point in a domain with a value representing the shortest distance to the interface. As such this function is equal to zero at the interface itself and non-zero in the fluids. To distinguish between the two fluids, one of them uses a signed function, being negative in one fluid and positive in the other. In Figure 3.1 a breaking wave is shown with several level set contours. Each contour represents those points that are a certain distance away from the interface. In the same figure the discretized flow domain is also shown. Each grid cell contains a value of the level-set function [54]. The LS function ϕ is a scalar parameter that is advected by the flow with the local flow velocity without influencing the flow itself; a passive scalar. It determines the location of the interface and thus the fluid properties to be used when a certain region is under consideration, but this can be seen as an indirect influence. The procedure of determining the interface can be performed after the flow has been solved. During the process of solving the flow itself the LS function is just simply advected with the flow. The advection equation can therefore be used to describe the motion of ϕ, and thus the evolution of the interface, in time.

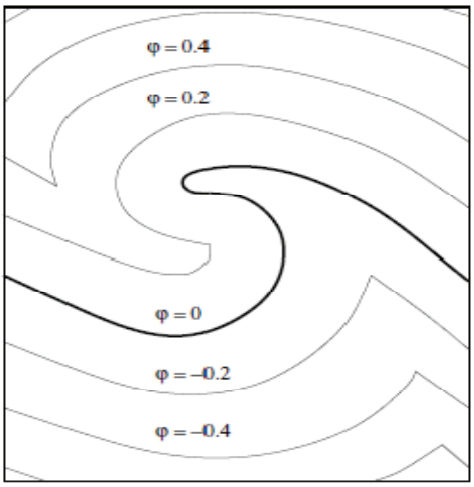

0.6	0.6	0.6	0.5	0.5	0.5	0.5	0.5	0.5	0.5	0.5	0.6	0.6
0.6	0.5	0.5	0.5	0.4	0.4	0.4	0.4	0.4	0.4	0.4	0.5	0.6
0.5	0.5	0.4	0.4	0.3	0.3	0.3	0.3	0.3	0.3	0.4	0.4	0.4
0.4	0.4	0.4	0.3	0.2	0.2	0.2	0.2	0.2	0.2	0.3	0.3	0.4
0.4	0.3	0.3	0.2	0.1	0.1	0.1	0.1	0.1	0.1	0.2	0.3	0.3
0.3	0.3	0.2	0.1	0	0	0	0	0	0	0.1	0.2	0.3
0.2	0.2	0.2	0.1	0	0	0	0	–0.1	0	0	0.1	0.2
0.1	0.2	0.2	0.2	0.1	0.1	0.1	0	–0.1	–0.1	0	0	0.1
0.1	0.1	0.1	0.2	0.2	0.2	0.1	0	–0.1	–0.2	–0.1	0	0
0	0	0	0.1	0.1	0.1	0.1	0	–0.1	–0.2	–0.2	–0.1	0
–0.1	0	0	0	0	0	0	0	–0.1	–0.2	–0.3	–0.2	–0.1
–0.2	–0.1	–0.1	0	0	0	–0.1	–0.1	–0.2	–0.3	–0.4	–0.3	–0.2
–0.3	–0.2	–0.2	–0.1	–0.1	–0.1	–0.2	–0.2	–0.3	–0.4	–0.4	–0.4	–0.3
–0.4	–0.3	–0.3	–0.2	–0.2	–0.2	–0.2	–0.3	–0.4	–0.4	–0.5	–0.4	–0.4
–0.5	–0.4	–0.4	–0.3	–0.3	–0.3	–0.3	–0.4	–0.4	–0.5	–0.5	–0.5	–0.5
–0.5	–0.5	–0.4	–0.4	–0.4	–0.4	–0.4	–0.4	–0.5	–0.5	–0.6	–0.6	–0.5

Figure 3.1. Interface definition with level set method (Left: level set contours, Right: level set function values) [54]

In the current study, the flow front tracking is accomplished by the Level Set Method, which COMSOL Multiphysics® allows as a solution option in the Chemical Engineering Module. The level set function, ϕ is defined for the whole mold cavity in which the preform has been placed. This function is a smoothed Heaviside step function and its value varies between 0 and 1, with 1 representing the resin impregnated regions and 0, the unfilled cavity portion, as presented in Figure 3.2. The interface between the impregnated and unfilled cavity is found by tracking the level set function value of 0.5. This interface denotes the flow front and propagates along the mold cavity with the actual flow velocity, $\vec{V}'$. The density and the dynamic viscosity should be defined as a function of level set function, ϕ. In the filled portion, the fluid is the suspension (where $\phi = 1$) and in the unfilled portion, the fluid is air (where $\phi = 0$). With the level set function, the material properties change continuously at the transition region. The scalar expressions for the density and dynamic viscosity are:

$$\rho = \rho_a + \phi(\rho_s - \rho_a) \tag{3.3}$$

$$\mu = \mu_a + \phi(\mu_s - \mu_a) \tag{3.4}$$

where the subscripts s and a denote the suspension and the air, respectively.

The level set function is governed by a conservation equation, the solution of which yields a transition region around the interface in which the function value changes from 0 to 1. The application mode solves the following equations in order to move the interface with the actual velocity field, $\vec{V}'$:

$$\frac{\partial \phi}{\partial t} + \vec{V}' \cdot \nabla\phi = \gamma\nabla \cdot \left(\varepsilon\nabla\phi - \phi(1 - \phi\frac{\nabla\phi}{|\nabla\phi|})\right) \tag{3.5}$$

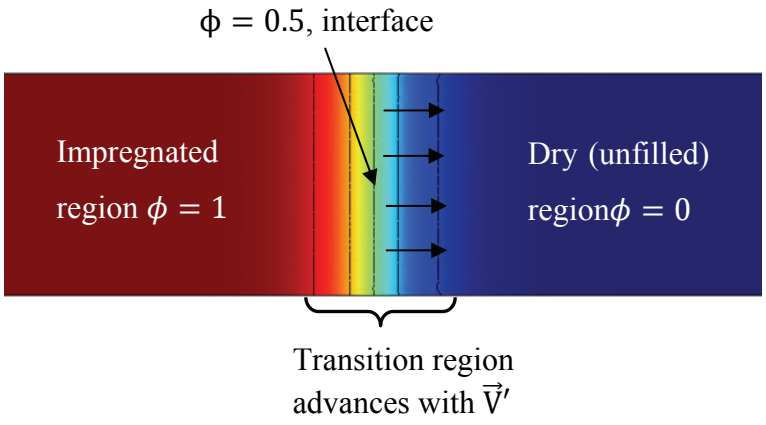

Figure 3.2. Propagation of level set function along the flow domain

The terms on the left-hand side give the correct motion of the interface, while those on the right-hand side are necessary for numerical stability. The parameter ε, determines the thickness of the region where the level set function should change from zero to one and should be of the same order as the size of the mesh elements. The solution domain is made-up two subdomain: the filled and unfilled portions. By default, ε is constant within each subdomain and equals the largest value of the mesh size, h, in each. The program allows the user control the narrowing or widening of this region by manipulating, ε. The parameter γ determines the amount of stabilization of the level set function. It needs to be tuned for each specific problem. If γ is too small, the thickness of the interface might not remain constant, and oscillations in may appear because of numerical instabilities. On the other hand, if γ is too large, the interface moves incorrectly. A suitable value for γ is the maximum magnitude of the velocity field in the subdomain and it is actual suspension velocity, $\vec{V}'$ in this study.

For accurate flow tracking, the transition must be very quick; hence a narrow transition region would be preferred. However, the numerical solution cannot handle steep derivatives associated with the fast transition (narrow transition

region), thus a compromise is made to widen the region to handle the associated derivatives while some loss of accuracy is present.

3.4 Arbitrary Lagrangian-Eulerian Method

After the injection phase is completed, the compression phase of the CRTM process begins. During the compression phase, the mold cavity volume changes and this change is handled with the Deformed Mesh application mode using Arbitrary Lagrangian Eulerin (ALE) description in Comsol Multiphysics module of the COMSOL Multiphysics®.

The problems including simulations of multidimensional fluid flow with free surface, fluid-fluid and fluid-solid interactions the kinematical description of the continuum is an important issue. This description will determine the relation between the moving (or deforming domain) and the solution domain. Then, using the kinematical description a numerical solution that can handle both large distortions and provide accurate solution is desired. Lagrangian and Eulerian are the two descriptions to describe the motion. Moreover, the arbitrary Lagrangian-Eulerian description is developed to use the advantages of Lagrangian and Eulerian descriptions while minimizing the disadvantages of these both descriptions [55].

In Lagrangian descriptions, the nodes in the computational solution domain moves with related material particle. Using Lagrangian description in the solution domain provides advantages on tracking of the free surface of the evolving domain. However, “its weakness is its inability to follow large distortions of the computational domain without recourse to frequent re-meshing operations.” [55]. Eulerian description is generally used for fluid flow problems. The solution domain is fixed and continuum moves with respect to grid. “In the Eulerian description, large distortions in the continuum motion can be handled with relative ease, but generally at the expense of precise interface definition and the resolution

of flow details" [55]. In this manner, taking the advantages and eliminate the drawbacks of both Lagrangian and Eulerian descriptions, the arbitrary Lagrangian-Eulerian technique is introduced. "In the ALE description, the nodes of the computational mesh may be moved with the continuum in normal Lagrangian fashion, or be held fixed in Eulerian manner, or be moved in some arbitrarily specified way to give a continuous rezoning capability" [55].

The built-in function Mesh Movement (ALE) of COMSOL Multiphysics is coupled with other equations during the compression phase of CRTM to include the changes in the model during the closure of the mold cavity. The boundary conditions are simply defined as the mold closing velocity which can be a function or a constant value.

CHAPTER 4

RESULTS AND DISCUSSION

In this chapter, the results obtained via the numerical solutions are presented and discussed. Firstly, the numerical results are compared with available analytical solutions to assess the accuracy of the numerical scheme. Then, some experimental results in the literature are used to express the validity of the model solutions. Following the validation studies, CRTM and RTM processes are compared through analyzing various scenarios for particle-filled composites. The study is concluded by assessing the effects of various process parameters in particle-filled CRTM.

4.1 Numerical Solution and Model Validations

In this part the available analytical solutions for the RTM and CRTM processes are derived and the numerical simulation results are compared with the analytical solutions, to assess the solution accuracy. In addition, some experimental results from the literature are investigated and compared with the model results to assess the model validity.

4.1.1 Comparison of Analytical and Numerical Results

4.1.1.1Fill Time and Flow Front Progression of 1-D RTM Process

The flow front progression with time and fill time for the particle-filled resin impregnation through fibrous preform can be determined analytically for constant inlet line gate velocity u_0. For the current test case, steady, particle-filled resin impregnation along a rectangular mold cavity with planar dimensions of 0.03 m x 0.5 m is investigated for the mold configuration shown in Figure 4.1 and the dimensions are taken from the study of Shojaei [22]. The rectangular cavity shape along with the line gate for which the flow cross-section is uniform assures one-dimensionality.

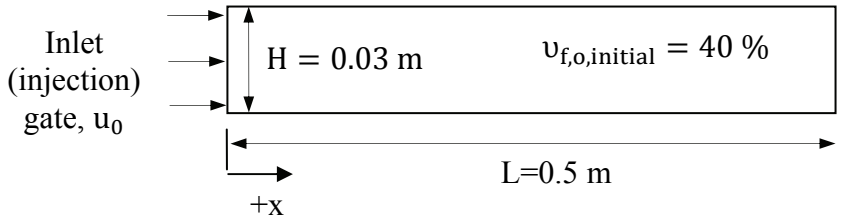

Figure 4.1. 1-D mold configuration for the RTM

One dimensional impregnation during the RTM process has an analytical solution for uniform constant injection velocity, u_0 at the inlet line gate. The superficial injection velocity, u_0 is constant along the mold cavity during the impregnation, but the actual velocity u' changes with the change is the porosity in the mold cavity, as in equation (2.3). There is no filtration at the flow front, so the actual velocity at the flow front is

$$u'|_{x_{front}} = \frac{u_0}{1 - \upsilon_{f,o}} = \frac{u_0}{\varepsilon_o} \tag{4.1}$$

where u_0 is the superficial suspension velocity, υ_f is the local fiber volume fraction, $1 - \upsilon_f$ the local porosity in the preform and t is time. Integrating equation (4.1) with respect to time and noting that at time t = 0, the flow front position x_{front}, yields:

$$x_{front} = \frac{u_0}{\varepsilon_o} \cdot t \tag{4.2}$$

For a mold cavity length of L, the fill time can be found as

$$t_{fill} = \frac{L}{\frac{u_0}{\varepsilon_o}} \tag{4.3}$$

For the simulation of 1-D impregnation of particle-filled resin in the explained cavity configuration, the process parameters used are listed in Table 4.1 and the parameters having * sign are taken from Erdal study [7]. The steps for generating COMSOL Multiphysics® model for 1-D CRTM process is described in Appendix A. The simulations for RTM process can be performed by changing the geometry and the values of the process parameters and following the steps for the impregnation phase.

Fill time results obtained from the numerical simulation and the analytical solution are given in Table 4.2. The flow front progressions in the numerical simulation are presented in Figure 4.2.a. The position of the flow front is determined by plotting the iso-level set function line corresponding to the value, ϕ = 0.5. The results show that the numerical fill time obtained through the numerical simulation and the analytical fill time obtained by using equation (4.3) are identical. Comparisons of numerical and analytical flow front progressions are presented in Figure 4.2.b. Both lines overlap in excellent agreement. In this

numerical analysis, 6400 triangular mesh elements have been used and the plot of the mesh elements is given in Figure 4.3. In Table 4.3, the numerical fill time and percent error ((True value-Numerical value)/True value) with different mesh element numbers are given.

Table 4.1 Process parameters for 1-D particle-filled RTM

Description	**Value**	**Description**	**Value**
Density of the resin $(\rho_p, kg/m^3)$	1200	Viscosity empirical constant* (A)	0.68
Viscosity of neat resin $(\mu_0, Pa \cdot s)$	0.1	Filtration coefficient constant (a_1)	1*
Fiber preform permeability $(K_{xx,o}, m^2)$	$3.75x10^{-11}$	Permeability relation constant (a_2)	1*
Fiber volume fraction $(v_{f,o,initial}, \%)$	40	Inlet gate resin velocity $(u_0, m/s)$	0.02
Inlet particle concentration in suspension (C_0)	0.3*	Injection volumetric flux per cavity width $(Q, m^2/s)$	0.0006
Initial filtration coefficient $(\alpha_0, 1/m)$	1*	Height of the mold $(H_{initial}, m)$	0.03
Ultimate specific deposit (σ_u)	0.5*	Length of the mold (m)	0.5

Table 4.2. Analytical and numerical fill time results for 1-D particle-filled impregnation in RTM process

Description	Analytical fill time (s)	Numerical fill time (s)
Value	15	15

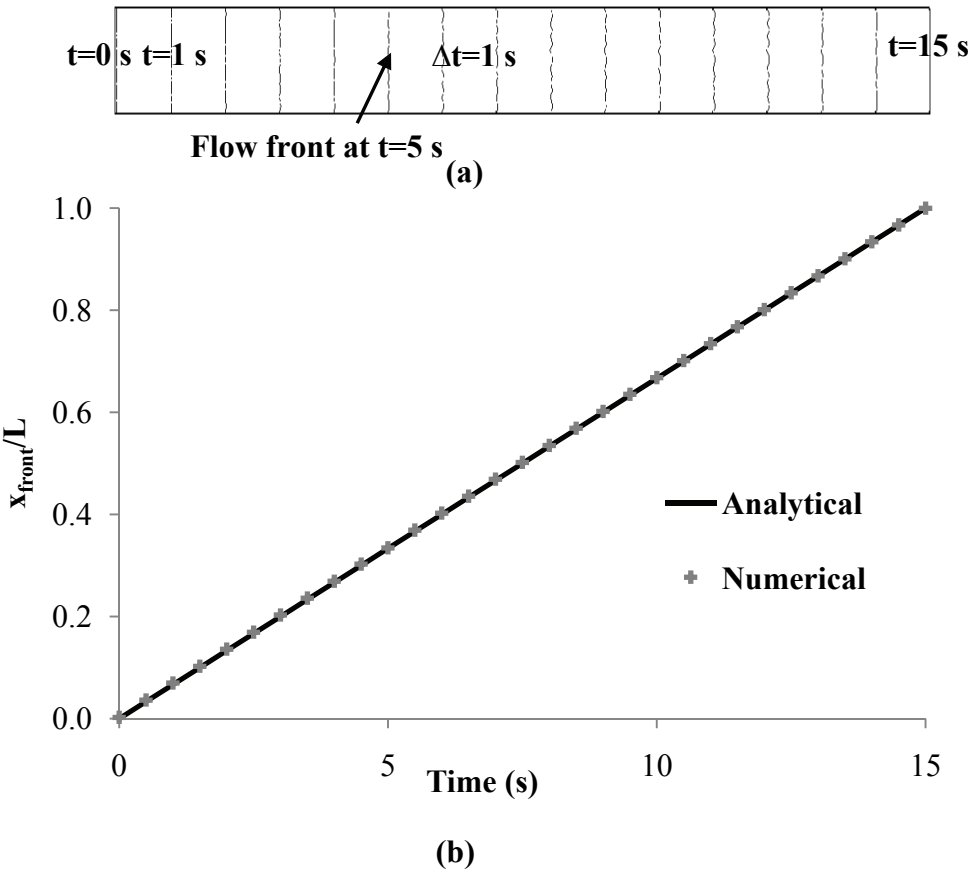

Figure 4.2. a) Flow front positions obtained via COMSOL Multiphysics® (Δt=1 s), b) flow front positions of analytical and numerical solutions for during 1-D particle-filled impregnation

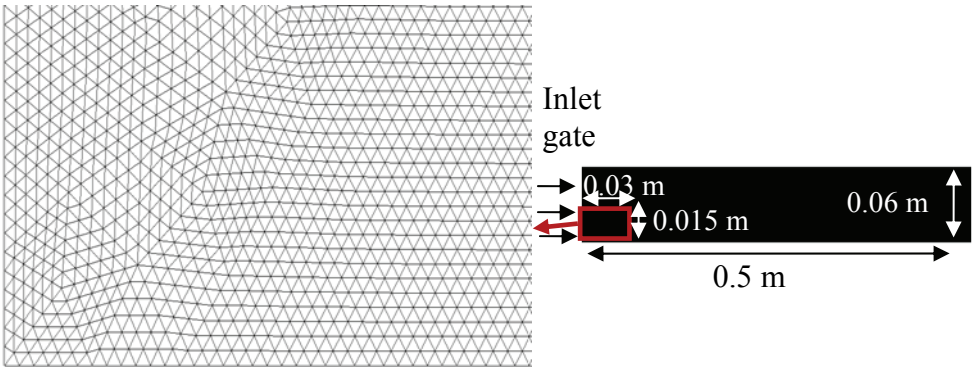

Figure 4.3. Mesh plot of the 1-D RTM analysis (number of mesh elements: 6400)

Table 4.3. The numerical fill time with different number of mesh elements

Number of mesh elements	Numerical fill time (s)	Error (%)
26	14.4	4
104	14.9	0.67
416	15	0
1600	15	0
6400	15	0

4.1.1.2 Fill Time and Flow Front Progression in 1-D CRTM Process

The flow front position and fill time for particle-filled impregnation can be calculated analytically for constant inlet line gate velocity, u_0 and with initial fiber volume fraction, $\upsilon_{f,o,initial}$, during the injection and the compression phases of CRTM. For the current test case, steady, one-dimensional particle-filled resin impregnation along the rectangular mold cavity with the planar dimensions of 0.06 m x 0.5 m is studied for the impregnation phase of the CRTM process, shown in Figure 4.4. The impregnation phase is followed by compression in which the cavity height drops down to 0.03 m. The final composite features (such as fiber volume fraction, final fiber preform permeability and composite part dimensions) are the same as those for the part used in the RTM simulation of the previous section.

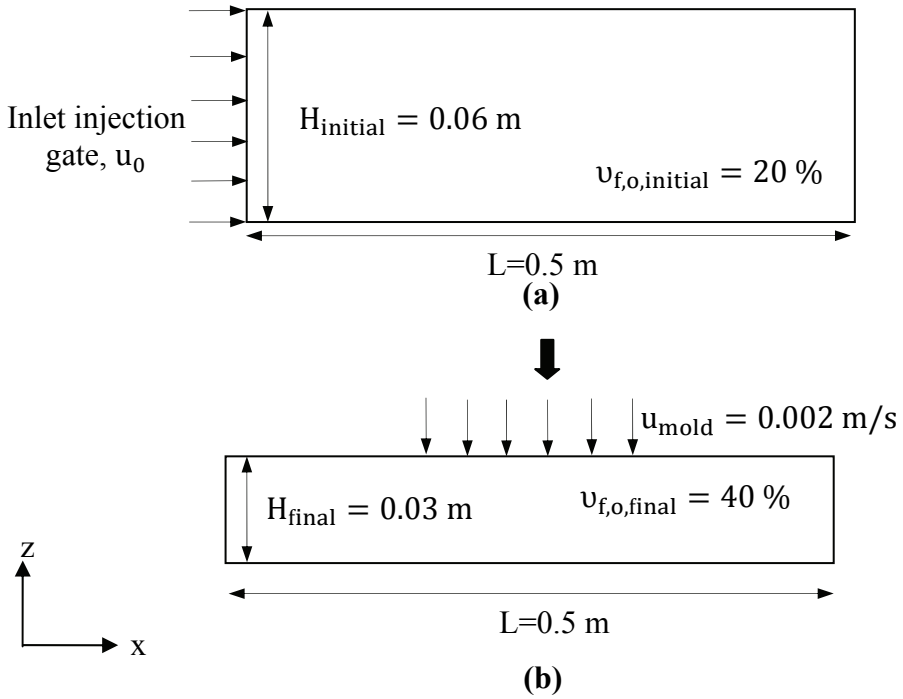

Figure 4.4. 1-D particle-filled impregnation mold cavity configuration for the CRTM a) impregnation phase, b) compression phase

The analytical flow front position and fill time can be calculated using equations (4.2) and (4.3) during the injection phase of the CRTM with $\upsilon_{f,o,initial}$ as the initial fiber volume fraction of the unfiltered domain. In the CRTM process, after sufficient amount of suspension - which will completely fill the final cavity volume - has been injected, the compression phase is initiated. The amount of empty volume per cavity width, once the fiber preform has been compressed to its final form is found as:

$$\forall_{final} = H_{final} \cdot L \cdot (1 - \upsilon_{f,o,final}) \tag{4.4}$$

Then, the injection is performed through the initial mold configuration and the volume of the suspension after $t_{injection}$ time passes will be equal to the available volume of the suspension. Thus, the injection time can be found as:

$$t_{injection} = \frac{\forall_{final}}{u_0 \cdot H_{initial}} = \frac{H_{final} \cdot L \cdot (1 - \upsilon_{f,o,final})}{u_0 . H_{initial}} \tag{4.5}$$

The fill time for the compression phase which is the time elapsed to spread the injected resin throughout the mold cavity, depends on the change between the initial and final mold gap (height) and the mold closing speed, u_{mold}. For a constant mold closing speed, the compression time is:

$$t_{compression} = \frac{H_{final} - H_{initial}}{u_{mold}} \tag{4.6}$$

The suspension flow during the compression phase remains one-dimensional for the current test case, as the results will show. The flow front moves parallel to the length of the mold with as a uniform front.

In order to determine the position of the flow front during the compression phase, the change of the height of the mold cavity and the unfiltered domain porosity with constant mold closing speed, u_{mold} should be expressed. The height of the mold cavity as a function of time during closing of the mold is:

$$H(t) = H_{initial} - u_{mold} \cdot t \tag{4.7}$$

During the compression phase the total volume of fiber preform does not change, so the volume of the fibers in terms of the fiber volume fraction and the volume of the mold cavity in Figure 4.4.a is

$$\forall_{fiber} = \upsilon_{f,o,initial} \cdot H_{initial} \cdot L \tag{4.8}$$

Using the relation between unfiltered fiber volume fraction, $\upsilon_{f,o}$ and the unfiltered domain porosity, $\varepsilon_{o,initial}$, the volume of the fibers is

$$\forall_{fiber} = (1 - \varepsilon_{o,initial}) \cdot H_{initial} \cdot L \tag{4.9}$$

As the mold is compressed, at a time instant the volume of the fibers in terms of the mold height $H(t)$ and the unfiltered domain porosity, $\varepsilon_o(t)$ at that instant is

$$\forall_{fiber} = (1 - \varepsilon_o(t)) \cdot H(t) \cdot L \tag{4.10}$$

Since the volume of the fibers does not change, the change of the unfiltered domain porosity as a function of time yields

$$\varepsilon_o(t) = 1 - (1 - \varepsilon_{o,initial}) \cdot H_{initial}/H(t) \tag{4.11}$$

The volume of the suspension at the end of injection; $\forall_{available}$ will spread out during the compression and is designed to completely fill the final configuration of the mold cavity (volume of the mold cavity in Figure 4.4.b). Then the available volume of the suspension for the CRTM process is

$$\forall_{available} = H_{final} \cdot L \cdot (1 - \upsilon_{f,final}) \tag{4.12}$$

During the compression phase, as the mold is compressed the volume of the suspension at any time instant is the product of flow front position, x_{front}, the height of the mold cavity, $H(t)$ and the unfiltered domain porosity $\varepsilon_o(t)$ at that time instant and it is equal to the volume of suspension at the end of injection phase (the inlet gate is closed at the end of injection). Thus, from that equality, the flow front position is

$$x_{front} = \frac{\forall_{available}}{H(t) \cdot \varepsilon_o(t)} = \frac{H_{final} \cdot L \cdot (1 - \upsilon_{f,final})}{H(t) \cdot \varepsilon_o(t)} \tag{4.13}$$

For the numerical solution of the impregnation and compression phases of the CRTM process for the mold cavity in Figure 4.4, the process parameters are given in Table 4.4 and the parameters having * sign are taken from Erdal study [7]. The process parameters in that table gives the same composite product with the RTM process in the previous part. The initial fiber volume fraction is assigned according to change in the volume of the mold cavity before and after the compression phase. For one-dimensional mold configuration the mold cap height is the parameter to determine the initial fiber volume fraction. Since the volume of the fibers does not change and for one dimensional analysis the mold length is constant, this relation is

$$\upsilon_{f,o,initial} = \frac{\upsilon_{f,o,final} \cdot H_{final}}{H_{initial}} \tag{4.14}$$

The initial permeability value is also assigned to have the same permeability value at the end of compression phase with the RTM process. For the determination of the fiber preform permeability value the relation in equation (2.61) is used as

$$K_{xx,o,initial} = K_{xx,o,final}\left[\left(\frac{\varepsilon_{o,initial}}{\varepsilon_{o,final}}\right)\left(\frac{\upsilon_{f,o,initial}}{\upsilon_{f,o,final}}\right)^{-2}\right]^{a_2} \tag{4.15}$$

The numerical solution is performed in two steps. First, the injection phase is modeled using a non-deforming solution domain and the resulting flow domain data at the end of injection is stored. Then, using the stored data, the compression phase is initiated and the solution domain is deformed while the mold upper plate is brought down, reducing the cavity gap. The steps of the numerical solution of the injection and compression stages are explained in details in Appendix A.

Analytical and numerical solution results for the injection time, the compression time and the total process time are shown in

Table 4.5. As before, the numerical and the analytical results are almost identical. For the impregnation phase using equation (4.2) and for the compression phase using equation (4.13), the flow front positions are calculated analytically and the analytical results are compared with the numerical ones. The comparison is presented graphically in Figure 4.5.a. In Figure 4.5.b the flow front progression during the compression phase as the mold is compressed is given for different time instants in terms of the total process time. As the total process time is reached t=29.9, the mold is completely impregnated. The analytical total process time is found to be 30 seconds for the process parameters given in the Table 4.5.

Table 4.4. Process parameters for 1-D particle-filled CRTM

Description	**Value**	**Description**	**Value**
Density of the resin ($\rho_p, kg/m^3$)	1200	Filtration coefficient constant* (a_1)	1
Viscosity of neat resin ($\mu_0, Pa \cdot s$)	0.1	Permeability relation constant* (a_2)	1
Initial Permeability ($K_{xx,o}, m^2$)	Initial: 2 x 10^{-10}	Inlet gate resin velocity ($u_0, m/s$)	0.01
	Final: 3.75x10^{-11}		
Initial fiber volume fraction ($v_{f,o}$ %)	Initial: 20	Injection volumetric flux per cavity width ($Q, m^2/s$)	0.0006
	Final: 40		
Inlet particle concentration in suspension (C_0)*	0.3	Height of the mold (H, m)	Initial: 0.06
			Final: 0.03
Initial filtration coefficient* ($\alpha_0, 1/m$)	1	Mold closing speed ($u_{mold}, m/s$)	0.002
Ultimate specific deposit* (σ_u)	0.5	Length of the mold (m)	0.5
Viscosity empirical constant* (A)	0.68		

Table 4.5. Results of fill time for impregnation and compression phases of 1-D particle-filled CRTM

Description	Analytical fill time (s)	Numerical fill time (s)
Injection	15.0	15.0
Compression	15.0	14.9
Total process time	30.0	29.9

In the numerical implementation of the compression phase, as the mold is compressed the deformed solution domain is handled via the addition of the ALE (Arbitrary Lagrangian-Eulerian) application method to the governing equations (Darcy's law, concentration and filtration equations and level set method to track the flow front). The compression phase is simulated with the change of the solution domain with compression. Using the ALE method, the initial mesh is deformed up to a considerable mesh element quality. If the deformation yields mesh elements with poor quality (a skewness value that adversely affect the accuracy of the solution), the mesh needs to be refined. For the current example, Figure 4.6 presents the mesh elements during the injection phase and at the end of compression. The number of triangular mesh elements is 12072, which is less enough to decrease the computational effort and high enough to have thinner transition region, during the injection and it is 12800 at the end of compression. This increase is the result of ALE. This method permits the deformation of the existing mesh elements up to some degree that affect the solution. If the mesh quality is decreased, this application mode generates new mesh elements in the solution domain to preserve the stability of the solution.

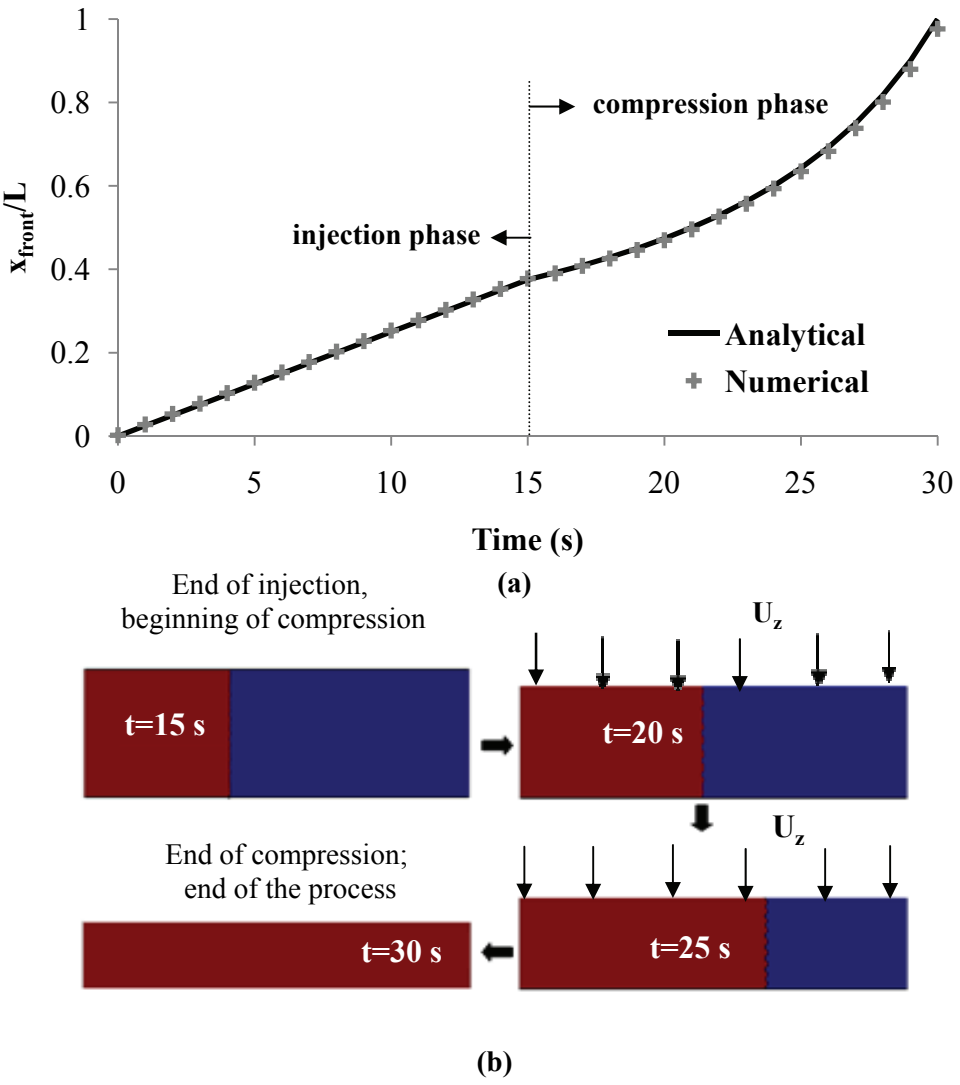

Figure 4.5. a) Flow front progression (normalized by cavity length L) in analytical and numerical solutions for 1-D particle-filled impregnation in injection and compression phases of CRTM. b) Flow front positions during the compression phase at various time instants during numerical solution

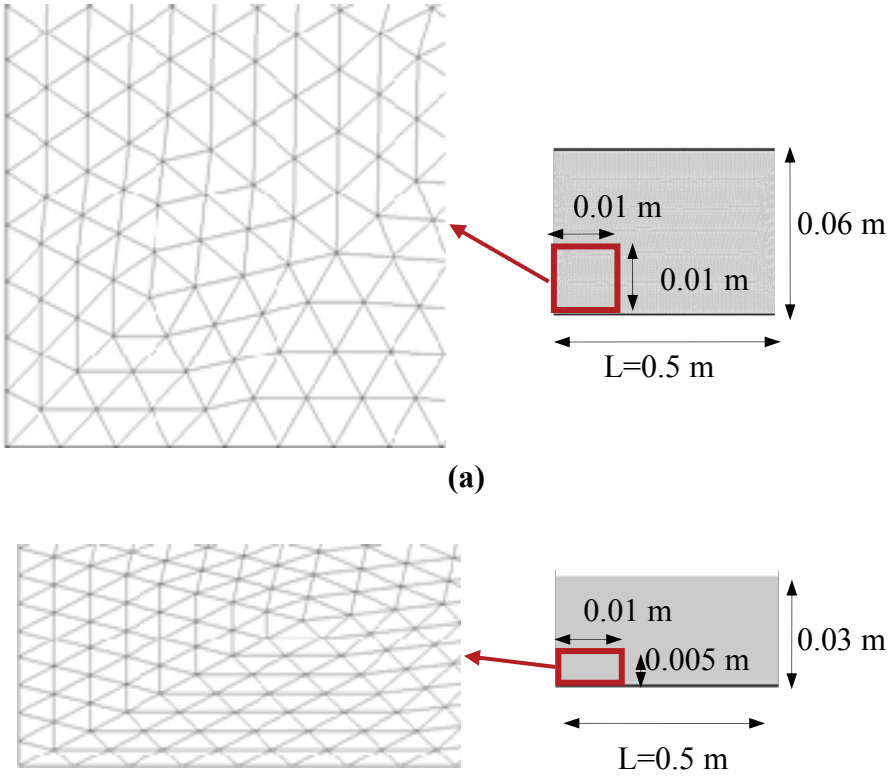

Figure 4.6. Mesh elements a) during injection, b) at the end of compression, for the simulation of 1-D particle-filled CRTM

4.1.1.3 Conservation of Particle-Fillers

In particle-filled impregnation in which the injection velocity/flow rate and particle concentration conditions are known, the total amount of particle volume injected into the mold cavity can be calculated. Referring to Figure 4.4 for the CRTM simulation, the volume of the particles injected into the mold cavity per cavity width, as a function of time can be expressed as:

$$\forall_{\text{partice}}(t) = \int u_0(t) H_{\text{initial}} C_0(t) dt \tag{4.16}$$

where the height of the line gate is H_{initial}. For constant inlet velocity, u_0 and constant inlet particle concentration in the suspension, C_0, equation (4.16) yields

$$\forall_{\text{partice}}(t) = u_0(t) H_{\text{initial}} C_0 t \tag{4.17}$$

For the compression phase of CRTM, the total volume of the particles at end impregnation phase does not change because the inlet gate is closed during the compression phase.

The concentration of the particles in the suspension is the ratio of volume of the particles in the resin to the volume of the suspension. Multiplying the concentration with porosity gives the ratio of the volume of the particles to the volume of the impregnated region. Also considering the filtered particles (volume of the filtered particles per volume of the impregnated region), total particle volume can be formulated as:

$$\forall_{\text{partice}} = (C \cdot \varepsilon + \sigma) \tag{4.18}$$

The numerical evaluation of the total particle volume per mold cavity is performed by using the "subdomain integration" option of the COMSOL Multiphysics® and the integrand is the expression in equation (4.18). Using this integrand the integral evaluation is performed only along the impregnated region because the C and σ has zero value at empty region in the mold cavity.

For the conservation of particle volume during the process, the analytical result of equation (4.17) and the numerical result of equation (4.18) are compared.

At the compression phase the inlet gate is closed so that the volume of the suspension and the volume of the particles in the suspension should remain the same as those at the end of impregnation phase. The analytical and the numerical

results are very similar to one another. The maximum error takes place at the end of injection at a value of 2.4 % (numerical result underestimates). During the compression phase the numerical calculations show a very minute increase in the particle volume. However, this is negligible as at the end of the process, the normalized average particle volume only differs by 0.06%; a very good match.

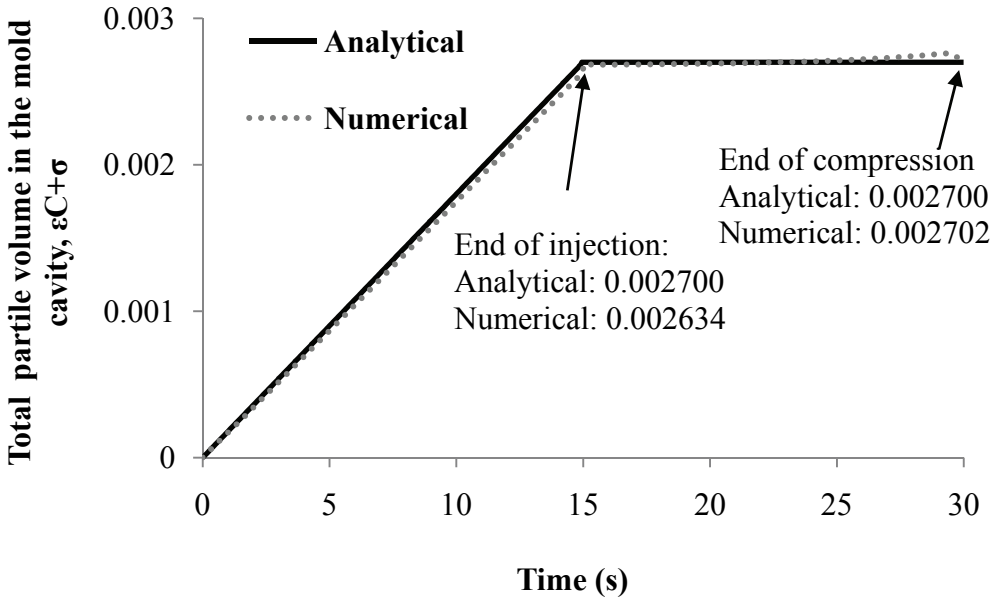

Figure 4.7. The variation of mean particle volume per cavity volume in the mold cavity, with time, during the impregnation and the compression phases of CRTM

4.1.1.4 Particle Concentration at the Flow Front during RTM or the Impregnation Stage of CRTM: Analytical and Numerical Solutions Comparison

The particle concentration at the flow front where the specific deposit is zero, can be determined analytically in RTM (or the injection phase of CRTM). The concentration equation during the impregnation phase (equation (2.45)) can be

expressed to obtain the concentration profile at the flow front for one dimensional modeling. Using equation (2.56) equation (2.45) can be expressed as for one dimensional flow

$$\frac{\partial[\varepsilon C]}{\partial t}+\nabla\cdot\{u'\varepsilon C\}=-\alpha u C\left(1-\frac{\sigma}{\sigma_u}\right) \tag{4.19}$$

Usign the product rule of the divergence operator, the equation (4.19) is

$$\frac{\partial[\varepsilon C]}{\partial t}+C\,\nabla\cdot\{u'\varepsilon\}+u'\varepsilon\cdot\nabla C=-\alpha u C\left(1-\frac{\sigma}{\sigma_u}\right) \tag{4.20}$$

Since, $u'\varepsilon$ is the actual velocity, using the continuity equation for the neat resin in equation (2.50), the equation (4.20) is reduced to

$$\frac{\partial[\varepsilon C]}{\partial t}+u'\varepsilon\cdot\nabla C=-\alpha u C\left(1-\frac{\sigma}{\sigma_u}\right) \tag{4.21}$$

From the boundary conditions presented in Figure 2.4, the specific particle deposit value, σ at the flow front is zero (no filtration at the flow front). Then, the porosity at the flow front is equal to initial (unfiltered) porosity, ε_0. Thus, equation (4.21) is

$$\frac{\partial[C]}{\partial t}+u'\cdot\nabla C=-\frac{\alpha u C}{\varepsilon_0} \tag{4.22}$$

At that point, the two terms at the left hand side of equation (4.22) is the total (substantial) derivative in the Eulerian description, as

$$\frac{D[C]}{Dt}=-\frac{\alpha u C}{\varepsilon_0} \tag{4.23}$$

If a control element is tracked at the flow front using Lagrangian description, equation (4.23) gives the time rate of change of the concentration at the flow front

with u and C is the superficial velocity and concentration value of that particle at the flow front. The the solution of the flow front concentration is

$$C = Be^{-\frac{\alpha u}{\varepsilon_0}\cdot t} \tag{4.24}$$

where B is a constant. The inlet particle concentration in suspension is expressed as C_0 initially at the flow front. Thus, the concentration profile at the flow front is obtained as:

$$C = C_0 e^{-\frac{\alpha u}{\varepsilon_0}\cdot t} \tag{4.25}$$

where α is the filtration coefficient that is expressed using the equation (2.60). Since porosity is equal to initial porosity at the flow front, the filtration coefficient is equal to initial filtration coefficient, α_0 at the flow front. Thus, the final form of the concentration profile at the flow front is:

$$C = C_0 e^{-\frac{\alpha_0 V}{(1-\upsilon_{f,0})}\cdot t} \tag{4.26}$$

The analytical calculations for the same case are performed using equation (4.26), with process parameters in Table 4.1 for the one dimensional mold cavity configuration of Figure 4.1. In Figure 4.8, the particle-filler concentration, C at the flow front is given with analytical and numerical calculations.

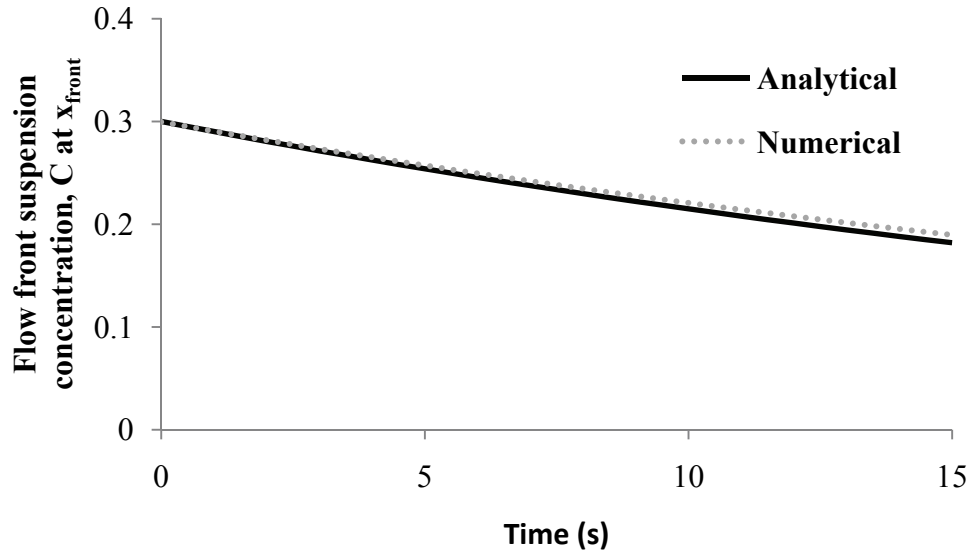

Figure 4.8. Variation of particle-filler concentration at the flow front with time during RTM comparison of analytical and numerical calculations

4.1.1.5 Fill Time in 2-D RTM Process

The fill time for particle-filled resin impregnation can be calculated analytically for constant inlet velocity u_0 through a gate with length L_{gate} and with fiber volume fraction $\upsilon_{f,o}$. The two dimensional geometry for the test case of steady, two dimensional particle-filled resin impregnation through a fibrous preform is a rectangular mold cavity with planar dimensions 0.03 m x 0.5 m. The particle-filled resin is injected at a constant flow rate and the positioning of the gate renders the flow two-dimensional. A sketch of the cavity is shown in Figure 4.9.

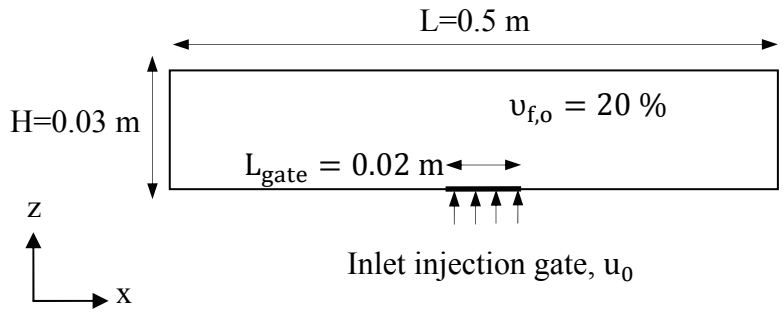

Figure 4.9. 2-D mold cavity configuration

The fill time to completely fill the fibrous preform can be calculated from the relation between the suspension that is injected and the available mold cavity volume (pore volume). The amount of suspension flux depends on the length of the gate, L_{gate} and the inlet injection velocity, u_0. If the total volume of the mold cavity is $\forall_0$, multiplying $\forall_0$ with the unfiltered domain porosity, $(1 - \upsilon_{f,o})$ gives the volume of the pores that can be filled with the suspension. Then, analytical fill time can be expressed as:

$$t_{fill} = \frac{\forall_0}{\frac{u_0}{(1-\upsilon_{f,o})} \cdot L_{gate}} = \frac{\forall_0(1-\upsilon_{f,o})}{u_0 \cdot L_{gate}} \tag{4.27}$$

The process parameters in the current analysis are the same as those in the one dimensional particle-filled resin impregnation, expressed in Table 4.1. In this 2-D simulation the permeability in the x and y directions are the same (isotropic permeability, $K_{xx,o} = K_{yy,o}$) and the principle axis coincides with the coordinate axis. Thus the permeability values at the transverse directions are neglected, $K_{xy,o} = K_{yx,o} = 0$.

During the numerical simulation, fill time is obtained by the tracking of the flow front, as the contours of the level set function, ϕ at the value 0.5. For two

dimensional resin impregnation the analytical fill time and numerical fill time are presented in Table 4.6.

Table 4.6. 2-D fill time result

Description	Analytical fill time (s)	Numerical fill time (s)
Value	45	45

As seen in Table 4.6, the fill times for numerical and analytic results are identical. The flow front progressions during impregnation for the isotropic preform are given in

Figure 4.10. Since the mold cavity mold cavity length is greater than the height of the mold cavity, the flow becomes a 1-D flow after some time. The outlets are defined along the height of the mold at two directions which leads an effective filling.

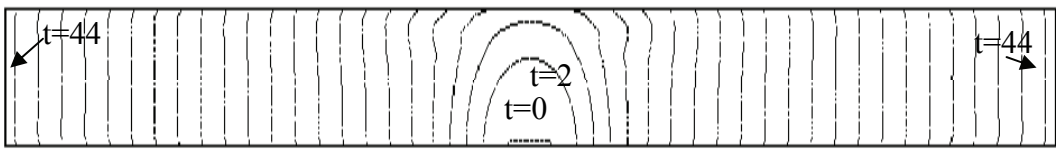

Figure 4.10. Flow front progressions during 2-D RTM ($\Delta t = 2$ sec)

4.1.1.6 Fill Time in 2-D CRTM Process

For the two dimensional suspension injection and compression stages of CRTM process, the injection time and the compression time can be calculated analytically. A sketch of the mold configuration for the injection and the

compression stages is given in Figure 4.11. The analytical injection time can be calculated using equation (4.5), with the parameters given in Figure 4.11. The case corresponds to that described in Table 4.4. The preform is assumed to be isotropic (the permeability values at –xx and –yy direction are same, $K_{xx,o} = K_{yy,o}$). Also, the principle axes is taken to coincide with the coordinate axes, so the permeability values at the transverse directions are zero ($K_{xy,o} = K_{yx,o}=0$).

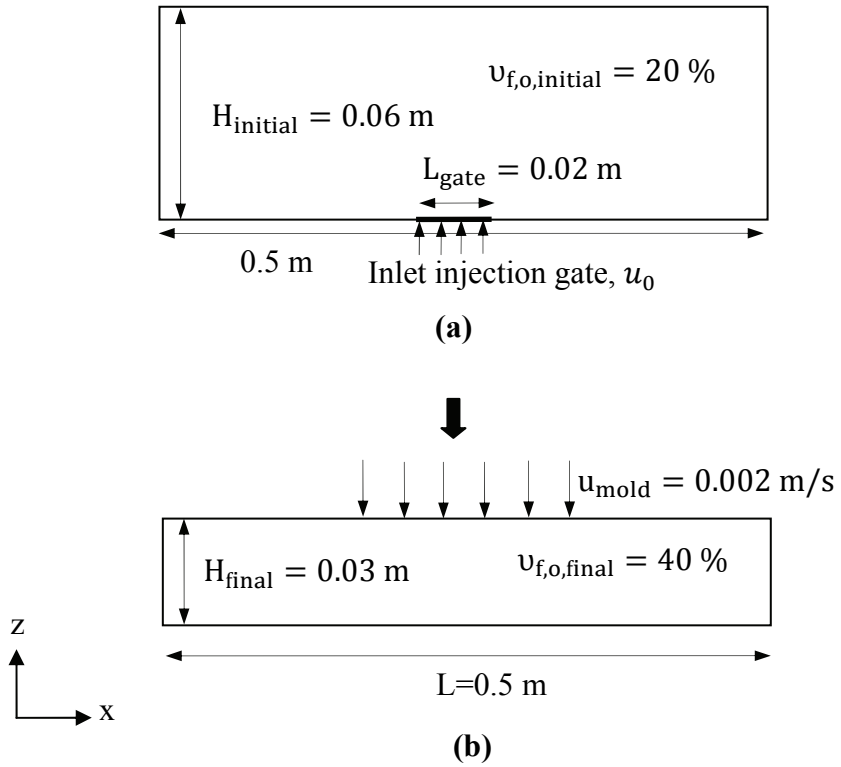

Figure 4.11. Mold configuration for t2-D CRTM, a) impregnation phase, b) compression phase

The analytical and numerical fill time results, given in Table 4.7 are identical. The fill time for injection is determined based on the available volume that will be completely filled by the suspension in the final composite form (as stated in

equation (4.5)) The time for compression is determined according to the mold closing speed and the amount of compression (as presented in equation (4.6)).

Table 4.7. Fill time for the impregnation and the compression phases of 2-D CRTM

Description	Analytical fill time (s)	Numerical fill time (s)
Injection	45	45
Compression	15	15
Total process time	60	60

Figure 4.12 shows the flow front progression for both injection and compression phases. At t=45 s, the injection is complete. Up until that instant, the gap height was constant. Then, the compression stage begins and the gap height begins to decrease, as seen in the figure. The process ends a the end of compression, at t=60, as shown in the Figure 4.12.

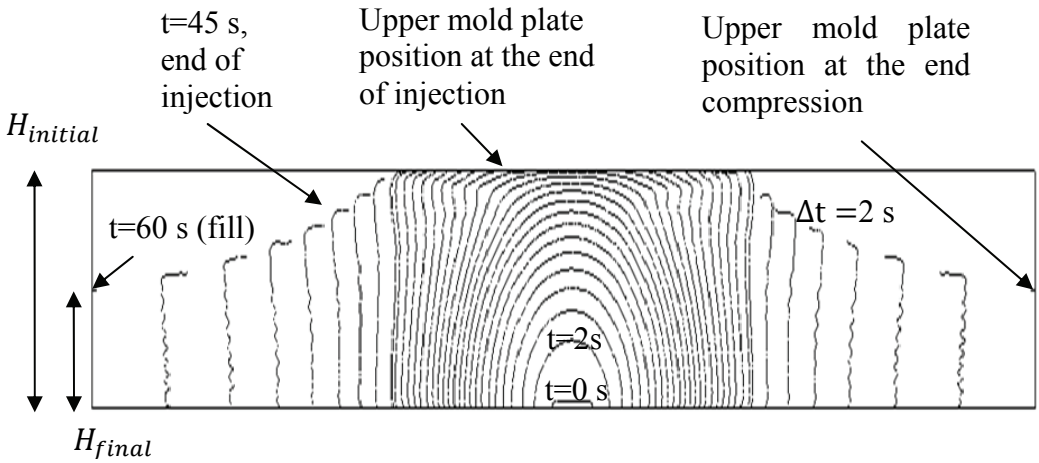

Figure 4.12. Flow front progression during the impregnation and the compression phases of 2-D particle-filled CRTM

4.1.2 Comparison of Numerical Results with Experimental Data

4.1.2.1 Particle Filled RTM

In this part, an experimental study, taken from the literature, on particle-filled resin impregnation in composite manufacturing is examined and results are compared with numerical ones. In the experiment, the resin is unsaturated polyester with a density of 1200 kg/m^3 and a viscosity 0.2 Pa.s. As particle-fillers, spherical glass micro-beads are used. In the experimental set up constant injection pressure (0.2 MPa) is applied to the mold cavity which is 90 mm wide, 4 mm thick (gap-width) and 400 m long [44]. The flow is one-dimensional as the width side of the cavity is a line gate.

The experiments are conducted with different particle-filler sizes and initial suspension concentration values. Depending on the size of the particles, the filtration trends differ. However, there is a clear deep-bed filtration effect seen in the experiment with the large particle-fillers (particle-fillers with large diameters, diameters in 100-200 μm range), which corresponds to the type of filtration that the current model relates to. The numerical analyses are performed for this experiment to demonstrate the applicability of the current mathematical model when model parameters are obtained empirically. The process parameters for the experiment are are given in Table 4.8.

Table 4.8. Process parameters for the particle-filled resin impregnation experimental study [44]

Description	Value
Filler diameters (μm)	48
Initial (inlet) filler content in the resin (C_0, %)	21.6
Fiber volume fraction (ν_f, %)	12.5
Length of the reinforcement (cm)	20
Injection time (s)	320

For the numerical analysis the flow front position is assumed to be a power function time as

$$x_{front} = bt^n \tag{4.28}$$

where b and n are numerical parameters. The velocity model is the same model used in the study [44], which has been obtained from the trend of the measured flow front progression. Then, the actual velocity at the flow front is obtained as

$$V'_{front} = \frac{dx_{front}}{dt} = bnt^{n-1} \tag{4.29}$$

From the mass conservation,

$$\varepsilon V' = \varepsilon_0 V'_{front} = U \tag{4.30}$$

where V' is the velocity at any location along the flow domain and ε is the corresponding porosity. ε_0 is the porosity at the flow front and since there is no specific deposit there, it is equal to the initial (unfiltered) porosity. Then, the Darcy velocity (superficial velocity) U, using equations (4.29), (4.30) and (2.3) is obtained as

$$U = \varepsilon_0 b n t^{n-1} \tag{4.31}$$

In the numerical solution, the Darcy velocity in equation (4.31) is used, without solving for the velocity profile. Since the flow length and fill time are known via Table 4.8, a relation between b and n exists in equation (4.28).

The variation of the filtration coefficient with respect to specific surface is neglected for the simulation. For the initial filtration coefficient, α_0 and specific particle deposit, σ_u values, rearranging the filtration kinetics equation (equation (2.56)) at the inlet (so that $C = C_0$) yields,

$$\frac{d\sigma}{\sigma_u - \sigma} = \frac{\alpha_0 U C_0}{\sigma_u} \tag{4.32}$$

Integrating the equation (4.32) gives

$$-\int \frac{d(\sigma_u - \sigma)}{\sigma_u - \sigma} = -\ln(\sigma_u - \sigma) = \frac{\alpha_0 C_0}{\sigma_u} \int U dt \tag{4.33}$$

Using equation (4.31) and (4.31), equation (4.33) becomes

$$\ln(\sigma_u - \sigma) = -\frac{\alpha_0 C_0 \varepsilon_0}{\sigma_u} \int dx_{front} + constant \tag{4.34}$$

Then equation (4.34) is

$$\ln(\sigma_u - \sigma) = -\frac{\alpha_0 C_0 \varepsilon_0}{\sigma_u} x_{front} + constant \tag{4.35}$$

At the inlet, when $t = 0$, $\sigma = 0$. At that instant, $x_{front} = 0$, so for the inlet specific deposit, equation (4.35) becomes

$$\ln(\sigma_u - \sigma) = -\frac{\alpha_0 C_0 \varepsilon_0}{\sigma_u} x_{front} + \ln \sigma_u \tag{4.36}$$

Then the specific particle deposit at the inlet can be defined as

$$\sigma = \sigma_u \left(1 - e^{-\frac{\alpha_0 C_0 \varepsilon_0}{\sigma_u} x_{front}}\right) \tag{4.37}$$

Using the experimental [44] value for the filler volume fraction at the inlet gate, the specific particle deposit value can be evaluated. The experimental study gives the the total filler volume fraction "$\varepsilon C + \sigma$" distribution in the cavity, when the cavity has been completely filled ($x_{front} = L$). Noting the experimentally measured total filler volume fraction at the inlet gate, $(\varepsilon C + \sigma)_{inlet}$ and knowing that the suspension concentration at the inlet is the known value, C_0 and using the relation between porosity and specific particle deposit from equation (2.42), the specific particle deposit value at the inlet can be calculated as shown in equation (4.38). From the graphicalresults of the experiment [44], the total volume fraction of the fillers at the inlet is read as 0.421633. Thus the specific particle deposit at theinlet is found as

$$\sigma_{inlet} = \frac{(\varepsilon C + \sigma)_{inlet} - (\varepsilon_0 C)_{inlet}}{(1 - C)_{inlet}} = \frac{0.421633 - C_0 \varepsilon_0}{1 - C_0} = 0.296726 \tag{4.39}$$

To determine n and b (numerical parameters), equation (4.28) is used. To determine the initial filtration coefficient, α_0 and specific particle deposit, σ_u values, equation (4.37) is used with inlet specific deposit value in equation (4.39) and a total flow length of $x_{front} = L = 20$ cm. After some trials, the process parameters are found as: $n = 1.3$, $b = 9.225x10^{-5}$, $\alpha_0 = 12\ 1/m$, and $\sigma_u = 0.85$ for an acceptable.

To simulate the experimental process with the mathematical model, the governing equations are; concentration equation (equation (2.45)) where ε is modified with equation (2.42), filtration kinetics equation (equation (2.56)) where the change of filtration coefficient with respect to specific surface is neglected ($\alpha = \alpha_0$) and the empirical relation for the Darcy velocity (superficial velocity, equation (4.31)) with the unknowns, U, C and σ.

In Figure 4.13, the experimental [44] and numerical results for the volume fraction of the fillers at the end of injection are given. With the proper selection of the numerical parameters (n, b, α_0, σ_u), good agreement between the results can be obtained. Thus, once empirical constants such as filtration coefficient or ultimate specific deposit are determined, the current model simulates the trend of filtration closely.

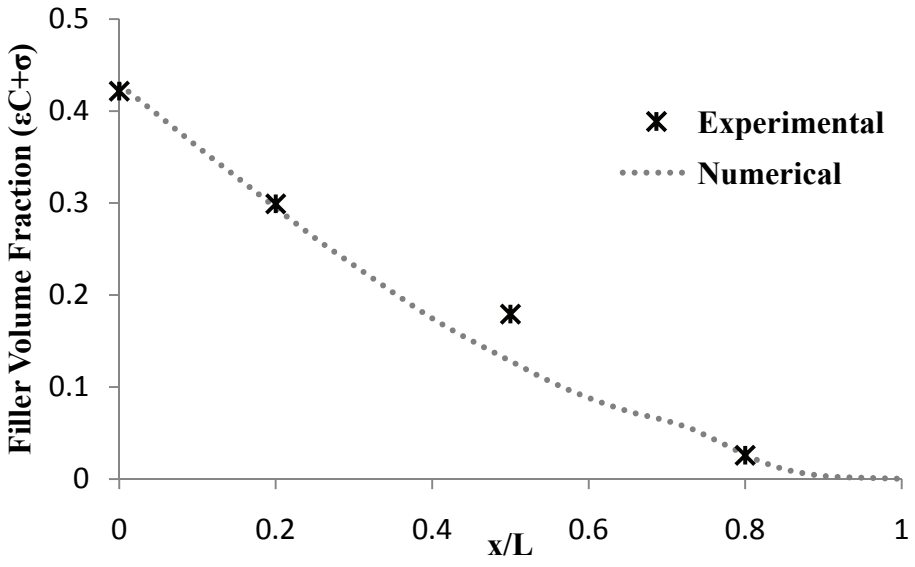

Figure 4.13. Comparisons of filler volume fraction with experimental and numerical solutions

4.1.2.2Comparison of Neat Resin CRTM

In this part the numerical model is validated with the experimental study from the literature. Pham and Trochu [1] presented the experimental analysis of Wirth and Gauvin to investigate the CRTM process. Wirth and Gauvin conducted a set of experiments to study neat resin flow for the mold configuration in Figure 4.14. P and T indicate the pressure sensors and thermocouples, respectively. The six pressure sensors measuring the resin pressure is located at 1.8 cm, 14.8 cm, 25.5

cm, 36.3 cm, 47 cm and 57.8 cm, respectively. The thermocouples measuring the resin temperature, gives the flow front progression in the mold cavity from the temperature gradient data. In the experimental set, loose continuous strand mat is used as reinforcement material and the resin injection and compression take place simultaneously during the CRTM process. As the neat resin is impregnated through fibrous preform, the final height is obtained during the compression of the upper mold plate at the same time. Moreover, Pham and Trochu [1] developed an analytical solution of the pressure distribution in the mold cavity for that description of the CRTM process.

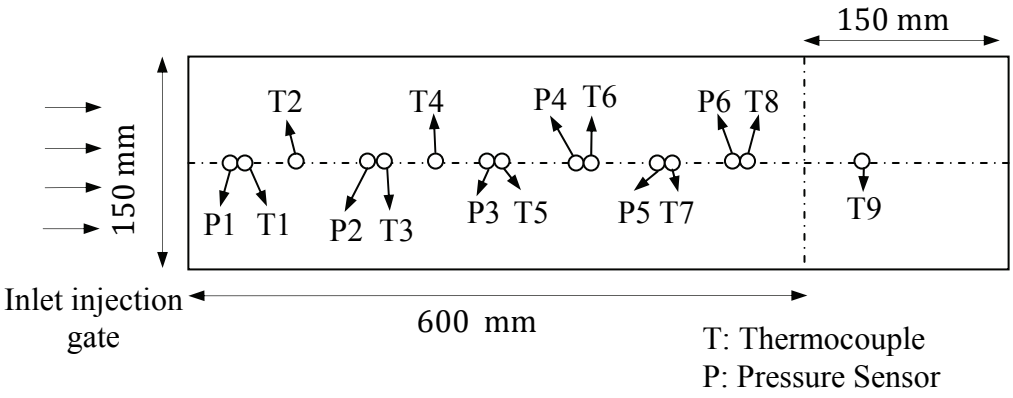

Figure 4.14. Mold cavity configuration of the Wirth and Gauvin experimental study [1]

600 mm is placed in the mold cavity and the process parameters of that experiment is given in Table 4.9. Moreover, the permeability of the OCF-8610 is measured by Pham and Trochu [1] and the change with porosity is given in Figure 4.15. The analytical solution of the pressure distribution along the mold length in the mold cavity for constant inlet gate pressure, p_0, flow front position, x_{front} and mold closing speed, U_z is presented as:

$$p = \frac{1}{2}\frac{U_z}{H}\frac{\mu}{K}x^2 - \left(\frac{1}{2}\frac{U_z}{H}\frac{\mu}{K}x_{front} + \frac{p_0}{x_{front}}\right)\cdot x + p_0 \quad (4.40)$$

Table 4.9. Process parameters of the experiment used in Pham and Trochu [1]

Description	Value	Description	Value
Density of the resin ($\rho_p, kg/m^3$)	1100	Viscosity of neat resin ($\mu_0, Pa \cdot s$)	0.160
Fiber volume fraction ($v_{f,0}$ %)	Initial: 11	Height of the mold (H, mm)	Initial: 5.1
	Final: 18		Final: 3.1
Mold closing speed ($u_{mold}, mm/s$)	0.09	Inlet gate resin pressure (MPa)	0.2
Injection tine (s)	20	Length of the preform (mm)	600

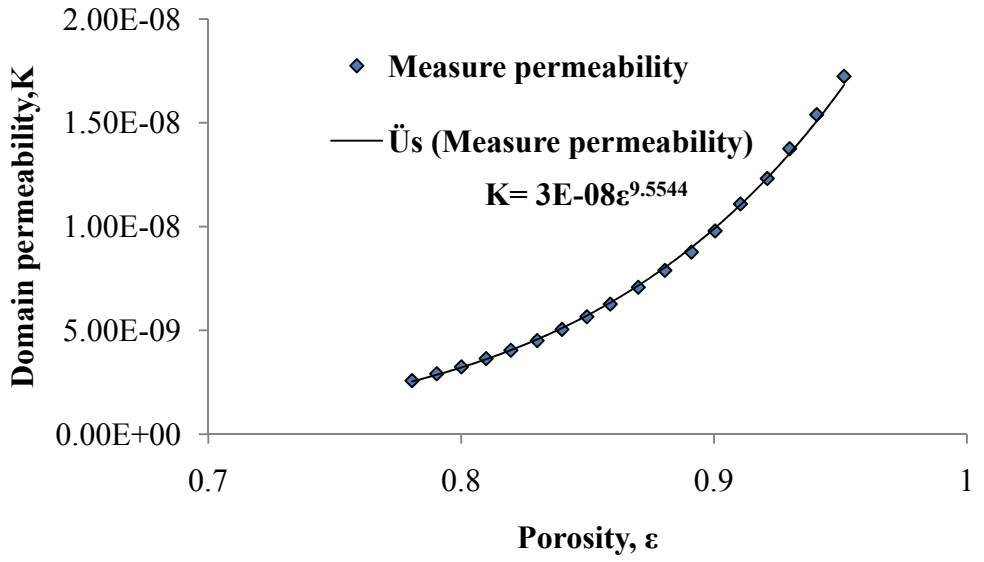

Figure 4.15. Permeability change with porosity from the measurements of Pham and Trochu [1]

In numerical application, the process parameters in Table 4.9are used except the inlet gate pressure. Pham and Trochu state that the inlet pressure is not constant; it is some function of time [1]. From experimental data they observe the inlet pressure is different than the given inlet gate pressure; even the pressure at the inlet gate is a function of time. Even though the injection is performed at constant injection pressure; it takes some time for the resin to reach the constant pressure value. Moreover, the characteristic of the fibrous preform affects the pressure variation in the mold cavity. For example, if the permeability of the fibrous preform is large, the mold cavity is filled before the pressure reaches the injection pressure value. Thus, the authors state that implementation of constant injection pressure is not proper for the numerical and analytical solutions. Thus, the analytical solutions given in [1] are given for inlet gate pressure as a function of time. The inlet pressure is determined using equation (4.40), the analytical results of the saturated cavity length versus time plot and pressure at point P1 versus time plot in that study. The inlet gate pressure is obtained at different time instants and the trend line of that change is used as inlet gate pressure function, as presented in Figure 4.16. The permeability as a function of changing porosity (Figure 4.15) as presented experimentally in [1] is used in the current simulation.

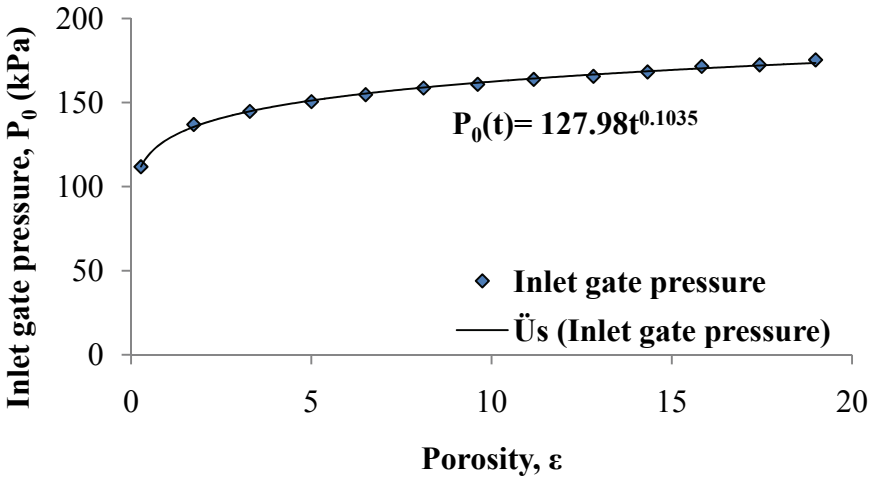

Figure 4.16. Inlet gate pressure distribution obtained from the analytical solution results of Pham and Trochu [1]

Using the inlet pressure of Figure 4.17, the numerical results are obtained via Darcy's law and Level Set Function applications modes of the COMSOL Multiphysics®. Comparison of the pressure variations at three different pressure sensors, P1, P2 and P3, obtained with the experimental study, analytical solution of Pham and Trochu [1] and the numerical result is given in Figure 4.18. As it can be seen in Figure 4.18, the agreement at points P1, P2 and P3 is acceptable. Furthermore, it can be observed from the Figure 4.18, there are fluctuations in the experimental data of the points P2 and P3, especially at point P3. That may stem from experimental conditions and properties of the continuous strand mat. The permeability value of the strand mat can show variations at different locations. Also, the injection pressure during the experiment may fluctuate due to experimental conditions.

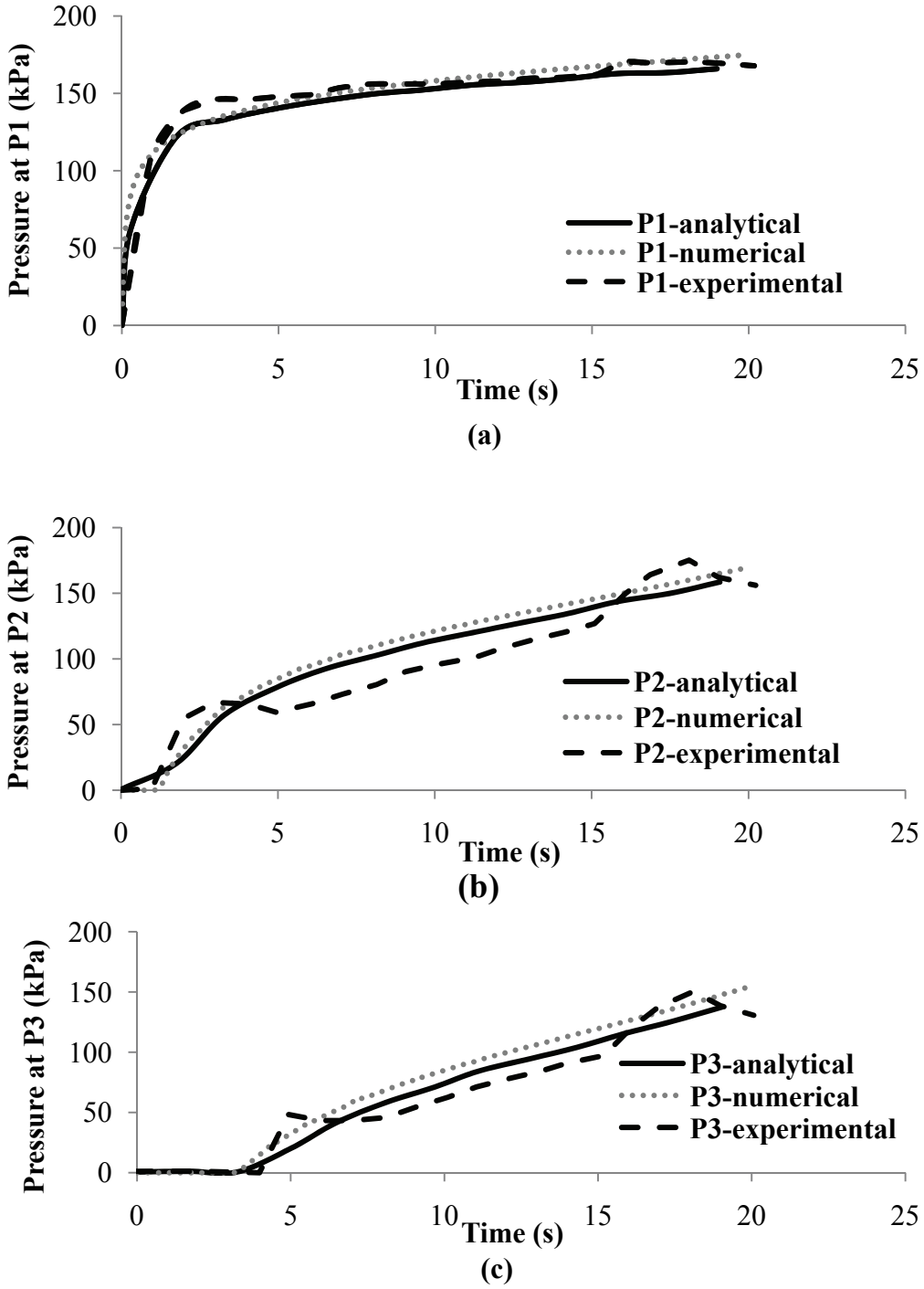

Figure 4.18. Comparisons of the pressure distribution with experimental, analytical and numerical solutions a) pressure at point P1, b) pressure at point P2, c) pressure at point P3

In Figure 4.19, the saturated length (flow front position) versus time is presented for analytical, experimental and numerical simulation. A good agreement is observed between the results. However, the numerical simulation gives flow front data untill t=20 seconds, but measurements for the experimental data and analytical solutions are performed until t=18 seconds.

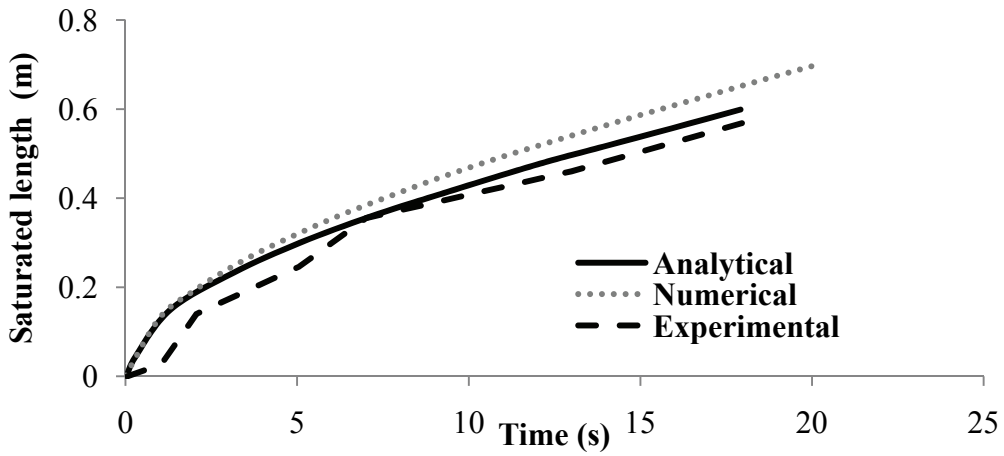

Figure 4.19. Comparison of the saturated length of analytical, numerical and experimental over time

4.2 Process Analysis of RTM and CRTM for 2-D Mold Cavity

In this part RTM and CRTM processes for two dimensional mold cavity configurations are studied. The properties of the final product, produced via RTM and CRTM are compared. In both processes, the same composite (same size/dimension and same fiber volume fraction) is produced. The shape of the composite part is presented in Figure 4.9 for RTM and in Figure 4.11 for CRTM process. In the CRTM process, the mold is initially partially closed thus the cavity thickness is larger. The fibrous preform is assumed to be homogenous and the

permeability is isotropic. The process parameters are presented in Table 4.1 for RTM and Table 4.4 for CRTM process, except the mold closing speed, U_z is defined as 0.0001 m/s, then, the compression time is 300 seconds and the initial filtration coefficient, α_0 is 5 1/m, in order to emphasis the advantages of the CRTM process over RTM process. The amount of particle filled suspension that must be injected during the injection phase of the CRTM is determined from the matrix volume that the composite part will have. This is determined using the final dimensions of the product and the final unfiltered fiber volume fraction (given in Figure 4.11.b). The calculations show that in order to have a final volume fraction of 40 %, $3/8^{th}$ of the initial pore volume (in Figure 4.11.a) must be filled during the injection phase of the CRTM process.

The pressure distribution in the mold cavity is presented at various time instants during the RTM process in Figure 4.20, during the injection phase of the CRTM process in Figure 4.21, and during the compression phase of the CRTM process in Figure 4.22. With the process parameters used in the simulations, the pressure in the mold cavity in CRTM is much lower than the maximum pressure reached in the RTM process as presented in Figure 4.23, which is a great advantage both in terms of the quality of the product which leads less deformation of the preform during the impregnation and in terms of the tooling cost. Since the injection phase of the CRTM takes place through the uncompressed preform where the porosity is higher than that in the RTM process, pressure values are lower than those in RTM process. However, it must be noted that the compression velocity, U_z is high enough plays an important role in the resulting pressure distributions in CRTM. If the compression velocity, U_z is high enough, the pressure levels in CRTM may exceed those in RTM. Thus, the CRTM process must be designed carefully if smaller processing pressures (compared to RTM) are desired.

Figure 4.24 presents the total particle distribution in the mold cavity at different time instants for RTM process. The total particle distribution during the injection and compression phases of CRTM process is given in Figure 4.25and Figure 4.26,

respectively. With CRTM process, the distribution of the particles is more uniform throughout the composite, compared to that in RTM, as shown in Figure 4.27. The effect of compression stage on particle filtration seems to be flattening out the gradients. A highly non-homogeneous particle distribution can yield property variations within the composite, which is undesirable, unless the composite is specially designed as such (e.g. a graded material). With CRTM, a more homogeneous micro structure could be obtained, compared to RTM with process parameters during that simulation set. However, CRTM doesn't give more homogenous products than RTM process at low initial filtration coefficient, α_0 values. For example with α_0 is 1 1/m, the total particle distribution at the end of RTM and at the end of CRTM process are given in Figure 4.28, respectively. As it can be seen in this figure, the total particle distributions at the end of the two processes doesn't show significant difference, even the total particle is slightly more homogeneous at the end of RTM.

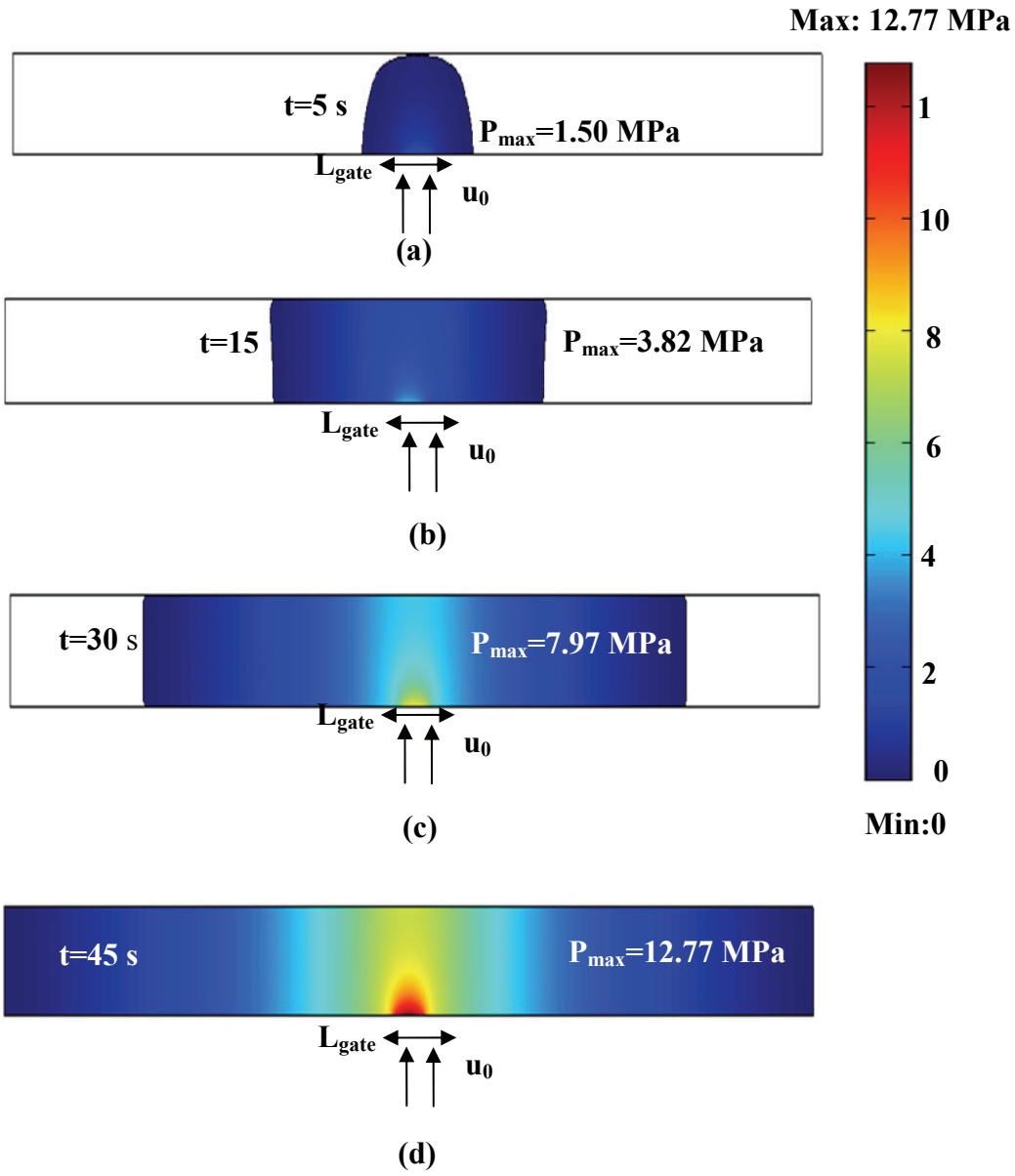

Figure 4.20. Pressure distribution in the mold cavity during RTM process at a) 5 s, b) 15 s, c) 30 s, d) 45s

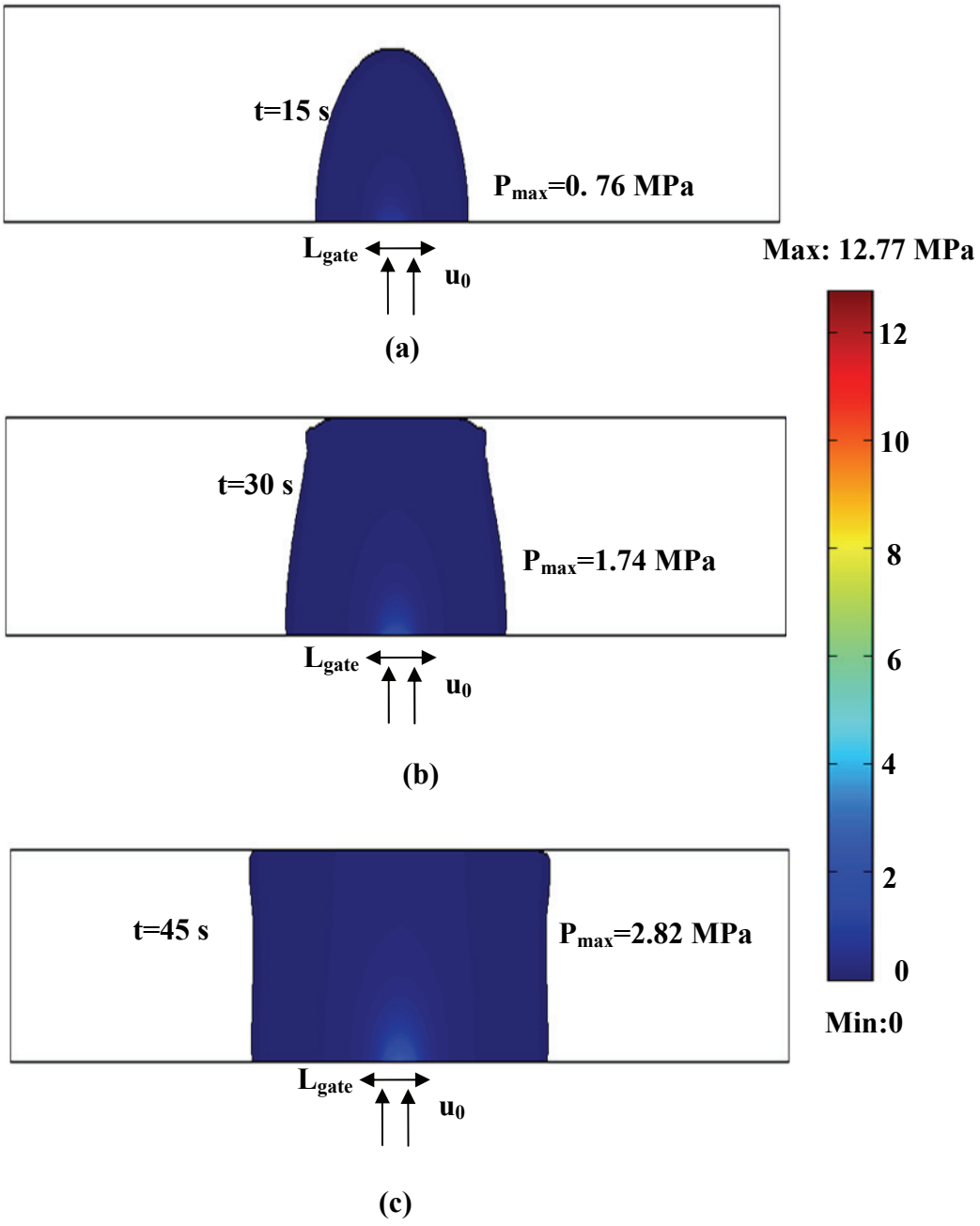

Figure 4.21. Pressure distribution in the mold cavity during the injection phase of CRTM: a) 15 s, b) 30 s, c) 45 s

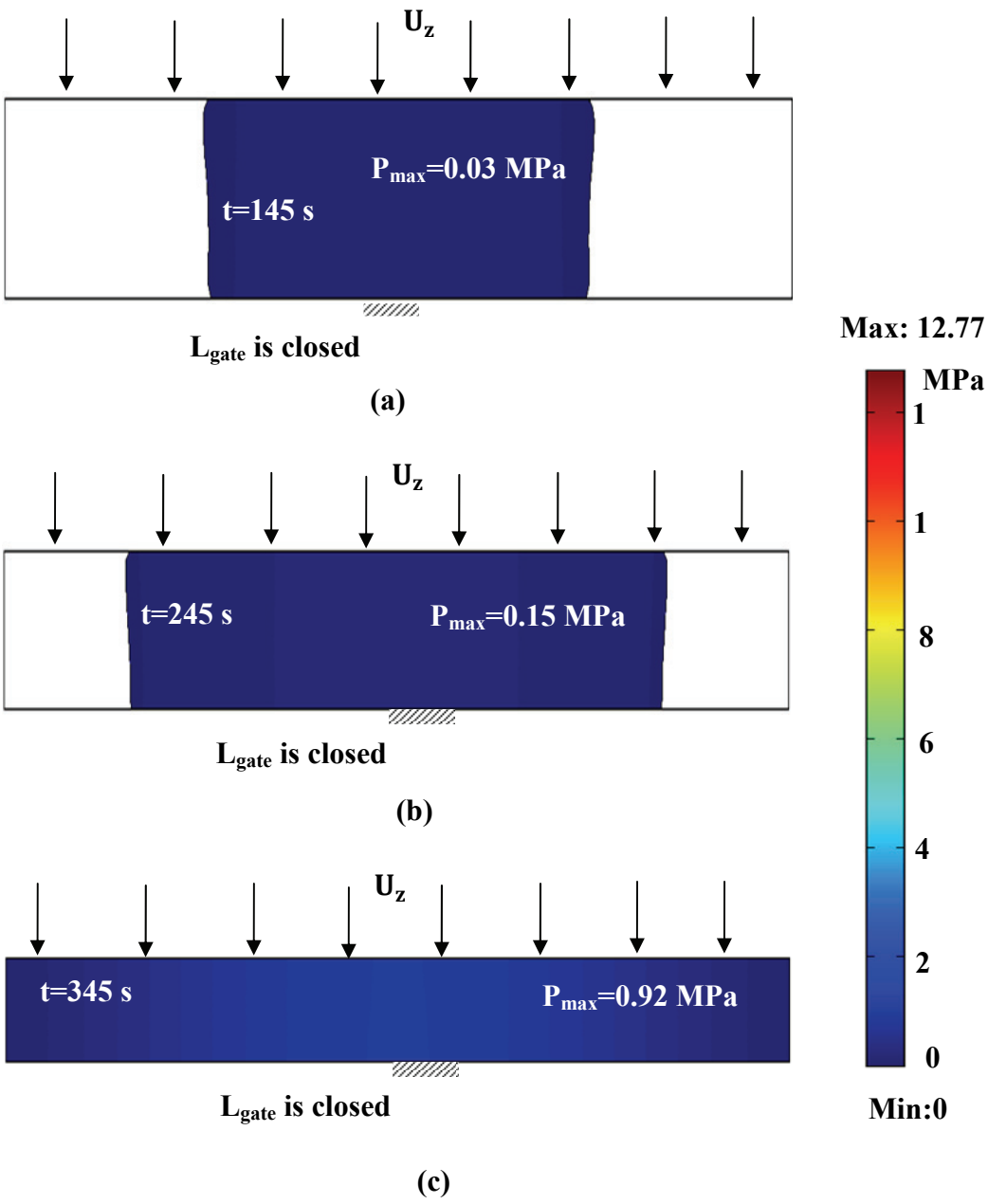

Figure 4.22. Pressure distribution in the mold cavity during the compression phase of CRTM: a) 145 s, b) 245 s, c) 345 s

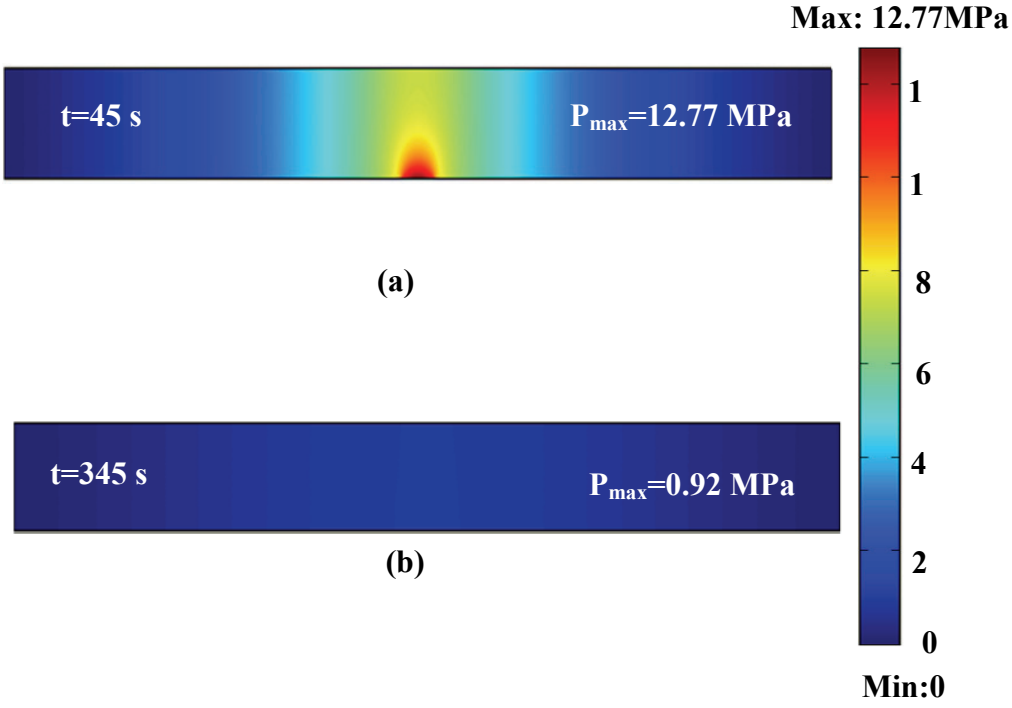

Figure 4.23. Pressure distribution in the 2-D mold cavity: a) at the end of RTM, b) at the end of CRTM

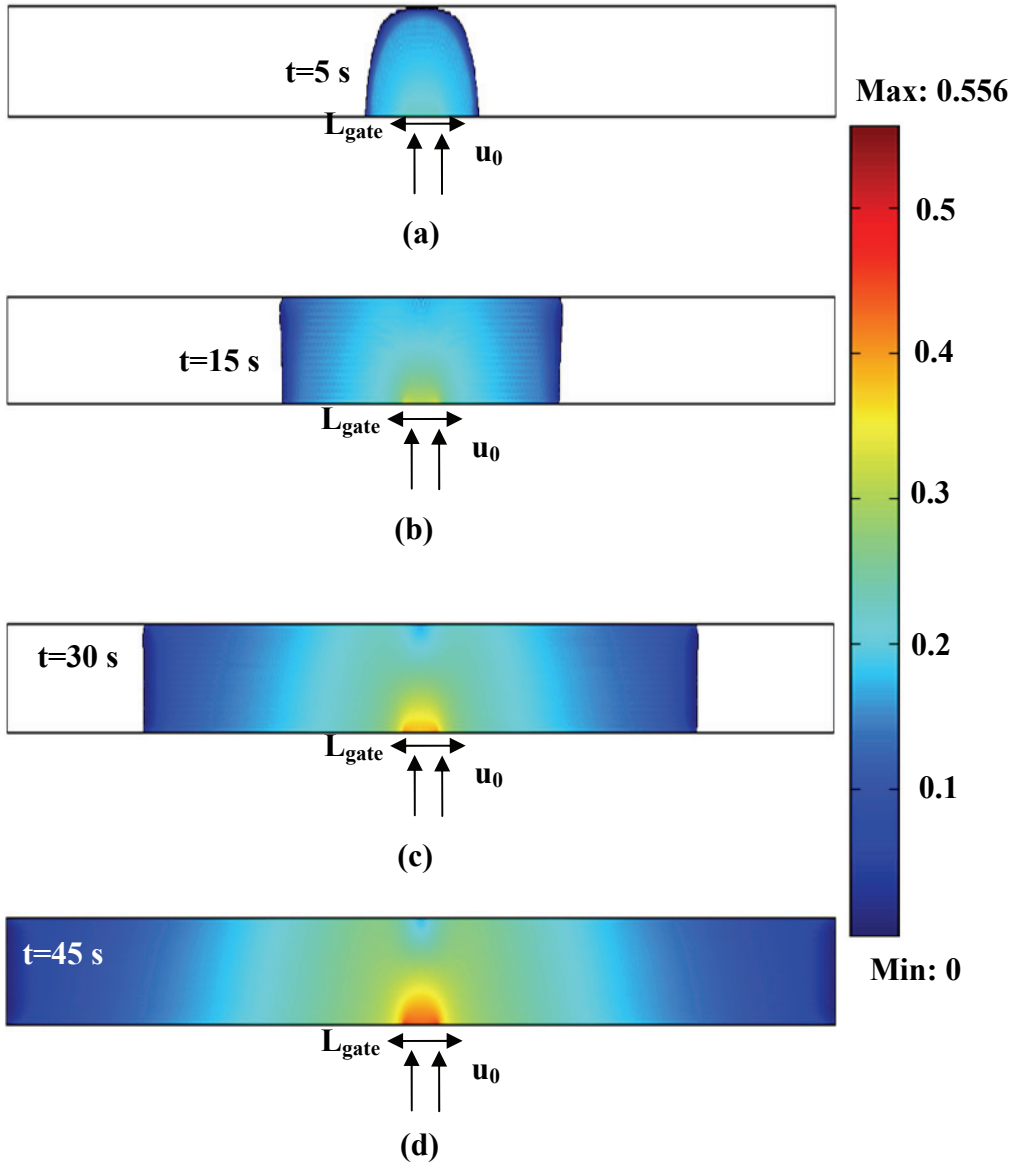

Figure 4.24. Total particle (εC+σ) distribution in the 2-D mold cavity during RTM at a) 5 s, b) 15 s, c) 30 s, d) 45s

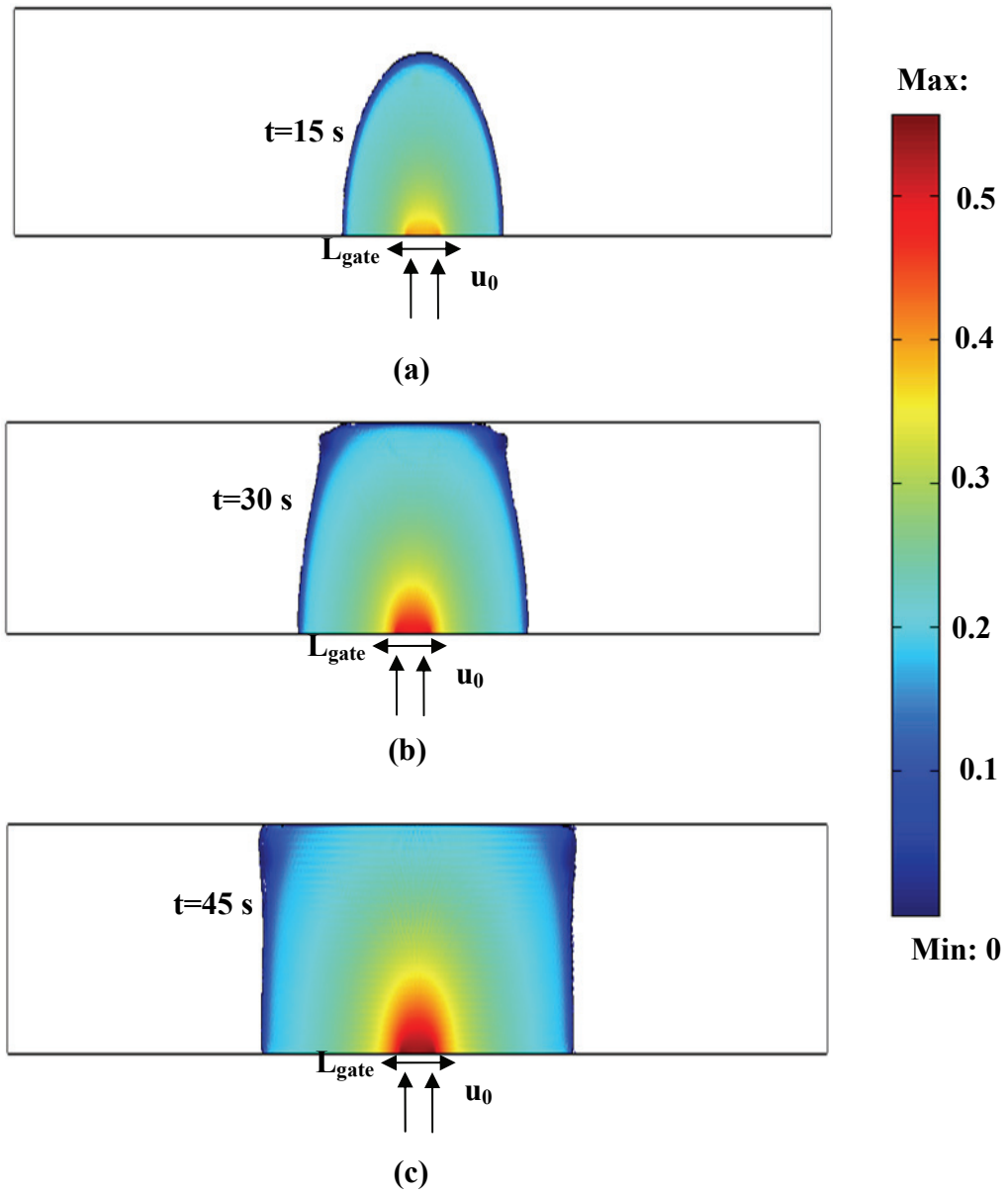

Figure 4.25. Total particle (εC+σ) distribution in the 2-D mold cavity during injection phase of CRTM at a) 15 s, b) 30 s, c) 45 s

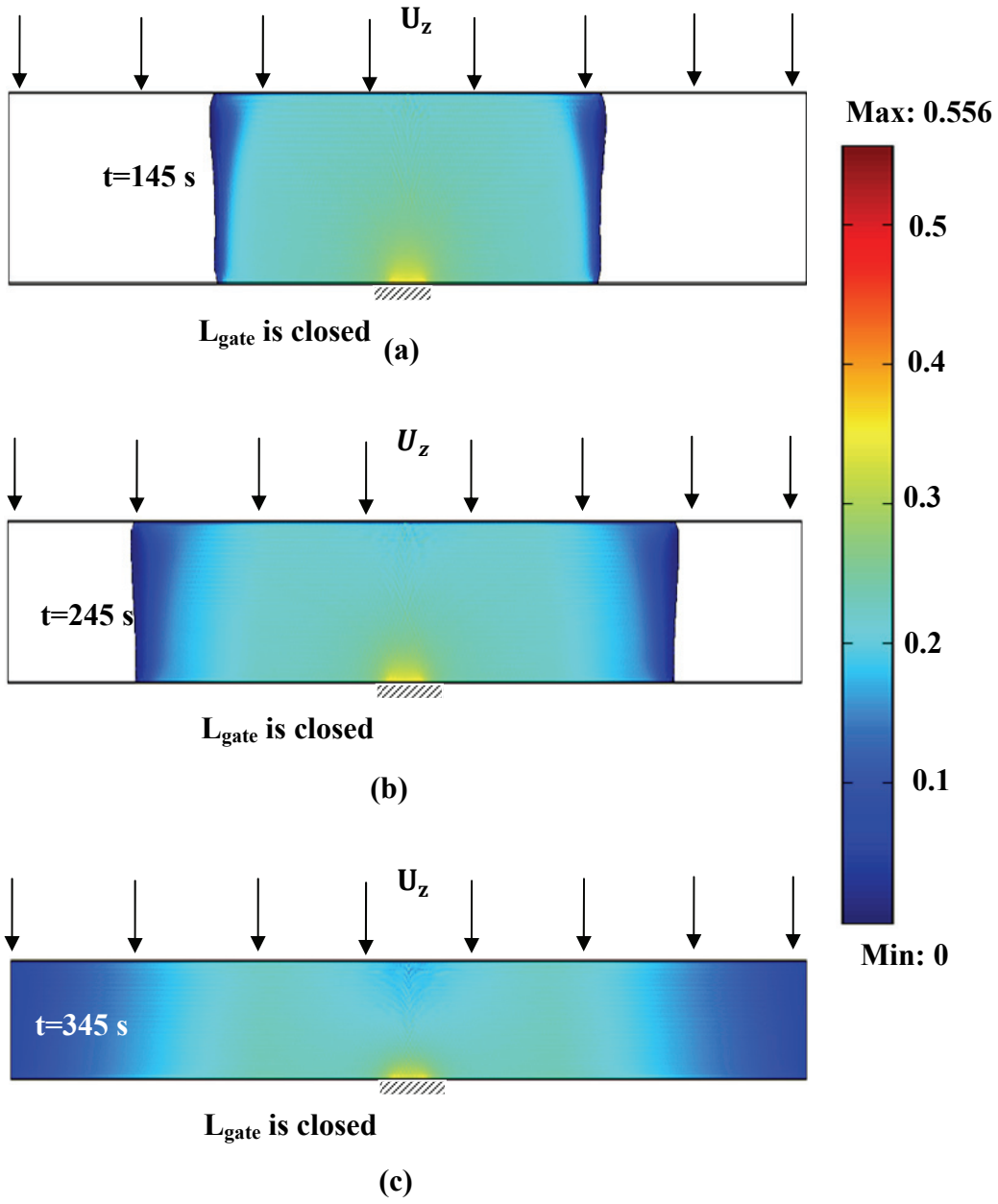

Figure 4.26. Total particle (εC+σ) distribution in the 2-D mold cavity during compression phase of CRTM at a) 145 s, b) 245 s, c) 345 s

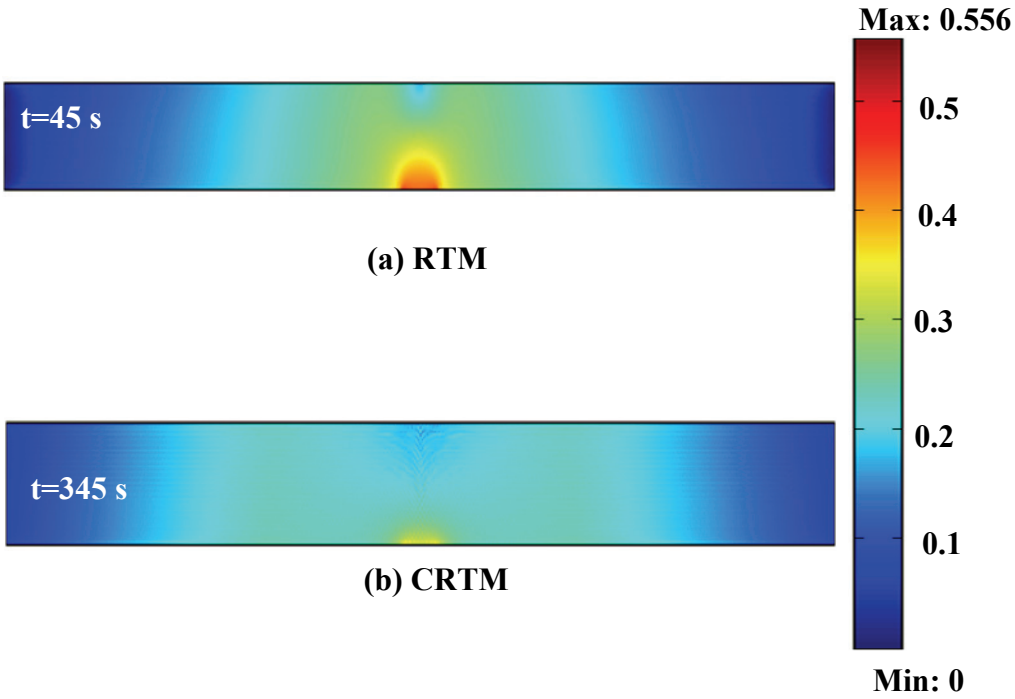

Figure 4.27. Total particle (εC+σ) distribution in the 2-D mold cavity with α_0=5 1/m: a) at the end of RTM, b) at the end of CRTM

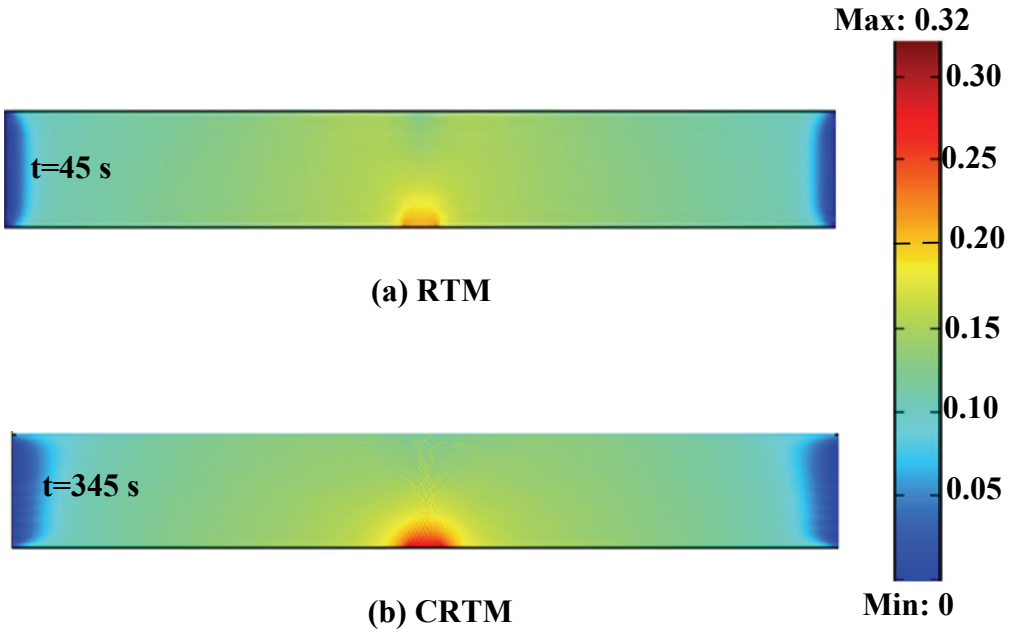

Figure 4.28. Total particle (εC+σ) distribution in the 2-D mold cavity with α_0=1 1/m: a) at the end of RTM, b) at the end of CRTM

4.3 Investigation of the Process Parameters of CRTM

CRTM process to be favorable than RTM process depends on the process parameters. These parameters, directly affecting the effectiveness of the CRTM process are the mold closing speed, U_z, injection volumetric flux per cavity width, Q and the change in the initial and final mold height and the initial, $H_{initial} - H_{final}$.

In Figure 4.29 the pressure distribution along the mold cavity at the end of RTM and CRTM processes with different mold closing speeds are given. The simulations are performed for the mold configuration in Figure 4.1 for RTM process and Figure 4.4 for the CRTM process with the process parameters given in Table 4.1and Table 4.4, respectively. Only parameter changed during the simulation is the mold closing speed, so as the compression time. As seen from Figure 4.29, the pressure values increases with the increase of mold closing speed, U_z. With the mold closing speed values less than 0.002, the pressure values reached at the end of CRTM process is less than RTM process. However, as the mold closing speed decreases, the compression time increase.

The total particle distributions along the mold cavity at the end of RTM and at the end of CRTM process with different mold closing speeds are given in Figure 4.30. The total particle distribution, $\varepsilon C + \sigma$ does not show significant difference with different mold closing speeds and with the distribution at the end of RTM process.

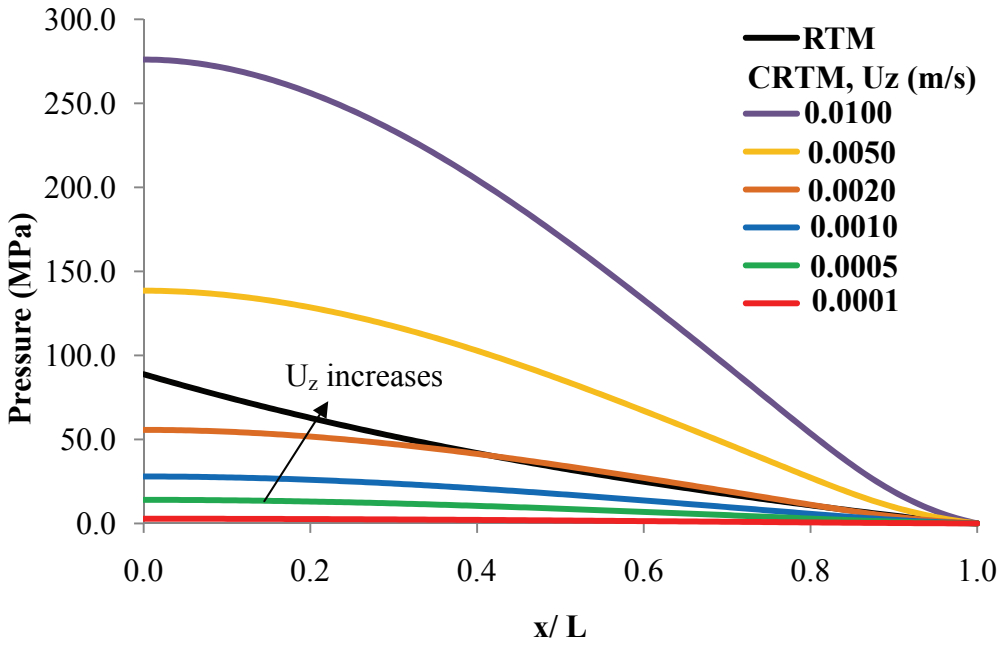

Figure 4.29. Pressure distributions along the mold cavity at the end of RTM and CRTM processes with different mold closing speeds

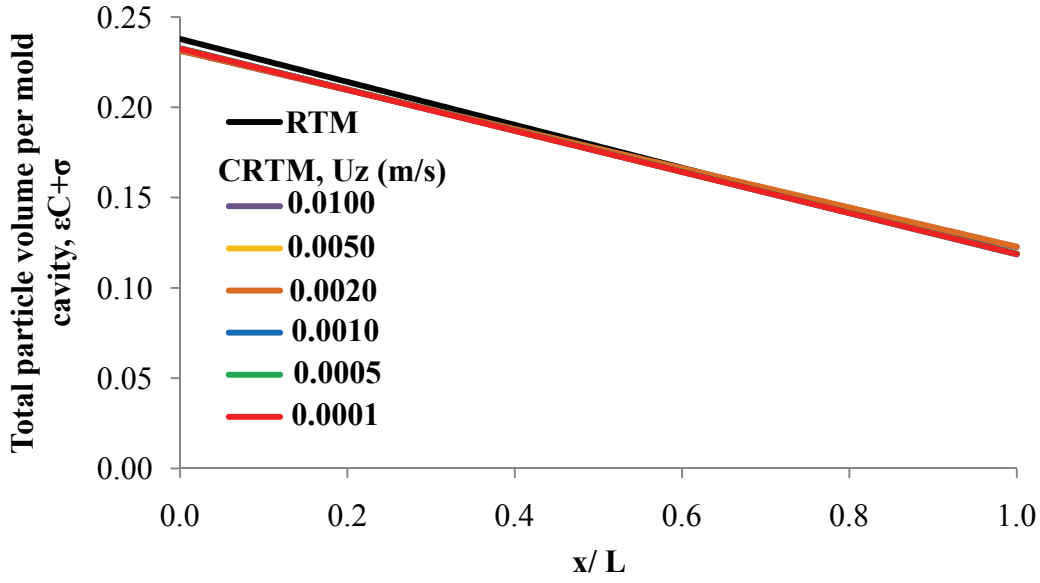

Figure 4.30. Total particle distribution along the mold cavity at the end of RTM and CRTM processes with different mold closing speeds

In Figure 4.31, the pressure distribution along the mold cavity at the end of RTM and CRTM processes with different injection volumetric flow per cavity width. The mold configuration in Figure 4.1 for RTM process and in Figure 4.4 for the CRTM process are used with the process parameters given in Table 4.1and Table 4.4, except the mold closing speed is 0.0005 m/s. The fill time is changed with the injection volumetric flow per cavity width. For the RTM process from Figure 4.31, the pressure values increases with increasing volumetric flux. The pressure values at the end of CRTM process is observed to decrease with increasing volumetric flux at the injection gate but this variation is not as significant as in the RTM process pressure distribution results. In Figure 4.32, the change in the total particle distribution with inlet volumetric flow per width is given. There is no considerable variations, that is there is no relation between inlet volumetric flow per width and particle distributions in the mold cavity in RTM and CRTM processes.

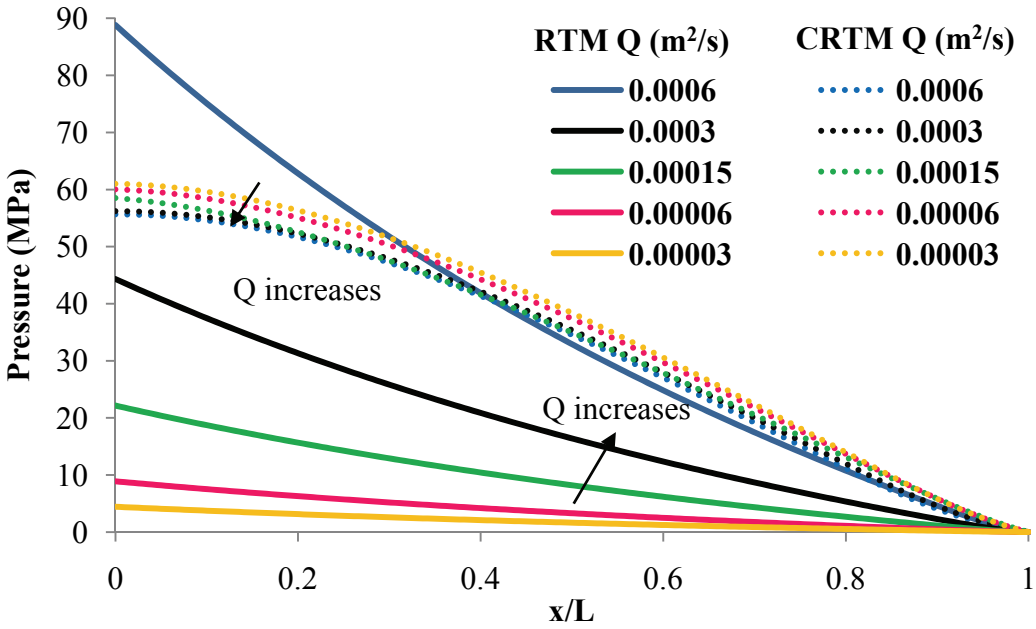

Figure 4.31. Pressure distributions along the mold cavity at the end of RTM and CRTM processes with different inlet gate fluxes

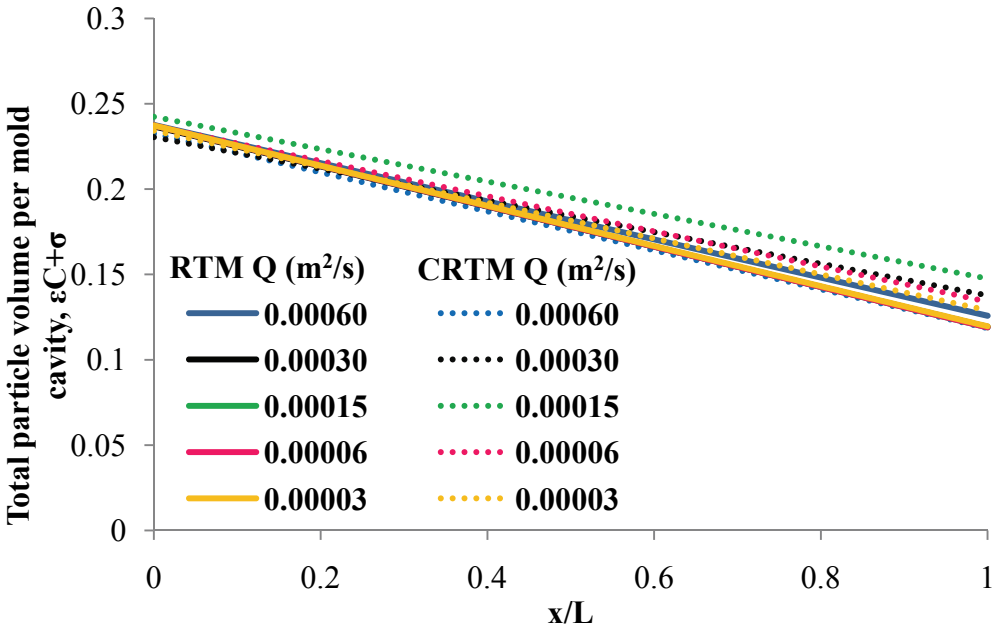

Figure 4.32. Total particle distribution along the mold cavity at the end of RTM and CRTM processes with different inlet gate fluxes

Finally, the initial mold gap (height) is changed to obtain the same composite product. Again, the mold configurations in Figure 4.1 for RTM process and in Figure 4.4 for the CRTM process are used with the process parameters given in Table 4.1and Table 4.4. However, the mold closing speed is 0.0005 m/s and the change in the process parameter to get the same composite product are given in Table 4.10. The pressure distribution at the end of RTM has larger pressure values than CRTM process and the pressure distribution has no difference for different inlet mold gap values, as presented in Figure 4.33. In Figure 4.34, the change in the total particle distribution for different initial mold gap (height) is given. There is no considerable variations, that is there is no relation initial mold gap (height) and particle distributions in the mold cavity in RTM and CRTM processes.

Table 4.10. The changes in the process parameters for different initial gap height analysis

$H_{initial}$ (m)	Initial fiber volume fraction ($\nu_{f,o,initial}$ %)	Initial Permeability (K_{xx}, m^2)
0.04	0.30	$7.78x10^{-11}$
0.05	0.24	$1.32x10^{-10}$
0.06	0.20	$2.00x10^{-11}$
0.08	0.15	$3.78x10^{-10}$
0.10	0.12	$6.11x10^{-10}$

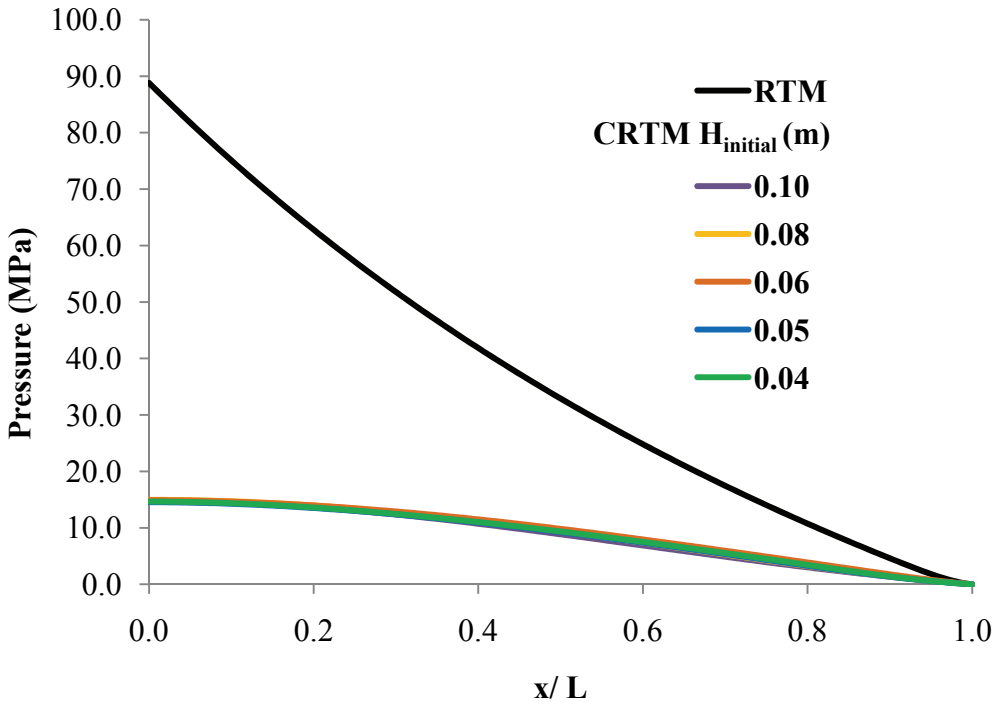

Figure 4.33. Pressure distributions along the mold cavity at the end of RTM and CRTM processes with different initial mold cavity height at the beginning of compression

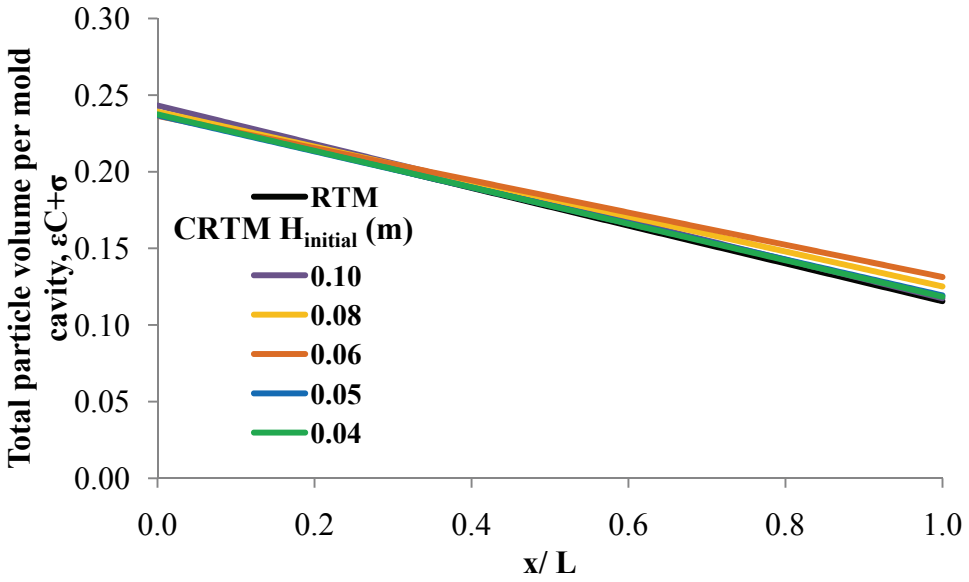

Figure 4.34. Total particle distribution along the mold cavity at the end of RTM and CRTM processes with different initial mold cavity height at the beginning of compression

CHAPTER 5

SUMMARY, CONCLUSIONS AND FUTURE WORK

5.1 Summary and Conclusions

In this study particle-filled resin impregnation through fibrous prefom for Compression Resin Transfer Molding (CRTM) has been studied. Since CRTM is a modification of resin transfer molding (RTM) process, the current research also involves RTM.

In this research, a mathematical model for the numerical modeling of the impregnation of particle-filled resin through the fibrous medium in CRTM has presented. The model is based on coupling Darcy flow with particle filtration, along with mass conservation applied to the two stages of the process: the particle-resin suspension injection and the compression stages. The injection stage model is identical to the resin impregnation in another process, the RTM process, with which CRTM is compared.

The numerical implementation and solution of the injection and the compression phases of CRTM are performed on COMSOL Multiphysics®, a commercial software package. The package is capable of solving a wide variety of well-known partial differential equations (PDE's) – coupled or uncoupled. It also allows the input of other PDE's (using a script) and boundary/initial conditions; such equations can be coupled and solved simultaneously with others. The program can handle geometrically complex solution domains. The package has many flow

modules and Darcy Law for porous flow is a built-in function in this software. The equations for the filtration kinetics and the conservation of particles in the suspension (concentration equation) are introduced via PDE application mode. The problem involves the tracking of the flow front (evolving free surface) which constitutes a freely expanding boundary and presents an irregular flow geometry throughout the impregnation (in both injection and compression stages). In the injection phase, the built-in Level Set Method (LSM) option in the package is used to track the moving flow front. In the compression phase, a moving boundary exists on the mold top plate, so the solution domain is deformed during the compression stage. In this case, the closing of the top plate is simulated by using the ALE (Arbitrary-Lagrangian-Eulerian) Method, which is another built-in module in COMSOL Multiphysics®. The software package allows the post-processing of the results for graphical presentation.

In order to validate numerical simulation results, analytical solutions for simple scenatios are derived and compared with the numerical ones. First, for the simulation of production of a rectangular composite with a line gate (1-D mold configuration) using CRTM and also RTM, fill time, flow front positions, conservation of total particle volume per mold cavity and concentration value at the flow front are obtained numerically and analytically. Following that, for 2-D mold cavity configuration using RTM and CRTM processes, the numerical fill time results are compared with the analytical solutions.

The numerical simulation results of the CRTM process using neat resin is compared with the analytical and experimental pressure distribution and saturated length (flow front position) results, taken from the literature. With the process parameters of the experiment, the simulations have been performed to determine pressure variation with time at several locations along the flow. As one of the input parameters to the solution, the injection pressure variation with time has been extracted from the results of the study from which the experimental case has been taken, and used in the numerical simulation.

To assess the validity of the filtration model, a 1-D resin impregnation experiment case from the literature has been used in the numerical simulation. In this part of the study, the model parameters for filtration which are empirical have been obtained from the results of the experiment.

After analytical and experimental validations of the numerical model, process analyses of 2-D RTM and CRTM have been performed. This was performed to assess whether CRTM did have the proposed advantages over RTM. In these simulations, the same composite was produced through CRTM and RTM, for the same final dimensions, fiber volume fraction and filler-particle volume.

Finally, the effect of the main process parameters of the CRTM process; mold closing speed, volumetric flow rate per mold width at the inlet gate during injection and the compression ratio of the mold upper plate, on process pressure and filler distributions in the composite have been investigated in a parametric analysis. The compression ratio has been varied by changing the initial cavity gap height, while keeping the final cavity gap thickness the same. The results were compared with the RTM results for the same composite production.

The following conclusions are reached in this study:

1. As one of the goals of the current research, the conservation equations for particle-filled compression stage in CRTM has been derived. The formulation for resin impregnation in CRTM process has been presented.

2. The commercial software COMSOL Multiphysics® can be successfully used to implement the simulation of particle-filled resin impregnation through fibrous preforms in RTM and CRTM processes.

3. The mesh size and the number of mesh elements affect the accuracy of the numerical solution. As the number of mesh elements increase, the accuracy of solution increases. However, beyond a certain number, the solution starts to become unstable and eventually blows up, without giving coherent answers.

4. As the dimension of the problem increases, the run-times increase significantly, with the increased number of mesh elements. The software becomes problematic in 3-D problems, especially in terms of particle filler distribution calculations. Such distributions become numerically unstable, yielding non-sensical results.

5. Numerical simulation results are found to be in very good agreement with the analytical results, in obtaining flow front progressions and fill time. The current numerical scheme yields accurate solutions, once the appropriate mesh architecture has been implemented.

6. The analytical solution for particle concentration on the flow front has been derived for RTM. Comparison with numerical simulations has yielded close agreement, once again confirming the accuracy of numerical solution

7. The flow front tracking is performed successfully with LSM. The analytical fill time and flow front tracking results are in good agreement with the numerical ones. With LSM the flow front is tracked with a scalar level set function value. It is has a value of one at the impregnated region and has a zero value at the unfilled region. The level set function value changes from one to zero at the transition region. The level set function value 0.5 is the flow front. The accuracy of the tracking depends on the thickness of that transition region. For a thin transition region the mesh elements should be high, but this time the gradients at the transition region will be very high and solution becomes unstable.

8. The filtration model has been shown to yield the expected, experimentally-confirmed filtration trends once the empirical filtration parameters are found.

9. The comparison of 2-D RTM and CRTM simulations for producing the same composite showed that the process pressure was lower and the particle distribution more uniform in CRTM than in RTM. However, the relative homogeneity of particle distribution in CRTM depended on the choice of process parameters. In other parameter settings, the particle distribution in CRTM can be less homogeneously distributed, which would not be an advantage of the CRTM process. However, processing pressures are significantly lower in CRTM. Lower

pressure values obtained with CRTM would lead to the decrease of the required clamping force.

10. The parametric analyses for the effect of various process parameters in CRTM have shown the following: As the mold closing is slowed down, the process pressure in CRTM decreases but the total process time is increased. An optimum mold closing speed can be selected to yield lower pressure values than in RTM process, while the process time is still reasonably low. As the volumetric flow rate per mold width at the inlet gate is increased in RTM, the pressure values reached at the end of the process increases. If the volumetric flow rate is increased in exactly the same manner in the injection phase of CRTM, the pressure levels at the end of the process is seen to decrease. However, this decrease is not as significant as the increase in pressure for the RTM process. As the cavity gap height during the compression phase of the CRTM process is changed (increased or decreased), the pressure values do not seem to be affected. The change in the three process parameters investigated, does not seem to have any considerable effect on particle-filler distribution in the mold cavity.

5.2 Future Work

Following the current thesis study, the presented mathematical model can be improved with;

- the inclusion of the elastic behavior of the fibrous preform to the model,
- the consideration of the individual fabric properties and orientations to take the layer characteristics of the preform into account,
- the implementation of different viscosity models from the literature,
- the inclusion of the effect of particle-filler size to the filtration model,
- the addition of thermal behavior of the resin in the mathematical formulations (i.e. the cure stage).

The following can be performed to further the numerical solution scheme,

- the solution can be performed with other commercial software packages, e.g. ANSYS® FLUENT®, and compared with COMSOL Multiphysics® (ANSYS® FLUENT® gain the ability to handle flow front tracking and PDE formulation after this study is initiated.)
- a custom computer program can be developed to have more flexibility (flow front tracking method) with lower cost (commercial package programs are expensive)

Using the present numerical solution obtained via COMSOL Multiphysics®,

- different models for viscosity, permeability can be studied for various irregular mold geometries,
- the effect of variation of the process parameters can be investigated in a more comprehensive manner,
- the effect of different gate and vent location/s can be investigated, e.g. double-gate injection,
- the numerical analysis can be performed with higher capacity computer resources, e.g. parallel processing
- the solution can be extended to the 3-D mold configurations.

Experimental study on the particle-filled injection and compression phases of the CRTM process can be included to

- determine the process parameters needed in the numerical model, e.g, permeability characteristics, empirical model constant of viscosity, the filtration coefficient model coefficient, etc.,
- undertake an extensive validation/modification (if necessary) of the numerical model.

REFERENCES

[1] Pham, X.-T., and Trochu, F., "Simulation of Compression Resin Transfer Molding to Manufacture Thin Composite Shells," *Polymer Composites*, vol. 20, no. 3, pp. 436-459, 1999.

[2] Shojaei, A., "A Numerical Study of Filling Process through Multilayer Preforms in Resin Injection/Compression Molding," *Composites Science and Technology*, vol. 66, no. 11-12, pp. 1546-1557, 2006.

[3] Young, W.-B., "Three-Dimensional Nonisothermal Mold Filling Simulations in Resin Transfer Molding," *Polymer Composites*, vol. 15, no. 2, pp. 118-127, 1994.

[4] Simacek, P., Advani, S. G., and Iobst, S. A., "Modeling Flow in Compression Resin Transfer Molding for Manufacturing of Complex Lightweight High-Performance Automotive Parts," *Journal of Composite Materials*, vol. 42, no. 23, pp. 2523-2545, 2008.

[5] Trochu, F., Gauvin, R., and Gao, D.-M., "Numerical Analysis of the Resin Transfer Molding Process by the Finite Element Method," *Advances in Polymer Technology*, vol. 12, no. 4, pp. 329-342, 1993.

[6] Tan, C. P., and Springer, G. S., "Composite Manufacturing: Simulation of 3-D Resin Transfer Molding," *Journal of Composite Materials*, vol. 33, no. 18, pp. 1716-1742, 1999.

[7] Erdal, M., "Impregnation Molding of Continuous Fiber-Reinforced Ceramic-Ceramic Composites Using Preceramic Polymer," Mechanical Engineering, University of Illinois at Chicago, 1998.

[8] Hieber, C. A., and Shen, S. F., "A Finite-Element/Finite-Difference Simulation of the Injection-Molding Filling Process," *Journal of Non-Newtonian Fluid Mechanics*, vol. 7, no. 1, pp. 1-32, 1980.

[9] Bruschke, M. V., and Advani, S. G., "A Finite Element/Control Volume Approach to Mold Filling in Anisotropic Porous Media," *Polymer Composites*, vol. 11, no. 6, pp. 398-405, 1990.

[10] Simacek, P., and Advani, S. G., "Desirable Features in Mold Filling Simulations for Liquid Composite Molding Processes," *Polymer Composites*, vol. 25, no. 4, pp. 355-367, 2004.

[11] Mathur, R., Advani, S. G., and Fink, B. K., "Use of Genetic Algorithms to Optimize Gate and Vent Locations for the Resin Transfer Molding Process," *Polymer Composites*, vol. 20, no. 2, pp. 167-178, 1999.

[12] Minaie, B., Chen, Y. F., and Mescher, A. M., "A Methodology to Obtain a Desired Filling Pattern During Resin Transfer Molding," *Journal of Composite Materials*, vol. 36, no. 14, pp. 1677-1692, 2002.

[13] Nielsen, D. R., and Pitchumani, R., "Closed-Loop Flow Control in Resin Transfer Molding Using Real-Time Numerical Process Simulations," *Composites Science and Technology*, vol. 62, no. 2, pp. 283-298, 2002.

[14] Lawrence, J. M., Hsiao, K.-T., Don, R. C., Simacek, P., Estrada, G., Sozer, E. M., Stadtfeld, H. C., and Advani, S. G., "An Approach to Couple Mold Design and on-Line Control to Manufacture Complex Composite Parts by Resin Transfer Molding," *Composites Part A: Applied Science and Manufacturing*, vol. 33, no. 7, pp. 981-990, 2002.

[15] Lin, M. Y., Murphy, M. J., and Hahn, H. T., "Resin Transfer Molding Process Optimization," *Composites Part A: Applied Science and Manufacturing*, vol. 31, no. 4, pp. 361-371, 2000.

[16] Simacek, P., and Advani, S. G., "A Numerical Model to Predict Fiber Tow Saturation During Liquid Composite Molding," *Composites Science and Technology*, vol. 63, no. 12, pp. 1725-1736, 2003.

[17] Frederick, R., and Phelan, J., "Simulation of the Injection Process in Resin Transfer Molding," *Polymer Composites*, vol. 18, no. 4, pp. 460-476, 1997.

[18] Bickerton, S., Sozer, E. M., Simácek, P., and Advani, S. G., "Fabric Structure and Mold Curvature Effects on Preform Permeability and Mold Filling in the Rtm Process. Part Ii. Predictions and Comparisons with Experiments," *Composites Part A: Applied Science and Manufacturing*, vol. 31, no. 5, pp. 439-458, 2000.

[19] Shojaei, A., Trochu, F., Ghaffarian, S. R., Karimian, S. M. H., and Lessard, L., "An Experimental Study of Saturated and Unsaturated Permeabilities in Resin Transfer Molding Based on Unidirectional Flow Measurements," *Journal of Reinforced Plastics and Composites*, vol. 23, no. 14, pp. 1515-1536, 2004.

[20] Bhat, P., Merotte, J., Simacek, P., and Advani, S. G., "Process Analysis of Compression Resin Transfer Molding," *Composites Part A: Applied Science and Manufacturing*, vol. 40, no. 4, pp. 431-441, 2009.

[21] Chang, C.-Y., "Simulation of Mold Filling in Simultaneous Resin Injection/Compression Molding," *Journal of Reinforced Plastics and Composites*, vol. 25, no. 12, pp. 1255-1268, 2006.

[22] Shojaei, A., "Numerical Simulation of Three-Dimensional Flow and Analysis of Filling Process in Compression Resin Transfer Moulding," *Composites Part A: Applied Science and Manufacturing*, vol. 37, no. 9, pp. 1434-1450, 2006.

[23] Buntain, M. J., and Bickerton, S., "Modeling Forces Generated within Rigid Liquid Composite Molding Tools. Part A: Experimental Study," *Composites Part A: Applied Science and Manufacturing*, vol. 38, no. 7, pp. 1729-1741, 2007.

[24] Young, W.-B., and Chu, C.-W., *Study on Compression Transfer Molding*, Sage, London, ROYAUME-UNI, 1995.

[25] Brocmann, C., and Michaeli, W., "Injection Compression Moulding–a Low Pressure Process for Manufacturing Textile-Covered Mouldings," *Proceedings of ANTEC' 97*, pp. 441-445, 1997.

[26] Wirth, #160, S., Gauvin, and R., *Experimental Analysis of Mold Filling in Compression Resin Transfer Molding*, Sage, London, ROYAUME-UNI, 1998.

[27] Han, K., Ni, J., Toth, J., Lee, L. J., and Greene, J. P., "Analysis of an Injection/Compression Liquid Composite Molding Process," *Polymer Composites*, vol. 19, no. 4, pp. 487-496, 1998.

[28] Bickerton, S., and Buntain, M. J., "Modeling Forces Generated within Rigid Liquid Composite Molding Tools. Part B: Numerical Analysis," *Composites Part A: Applied Science and Manufacturing*, vol. 38, no. 7, pp. 1742-1754, 2007.

[29] Nordlund, M., Fernberg, S. P., and Lundström, T. S., "Particle Deposition Mechanisms During Processing of Advanced Composite Materials," *Composites Part A: Applied Science and Manufacturing*, vol. 38, no. 10, pp. 2182-2193, 2007.

[30] Erdal, M., Güçeri, S. I., and Danforth, S. C., "Impregnation Molding of Particle-Filled Preceramic Polymers: Process Modeling," *Journal of the American Ceramic Society*, vol. 82, no. 8, pp. 2017-2028, 1999.

[31] Chang-Upp, C., and Chi, T., "Hydrosol Deposition in Fibrous Beds," *Separations Technology*, vol. 1, no. 3, pp. 122-131, 1991.

[32] Herzig, J. P., Leclerc, D. M., and Goff, P. L., "Flow of Suspensions through Porous Media—Application to Deep Filtration," *Industrial & Engineering Chemistry*, vol. 62, no. 5, pp. 8-35, 1970.

[33] Alvarez, A. C., and Et Al., "A Fast Inverse Solver for the Filtration Function for Flow of Water with Particles in Porous Media," *Inverse Problems*, vol. 22, no. 1, pp. 69, 2006.

[34] Bedrikovetsky P G, M. D., Shecaira F, Serra a L, and E, R., "Characterization of Deep Bed Filtration System from Laboratory Pressure Drop Measurements," vol. 32, no. 2-4, pp. 167, 2001.

[35] Vengimalla, R., Chase, G. G., and Ramarao, B. V., "Modeling of Filler Retention in Compressible Fibrous Media," *Separation and Purification Technology*, vol. 15, no. 2, pp. 153-161, 1999.

[36] Jung, Y., and Tien, C., "Granular Filtration of Polydispersed Aerosols," *Filtration & Separation*, vol. 30, no. 3, pp. 253-257, 240, 1993.

[37] Sahimi, M., Gavalas, G. R., and Tsotsis, T. T., "Statistical and Continuum Models of Fluid-Solid Reactions in Porous Media," *Chemical Engineering Science*, vol. 45, no. 6, pp. 1443-1502, 1990.

[38] Sahimi, M., and Imdakm, A. O., "Hydrodynamics of Particulate Motion in Porous Media," *Physical Review Letters*, vol. 66, no. 9, pp. 1169, 1991.

[39] Chohra, M., Advani, S. G., Gokce, A., and Yarlagadda, S., "Modeling of Filtration through Multiple Layers of Dual Scale Fibrous Porous Media," *Polymer Composites*, vol. 27, no. 5, pp. 570-581, 2006.

[40] Chohra, M., Advani, S., and Yarlagadda, S., "Filtration of Particles through a Single Layer of Dual Scale Fibrous Porous Media " *Advanced Composites Letters*, vol. 16, no. 6, pp. 205-221, 2007

[41] Li, Y., and Park, C. W., "Effective Medium Approximation and Deposition of Colloidal Particles in Fibrous and Granular Media," *Advances in Colloid and Interface Science*, vol. 87, no. 1, pp. 1-74, 2000.

[42] Nazarbol M. A., Chen X., Hearle J. W. S., Lydon R., and Moss M., "Effect of Different Particle Shapes on the Modelling of Woven Fabric Filtration," *Journal of Information and Computing Science*, vol. 2, no. 2, pp. 111-118, 2007.

[43] Lefevre, D., Comas-Cardona, S., Binetruy, C., and Krawczak, P., "Coupling Filtration and Flow During Liquid Composite Molding: Experimental Investigation and Simulation," *Composites Science and Technology*, vol. 69, no. 13, pp. 2127-2134, 2009.

[44] Lefevre, D., Comas-Cardona, S., Binétruy, C., and Krawczak, P., "Modelling the Flow of Particle-Filled Resin through a Fibrous Preform in Liquid Composite Molding Technologies," *Composites Part A: Applied Science and Manufacturing*, vol. 38, no. 10, pp. 2154-2163, 2007.

[45] Ives, K. J., "The Scientific Basis of Filtration," *Proceedings of the NATO Advanced Study Institute on the Scientific Basis of Filtration, Leyden, Noordhoof Int. Pub. Co.*, pp. 183-224, 1975.

[46] Adin, A., and Rebhun, M., "A Model to Predict Concentration and Head-Loss Profiles in Filtration " *Journal AWWA*, vol. 69, no. 8, pp. 444-453, 1977.

[47] Tobiason, J. E., and O'melia, C. R., "Physicochemical Aspects of Particle Removal in Depth Filtration," *Journal AWWA*, vol. 80, no. 12, pp. 54-64, 1995.

[48] Tobiason, J. E., Johnson, G. S., Westerhoff, P. K., and Wigneswaran, B., "Particle Size and Chemical Effects on Contact Filtration Performance," *ASCE Journal of Environmental Engineering*, vol. 119, no. 3, pp. 520-538, 1993.

[49] Moguedet, M., Namy, P., and Bereaux, Y., "On the Use of Comsol Multiphysics to Understand and Optimize the Filling Phase in the Injection and Micro-Injection Molding Process," *Proceedings of COMSOL Users Conference*, Grenoble, 2007.

[50] Otmani R. El., M. Zinet, M. Boutaous, P. Chantrenne, and Benhadid, H., "Numerical Simulation of the Filling Stage in the Polymer Injection Moulding Process," *Proceedings of COMSOL Users Conference* Grenoble, 2007.

[51] Varela, A. E., "Isothermal Filling of an Injection Molding Cavity Simulated with the Level Set Method," *Proceedings of Modelling and Simulation*, Montreal, QC, Canada, 2007.

[52] Comsol, "Comsol Multiphysics User's Guide," November 2008.

[53] Zimmerman, W. B. J., *Process Modelling and Simulation with Finite Element Methods*, World Scientific, Singapore, 2006.

[54] Naber, J., "A Runge-Kutta Discontinuous-Galerkin Level-Set Method for Unsteady Compressible Two-Fluid Flow," Department of Aerospace Engineering, Delft University of Technology, December 2005.

[55] Donea J., H. A., Ponthot J.P., Rodr´ıguez-Ferran A., *Encyclopedia of Computational Mechanics*, John Wiley & Sons, Ltd, 2004.

APPENDIX A

A GUIDE FOR COMSOL MULTIPHYSICS MODELING

In this part, the steps of the simulations performed in the study using COMSOL Multiphysics® version 3.5a are presented in detail. One-dimensional CRTM simulation with the geometric properties given in Figure 4.4, with the process parameters listed in Table 4.4 is explained. First the steps of the simulation of the injection phase are as below.

1. Start COMSOL Multiphysics

2. In the Model Navigator set the Space Dimension to 2D (by default)

3. In the list of application modes select Chemical Engineering Module → Momentum Transport → Porous Media Flow → Darcy's Law → Transient analysis → click to Multiphysics (right of the model navigator window) → Add. (The Darcy's Law is added to the list of the equations to be solved)

4. In the list of application modes select Chemical Engineering Module → Momentum Transport → Multiphase Flow → Level Set →Add. (The level Set Method is added to the list of the equations to be solved to track the flow front)

5. In the list of application modes select Comsol Multiphysics Module → PDE Modes → PDE, Coefficient Form → Time-dependent analysis →Change dependent variable name to "sigma"→Add. (The PDE form to handle filtration is added)

6. In the list of application modes select Comsol Multiphysics Module → PDE Modes → PDE, Coefficient Form → Time-dependent analysis →Change dependent variable name to "C"→Add. (The PDE form to handle concentration equation is added).

In Figure A.1 the final form of the Model Navigator is given. Then, click "OK" to continue.

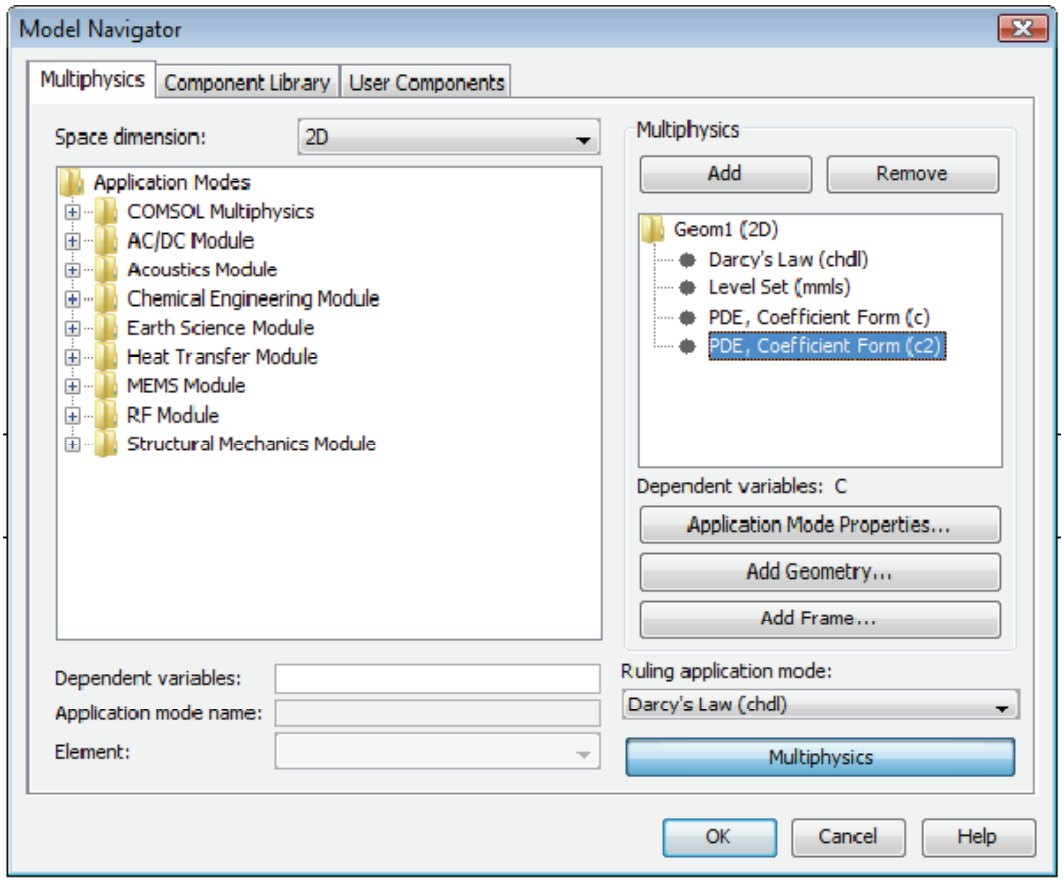

Figure A.1. Snapshot of the model navigator for the simulation of injection phase

After clicking "OK", the program is opened with Draw Mode.

7. To draw the geometry, shift+click to rectangle/squre box in the column at the left side. To draw the 0.5x0.06 rectangle, of which width and height is defined as in Figure A.2. The geometry is obtained after clicking "OK".

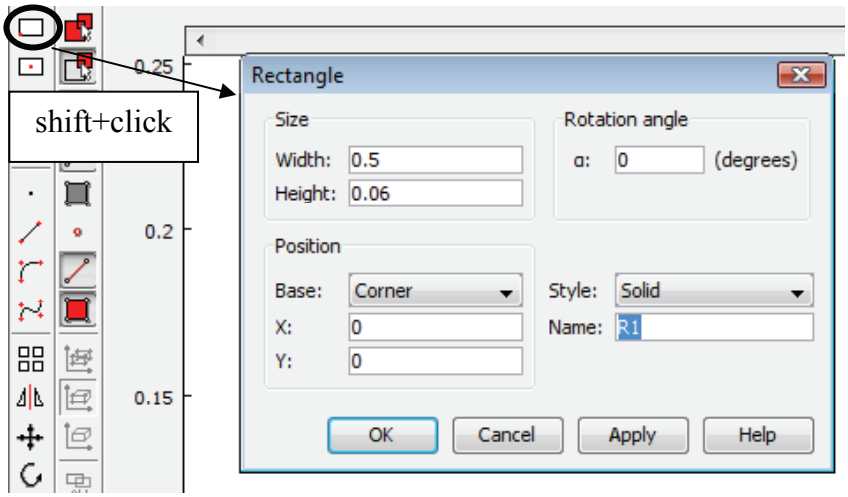

Figure A.2. Snapshot of drawing the geometry

Then, the constants and the expressions are defined.

8. Open the Constant dialog from Options menu.

9. Enter the constant in the following table.

Table A.1. The constants used in the simulation of the injection phase

Name	Expressions	Name	Expressions
rho_a	1200[kg/m^3]	kappa_0	0.2e-9 [m^2]
rho_p	1200 [kg/m^3]	epsilon_0	0.8
eta_a	0.01e-1 [Pa*s]	sigma_u	0.5
eta_p0	1e-1 [Pa*s]	a1	1
alpha_0	1 [1/m]	u_0	0.01 [m/s]
C_0	0.3	H	0.06 [m]
A	0.68	u_ale	0.002 [m/s]
a2	1	t_fill	15 [s]

10. Open the Scalar Expressions dialog from Options→Expressions menu.

11. Enter the expressions in the following table.

Table A.2. Scalar expressions used in the simulation of the injection phase

rho	rho_a+phi*(rho_p-rho_a)
eta_p	eta_p0*(1-C/A)^(-2)
eta	eta_a+phi*(eta_p-eta_a)
kappa	kappa_0*((epsilon_chdl/epsilon_0)*((1-epsilon_chdl)/(1epsilon_0))^(-2))^a2
alpha	alpha_0*((kappa/kappa_0)^(-0.5)*((epsilon_chdl)/(epsilon_0))^(1.5))^a1
U	abs(U_chdl)
const_sigma	((phi<=0.5)*0+(phi>0.5)*1)
const_C	((phi<0.5)*0+(phi>=0.5)*1)

12. For the subdomain settings of the equations inserted to the program, first Dacy's Law settings are performed. From Multiphysics menu, select Darcy's Law (chdl). Then, select Subdomain setting dialog in the Physics menu. The Darcy's Law and the continuity equations in the mathematical formulation (equation (2.1) and equation (2.51), respectively) are implemented to the program. The general form of the equation defined in the software is given on the top of the snapshot given in Figure A.3. In order to obtain the mathematical relations developed in the Chapter 2, the value/expression part should be filled properly. First the time scaling coefficient is necessary for numerical stability. For example, if the time scaling coefficient, δ_{ts} and source term, F are set to zero, solution does not converges due to the numerical instabilities. Then time scaling coefficient is set to 1. The change of the porosity with filtration in equation (2.42), is written as "epsilon_0 – sigma", where epsilon_0 is the unfiltered domain porosity and sigma is the specific particle deposit. The definition of the density and the viscosity as a function of level set function is defined in the Scalar Expression part. The change of the domain permeability is also handled with assigning the K value as "kappa" where kappa is defined as a function in the expression part according to the relation given in equation (2.61).

The expression for the source term, F in Figure A.3 is necessary to obtain the form in the mathematical formulation in Chapter 2, which is the combination of equations (2.1) and (2.51). In the description of source term, F the "d(epsilon_chdl*rho_chdl,t)" indicates the time derivative of the multiplication of porosity and density expressions, that are entered in the Subdomain Setting of the Darcy's Law. "u_chdl" is the superficial velocity obtained via the solution of the Darcy's Law.

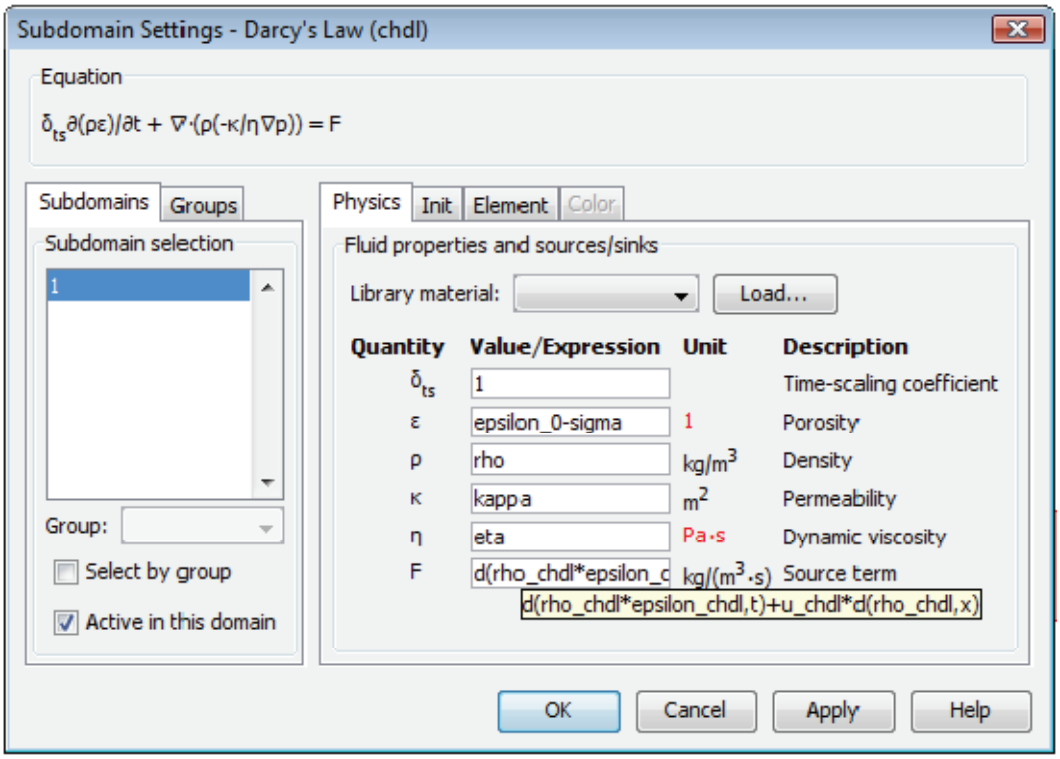

Figure A.3. Subdomain setting of the Darcy's Law

13. For the boundary condition definitions for the Darcy's Law, from Physics menu, select Boundary Settings. The available boundary conditions are; inflow/outflow, pressure condition and insulation/symmetry. The boundary conditions are as given in Table A.3

Table A.3. Boundary conditions for Darcy's Law

	Inflow/outflow	**Pressure**	**Insulation/symmetry**
1	u_0		
2,3			✓
4		0	

14. For the subdomain settings for the Level Set, from Multiphysics menu, select Level Set (mmls). Then, select Subdomain setting dialog in the Physics menu. In Figure A.4, the equation of the level set method and the values/expressions of the quantities are given. Reinitialization parameter γ is to be selected as the maximum value of the flow velocity and it is assigned to the initial velocity. Parameter controlling the interface thickness, ε determines the thickness of the transition region and it is assigned to the half value of the maximum dimension of the mesh elements, hmax_mmls/2. "x-velocity" and "y-velocity" are the components of **u** velocity vector in the formulation and the level set function ϕ is advected with the actual velocity obtained from the Darcy's Law. The components of the actual velocities in the x and y directions are, "u_chdl/epsilon_chdl" and "v_chdl/epsilon_chdl", respectively.

15. For the boundary condition settings for the Level Set, from Physics menu, select Boundary Settings. The available boundary conditions are: inflow, insulation/symmetry and outflow. The boundary conditions are given in Table A.4.

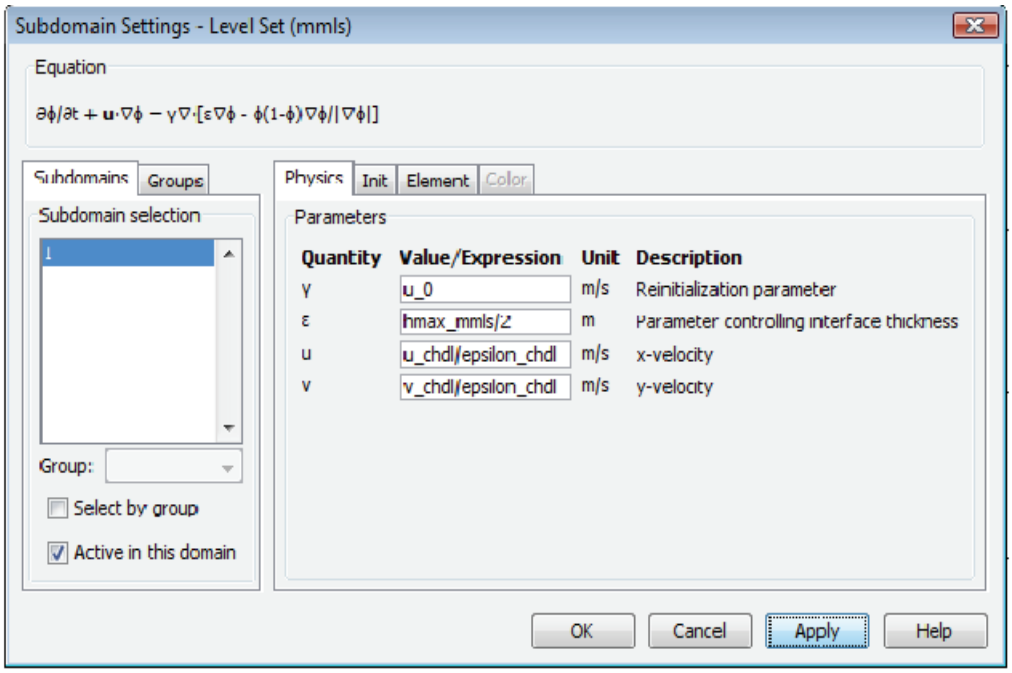

Figure A.4. Snapshot of the subdomain settings of the Level Set

Table A.4. Boundary conditions for Level Set

	Inflow	**Outflow**	**Insulation/symmetry**
1	$\phi = 1$		
2,3			✓
4		✓	

16. For the subdomain settings for the Filtration Kinetics Equation, from Multiphysics menu, select PDE, coefficient form (c). Then, select Subdomain setting dialog in the Physics menu. Referring to the equation (2.56) and Table 3.3, with the constants and scalar expressions defined into the program, the setting of Filtration Kinetics Equation is given in Figure A.5. Here "a" is "alpha*U*C/sigma_u*const_sigma", "f" is "alpha*U*C*const_sigma" and "d_a" is "1". "const_sigma" is defined using the level set function, so specific particle deposit value is zero at the flow front and beyond the flow front. The initial value is assigned at the "init" tab of the subdomain setting is Figure A.5.

17. For the boundary condition settings for the Filtration Kinetics Equation, from Physics menu, select Boundary Settings. Since, Filtration Kinetics Equation has only time derivative, there is no need to define any other boundary condition. For all boundaries, select "Dirichlet boundary condition" and set "h" to 1. So insulation/symmetry is assigned for all boundaries.

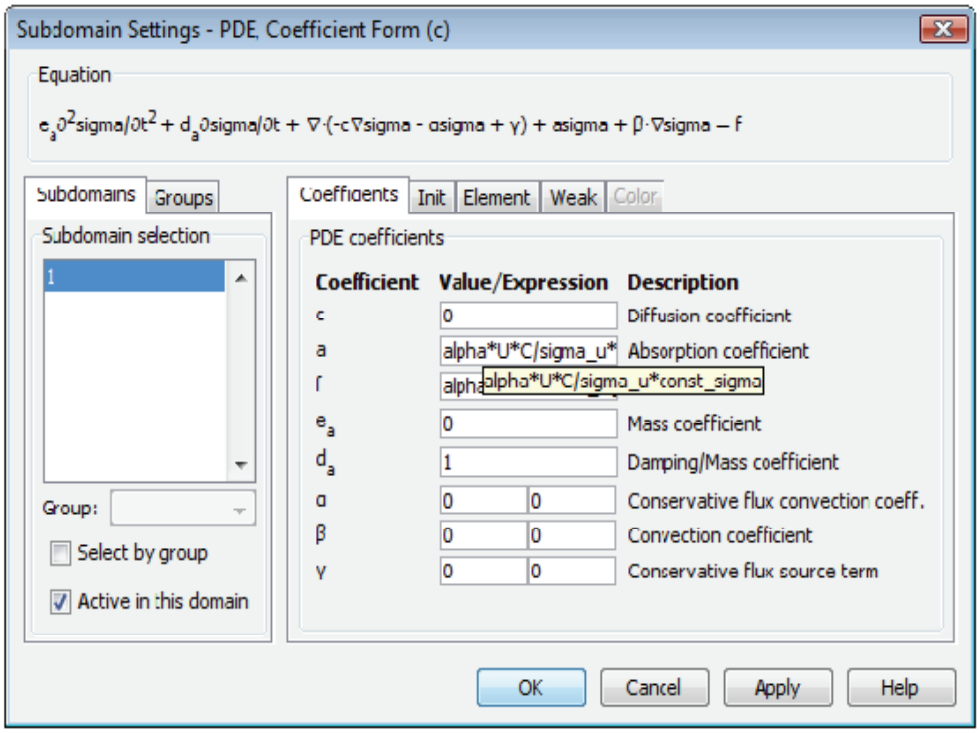

Figure A.5. Snapshot of the subdomain settings of the Filtration Kinetics Equation

18. For the subdomain settings for the Concentration Equation, from Multiphysics menu, select PDE, coefficient form (c2). Then, select Subdomain Setting dialog in the Physics menu. Referring to the equation (2.45) and Table 3.3, with the constants and scalar expressions defined into the program, the setting of concentration equation is given in Figure A.6. Here "a" is "d(epsilon_chdl,t)*const_C", "f" is "-d(sigma,t)*const_C", "d_a" is "epsilon_chdl" and "β" is a vector with components "u_chdl*const_C" and "v_chdl*const_C" . "const_C" is defined using the level set function, so concentration value is zero

beyond the flow front. The initial value is assigned at the “init” tab of the subdomain setting is in Figure A.6.

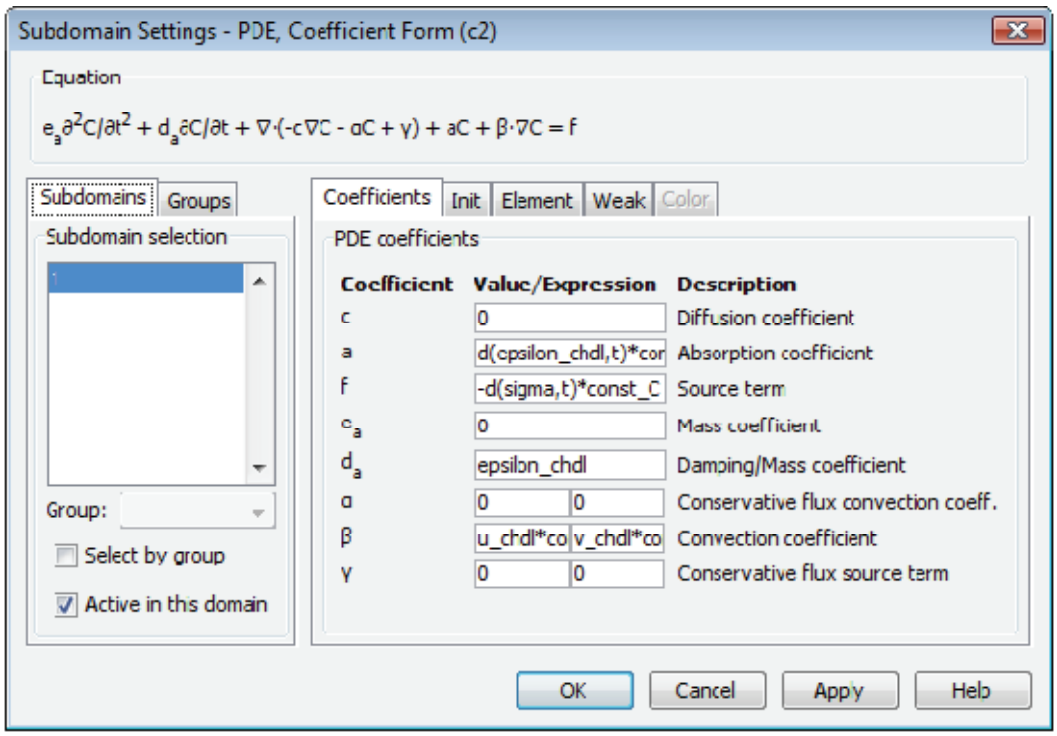

Figure A.6. Snapshot of the subdomain settings of the Concentration Equation

19. For the boundary condition settings for the Concentration Equation, from Physics menu, select Boundary Settings. Since, Concentration Equation has only one time derivative and one first order space derivative, one initial condition and one boundary condition should be defined. There is no need to define any other boundary condition. At the inlet, initial concentration is defined, selecting the “Neumann boundary condition” and setting “q” to 1 and “g” to “C_0”. For the rest of the boundaries, select “Dirichlet boundary condition” and set “h” to 1.

After setting the subdomain and boundary conditions, mesh elements are generated. The mesh elements can be generated from “Initialize Mesh” under Mesh menu and then refinement can be done with “Refine Mesh”. The program offers flexibility on mesh generation. Free Mesh, Mapped Mesh and/or Boundary

Layer Mesh elements can be generated with size functions and/or defining maximum mesh element sizes.

20. From Mesh menu, select Free Mesh Parameters. Under “subdomain” tab, select “Extremely fine” from “Predefined mesh sizes”. (The same solution can be obtained with “Extra fine” or “Refine Mesh” options). The properties of the mesh elements can be obtained from “Mesh Statistics” under Mesh menu.

After mesh generation, solution computation takes place. First, the level set method is initialized.

21. In order to determine the time step, click to “Get Initial Value” under Solve menu. Then, from “Plot Parameters” dialog under Postprocessing menu, write “5*epsilon_mmls/gamma_mmls” to Expression in the “Surface” tab. The obtained value gives the proper time step for the solution. However, the convergence can be tested with smaller time steps. With time step, 0.05 s the solution converges, so the time step is selected to be 0.05 s.

22. Click the Solver Parameters button on the Main toolbar. Select “transient initialization” for the Level Set (mmls) and write “range(0,0.05,0.05)” in the Times field. Click “OK”.

23. Click the Solver Manager button on the Main toolbar. From Solve For tab select only the Level Set (mmls) and click Apply. From Initial Value tab, click Initial value expression evaluated using current solution. First click Apply, and then click Solve.

24. Click the Solver Parameters button on the Main toolbar. Select “transient” for the Level Set (mmls) (also for the Darcy’s Law (chdl)). For the Times field, using the required time for injection formulation in equation (4.5), write range(0,0.05,15). Click “OK”.

25. Click the Solver Manager button on the Main toolbar. From Solve For tab select four equations in the list and click Apply. From Initial Value tab, click

"Store Solution…" button and select 0.05 from the list, click OK. From the initial value part, select "stored solution" and select 0.05 for "solution at time". For the Solver Type, the default one, Direct (UMFPACK) is used. First click Apply, and then click Solve.

The impregnation phase is completed. Save the file.

For the post-processing, from Plot Parameters in the Main toolbar; the time can be set from "solution at time" in the general tab. In the surface tab, for the pressure distribution write "P", for velocity field, write "U", for specific particle deposit, enter "sigma", for concentration enter "C", for the total particle distribution write "C*epsilon_chdl+sigma", etc.. To visualize the flow front position at any time, from Contour tab enter "phi" and select "vector with isolevels" and enter 0.5.

Save the file with a different name and continue. This is necessary to preserve the results of impregnation phase.

For the compression phase the solution domain is deformed with the compression and this is handled with ALE.

26. From Multiphysics menu go to Model Navigator.

27. In the list of application modes select Comsol Multiphysics Module → Deformed Mesh→ Moving Mesh (ALE) → Transient analysis → Add. The final form of the Model Navigator is given in Figure A.7.

NOTE: With the addition of ALE, a reference frame (**X,Y,Z**) and a new time frame (**TIME**) is added to the model. Thus, the expressions should be defined according to those new frames which moves with the solution domain.

28. Add the following expressions from Options → Expressions → Scalar Expressions.

- H_t: H-(t-t_fill)*u_ale
- sors: -u_ale/H_t

- epsilon_t: 1-(1-epsilon_0)*H/H_t

29. From Multiphysics menu, select Darcy's Law. Then from Physics menu click "subdomain settings". As the mold is closed, the unfiltered domain porosity changes, so, change "epsilon_0-sigma" to "epsilon_t-sigma". Also the continuity equation changes as given in equation (2.90). Add "-rho_chdl*sors" and change "d(epsilon_chdl*rho_chdl,t)" to "d(epsilon_chdl*rho_chdl,**TIME**)" and "u_chdl*d(rho_chdl,x)" to "u_chdl*d(rho_chdl,**X**)" for the F, source term. The expression for F is changed as "d(rho_chdl*epsilon_chdl,TIME)+ u_chdl*d(rho_chdl,X)-rho_chdl*sors". Then click Apply and OK.

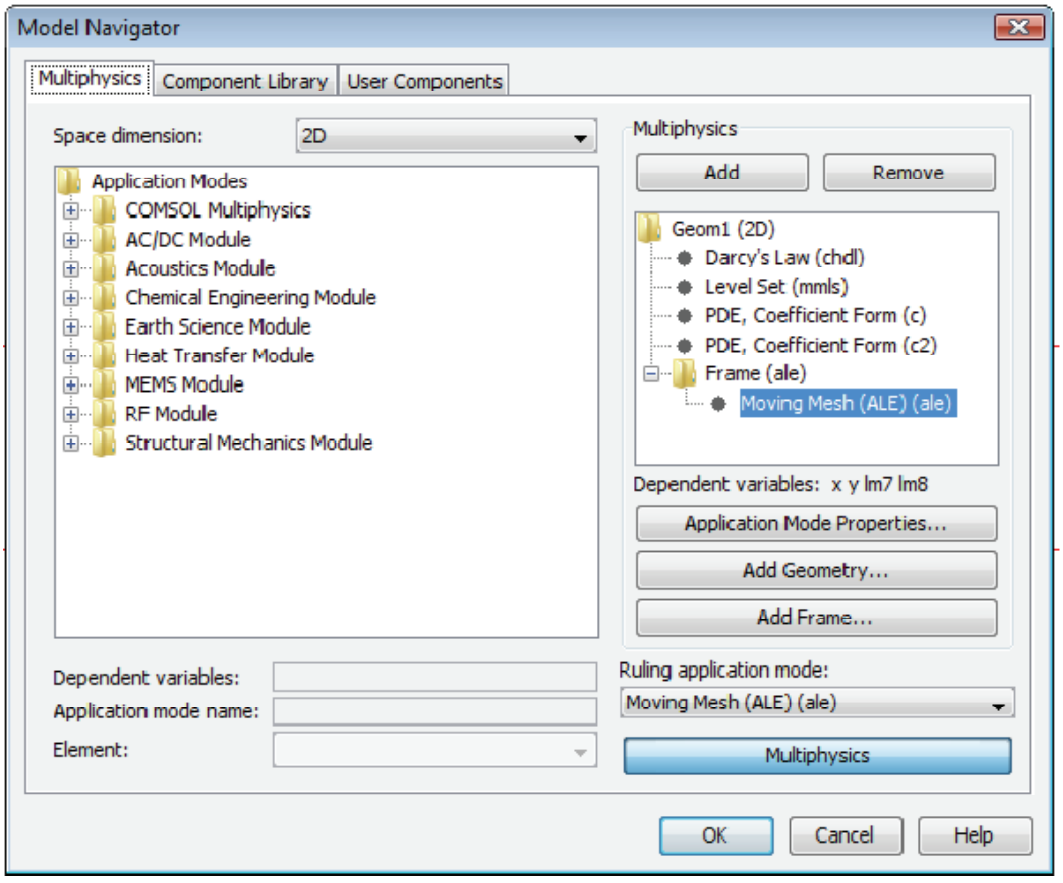

Figure A.7. Snapshot of the model navigator for the simulation of compression phase

30. From Physics menu, select “Boundary Settings”. To close the inlet gate, change the boundary condition at the inlet to “slip/symmetry”. Then click apply and OK.

31. No change is necessary for the subdomain settings of the Level Set, but the boundary condition at the inlet should be changed. From Multiphysics menu, select Level Set. Then from Physics menu click “boundary settings”. Change the inlet boundary condition from “inflow, $\Phi = 1$” to “insulation/symeetry”.

32. No change is necessary for the subdomain and boundary settings of the Filtration Kinetics Equation.

The subdomain and boundary settings should be changed for the concentration Equation.

33. From Multiphysics menu, select PDE, coefficient form (c2). Then from Physics menu click “subdomain settings”. The equation should be changed as in equation (2.81). Change,

a: (d(epsilon_chdl,TIME)+(epsilon_chdl-1)*sors)*const_C

f: (-d(sigma,TIME)-sigma*sors)*const_C

but “β” and “da” remain same.

34. From Physics menu click “boundary settings”. The initial concentration, C_0 should be changed, because the inlet gate is closed during the compression phase. Change the condition at the inlet to “Dirichlet boundary condition” and set “q, g, h r” all to zero.

35. From Multiphysics menu, select Moving Mesh (ALE) (ale). Then from Physics menu click “subdomain settings”. From Mesh tab select “Free Displacement” (it is selected by default).

36. From Physics menu, click “boundary settings”. The mold is closed from upper part, so the mold closing speed, u_ale is defined as velocity at that boundary. The lower part of the mold shouldn’t move, so zero mesh velocity is defined. At the upper part, the definition of the mesh velocity is shown in Figure A.8. At the lower part (boundary number 2), click both v_x and v_y and enter zero velocity.

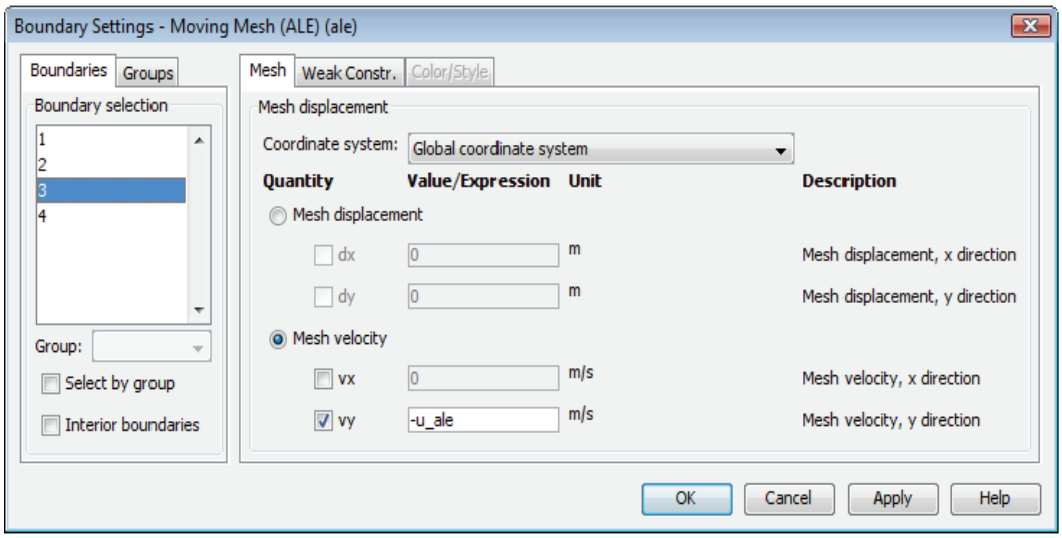

Figure A.8. Snapshot of the boundary settings of Mesh Movement (ALE) at the upper part of the mold cavity

At left and right boundaries to define insulation/symmetry condition, just click to Mesh displacement and do not click the boxes of dx and dy. Then click Apply and OK.

37. Do not repeat the mesh generation operation; same mesh elements with the injection phase will be used.

38. For the computation of the problem, the solution at the end of injection will be stored and will be used as an initial condition. Open “Solution Parameters” from the Main toolbar. Calculate the time for compression using equation (4.6). Edit the Times field as range(15,0.05,30). Here 15 is the time at the end of injection

and compression will continue 15 seconds according the equation (4.6), and total process time is 30 seconds. Then click Apply and OK.

39. From Main toolbar click “Solution Parameters”. By default all equations are selected in the Solve For tab. From Initial Value tab, from “Store Solution…” button select time 15 (end of injection), click OK. Select the time at the Stored Solution field as 15. Click Apply and Solve. The solution takes some time according to mesh elements and time step.

As the solution is finalized, the post-processing for visualization can be performed same with impregnation phase.